A PRIORI ERROR ANALYSIS FOR THE FINITE ELEMENT APPROXIMATIONS TO VARIOUS INTERFACE PROBLEMS ARISING IN BIOLOGICAL MEDIA

by

JOGEN DUTTA

DEPARTMENT OF MATHEMATICS
INDIAN INSTITUTE OF TECHNOLOGY GUWAHATI
GUWAHATI-781039, INDIA

January, 2021

TH-2392_146123010

TH-2392_146123010

A PRIORI ERROR ANALYSIS FOR THE FINITE ELEMENT APPROXIMATIONS TO VARIOUS INTERFACE PROBLEMS ARISING IN BIOLOGICAL MEDIA

A thesis submitted

in partial fulfillment of the requirements

for the degree of

DOCTOR OF PHILOSOPHY

by

JOGEN DUTTA

(Roll No. 146123010)

Department of Mathematics

INDIAN INSTITUTE OF TECHNOLOGY GUWAHATI

January, 2021

TH-2392_146123010

TH-2392_146123010

Dedicated

to

my mother

TH-2392_146123010

TH-2392_146123010

CERTIFICATE

It is certified that the work contained in this thesis entitled **"*A priori* error analysis for the finite element approximations to various interface problems arising in biological media"** by **Jogen Dutta,** a student of Department of Mathematics, Indian Institute of Technology Guwahati, for the award of the degree of Doctor of Philosophy has been carried out under my supervision and that this work has not been submitted elsewhere for a degree.

January, 2021

Dr. Bhupen Deka
Associate Professor
Department of Mathematics
Indian Institute of Technology Guwahati

TH-2392_146123010

TH-2392_146123010

Acknowledgement

This thesis is the most important phase in my academic career and the journey would not have been possible without the love and support of some people, who are always with me directly or indirectly. It is the most pleasurable moment when I can sincerely express my gratitude to all of them .

First and foremost, I would like to take this opportunity to express my gratitude and indebtedness to my supervisor Dr. Bhupen Deka for his ceaseless encouragement and guidance throughout the time of research and writing of this thesis. His attitude and devotion towards research has always been my constant source of inspiration. I am grateful to him for all those countless hours of discussions which enabled my growth as a researcher and as a person.

I acknowledge my gratitude to all the members of my doctoral committee: Dr. A. K. Chakrabarty, Prof. D.C. Dalal and Prof. R. K. Sinha for their useful suggestions and motivations during the progress of my research. Further, I would like to heartily thank Prof. R. K. Sinha for his insightful comments which led to improvement in the quality of my research work.

I also take this opportunity to express my gratitude to all the faculty members of the Department of Mathematics, IIT Guwahati for their help on various occasions. Specially, I thank Dr. Anjan K. Chakrabarty for all the discussions and insights that helped me broaden my knowledge in Mathematics. I am also grateful to all the technical and nontechnical staff members of the department for their help and cooperation throughout the period of my research.

I sincerely acknowledge IIT Guwahati for providing me various facilities necessary to carry out my research. I am most grateful to Ministry of Human and Resource Development, Government of India, for providing me financial assistance for the completion of my thesis work.

I would like to extend my sincere gratitude to Dr. Bhupen Deka and his wife Surobhi(ma'am) for their care, affection and support which gave me homely feeling during my stay at IIT Guwahati.

I could not thank enough Prof. Swaroop Nandan Bora and his wife Swapnali(ma'am)

TH-2392_146123010

for all the love, care and support during these years.

I am forever grateful to my teacher Dr. Dhiren Kumar Basnet for his immense support and encouragements to go for higher studies.

I thank my senior research mates Ankur bhaiya, Naba da, Swarup da and Sougata da for their valuable advice and suggestions during the initial years of my research. I also acknowledge the love and support of my friends Ashish, Maneesh, Ramesh, Ranjan, Tamal, Dipankar, Jibrail, Shivaji, Gautam, Nilay, Kuldeep, Kuwari, Naresh and my friends on the badminton court Anupal, Bastav, Dhanesh, Gyandeep, Jagadish, Nilutpal, Sabnam, Shekhar, who contributed in their own way towards making the time spent in these years really fun and memorable. Practically, it is impossible to mention the names of all the people who have influenced me in this journey. I express my heartiest gratitude to all of them.

I express my heartful gratitude to Jayanta da and his wife Jayashree(sister-in-law) for their unconditional love and support throughout my journey. I owe thanks to my friends: Nandita, Bandita, Debabarata, Nashim and Shailendra, who has always been by my side and whose love and support knows no limits.

I am deeply indebted to my family, especially my parents, without their blessings I would not have made it here. The constant encouragement, love, patience and immense support from my siblings always boosted me.

Finally, I remain ever grateful to Almighty God for His blessings.

January, 2021

(Jogen Dutta)

Department of Mathematics

Indian Institute of Technology Guwahati

TH-2392_146123010

Abstract

The main objective of this thesis is to study *a priori* error analysis of finite element Galerkin methods for some interface problems arising in biological media. Interface problems are often referred to as differential equations with discontinuous coefficients. The discontinuity of the physical coefficients is due to the presence of different material properties across the interface. In biological system it is natural to have heterogeneity in the underlying medium as properties of biological media vary between different layers. Due to the presence of discontinuous coefficients across the interface, interface problems usually lead to non-smooth solutions. Owing to its mathematical complexity and low regularity of its solutions, the study of interface problems has remained a major part of the mathematical study up to the present day. In this thesis we attempt to study the *a priori* error analysis of some of the interface problems arising in biological media using fitted finite element method.

In our first problem, we analyze finite element Galerkin methods applied to pulsed electric model arising in biological tissue when a biological cell is exposed to an electric field. Considering the cell to be a conductive body, embedded in a more or less conductive medium, the governing system involves an electric interface (surface membrane), and heterogeneous permittivity and a heterogeneous conductivity. A fitted finite element method with straight interface triangles is proposed to approximate the voltage of the pulsed electric model across the physical media. Optimal pointwise-in-time error estimates in L^2-norm and H^1-norm are shown to hold for semidiscrete scheme even if the regularity of the solution is low on the whole domain. Further, a fully discrete finite element approximation based on Crank-Nicolson scheme is analyzed and related optimal error estimates are derived. Finally, we give numerical examples to verify the theoretical results.

We next proceed to the *a priori* error analysis of non-Fourier bio heat transfer model in multi-layered media. Specifically, we employ the Maxwell-Cattaneo equation on the physical media with discontinuous coefficients. A fitted finite element method is proposed and analyzed for a hyperbolic heat conduction model with discontinuous coefficients. Typical semidiscrete and fully discrete schemes are presented for a fitted finite element discretization with straight interface triangles. The fully discrete space-time finite element discretizations is based on second order in time Newmark scheme. Optimal *a priori* error estimates for both semidiscrete and fully discrete schemes are proved in $L^\infty(L^2)$ norm. Numerical experiments are reported for several test cases to confirm our theoretical convergence rate. Finite element algorithm

TH-2392_146123010

presented here can be used to solve a wide variety of hyperbolic heat conduction models for non-homogeneous inner structures.

Finally, we have extended our analysis to study the dual-phase-lag(DPL) bio heat model in heterogeneous medium. Well-posedness of the model interface problem and *a priori* estimates of its solutions are established. A new non-standard elliptic type projection operator is introduced to derive optimal convergence result for the semidiscrete solution in $L^{\infty}(L^2)$ norm. The fully discrete space-time finite element discretizations is based on second order in time Newmark scheme. Optimal *a priori* error estimate for the fully discrete scheme is proved in $L^{\infty}(L^2)$ norm. Finally, numerical results for two dimensional test problems are presented in support of our theoretical findings. Finite element algorithm presented here can contribute to a variety of engineering and medical applications.

TH-2392_146123010

Contents

TH-2392_146123010

TH-2392_146123010

List of Figures

TH-2392_146123010

भारतीय प्रौद्योगिकी संस्थान गुवाहाटी • Indian Institute of Technology Guwahati •

TH-2392_146123010

List of Tables

TH-2392_146123010

TH-2392_146123010

1 Introduction

The main purpose of this thesis is to study *a priori* error analysis of finite element Galerkin methods for some interface problems arising in biological media. This chapter contains the description of the problems, notations and preliminary materials to be used in the thesis. It also provides the survey for relevant literature and motivation for the present study. The chapter-wise description of the thesis is presented in the last section of this chapter.

1.1 Problem Description

Interface problems are often referred as differential equations with discontinuous coefficients. The discontinuity of the coefficients corresponds to the fact that the medium consists of two or more physically different materials or fluids.

Electric interface model problem: Let Ω be a bounded domain in $\mathbb{R}^d (d = 2,\ 3)$ with boundary $\partial\Omega$ occupied by the concerned physical media having conductivity $\beta = \beta(x)$ and permittivity $\epsilon = \epsilon(x)$. We now consider the pulsed electric field model for biological media [8, 114, 135]

$$-\nabla \cdot \big(\epsilon \nabla u' + \beta \nabla u\big) = f \quad \text{in } \Omega \times (0, T], \tag{1.1.1}$$

with initial and boundary conditions

$$u(x, 0) = u_0 \ \text{ in } \Omega; \quad u(x, t) = 0 \quad \text{on } \partial\Omega \times (0, T], \tag{1.1.2}$$

where u and f are the voltage potential and electric pulse of the model, respectively. Further, u_0 is the initial voltage and T is the finite terminal observation time, and u' denotes the derivative of u with respect to time variable[1].

[1]For our notational convenience, we will be using $\frac{\partial \phi}{\partial t}$ or ϕ_t or ϕ' interchangeably to denote time differentiation of ϕ. Similar remarks hold for other higher order time derivatives.

TH-2392_146123010

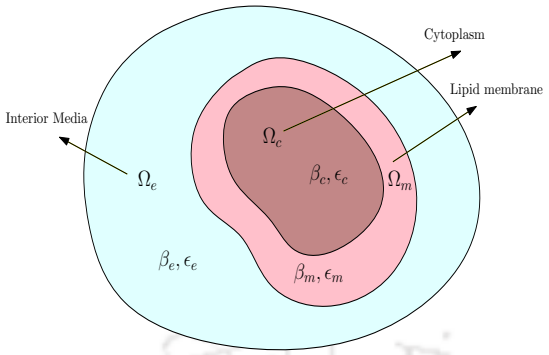

Figure 1.1: A cell comprising of the cell cytoplasm and the cell membrane.

The basic effects of an electric field on a biological cell can be described by considering the cell to be a conductive body (cytoplasm) surrounded by a dielectric layer (surface membrane), embedded in a more or less conductive medium. When an electric field is applied to this cell (by placing the cell in a conductive medium between two electrodes and applying an unipolar voltage pulse to the electrodes), the resulting current causes accumulation of electric charges at the membrane and consequently a voltage across the membrane. Figure 1.1 shows cross section of a single cell structure comprising of the cell cytoplasm and the cell membrane. Here β_j and ϵ_j define the conductivity and permittivity of each medium with subscripts c, m and e describing the cell cytoplasm, membrane, and exterior media, respectively. Therefore the governing system involves interface (surface membrane) and discontinuous media parameters, which may find wide applications in electromagnetism, medicine, food sciences, and biotechnology. Of our special interest is the case when the physical coefficient functions are discontinuous and piecewise positive constants in Ω. We can restrict ourselves to the case when domain Ω consists of two open subdomains Ω_1 and Ω_2 with C^2 smooth interface Γ (see, Figure 1.2). We write

$$(\epsilon, \beta) = \begin{cases} (\epsilon_1, \beta_1) & \text{in } \Omega_1, \\ (\epsilon_2, \beta_2) & \text{in } \Omega_2. \end{cases}$$

Then the information between both the domains are transferred via some interface conditions

$$[u] = 0, \quad \left[\epsilon \frac{\partial u'}{\partial \mathbf{n}} + \beta \frac{\partial u}{\partial \mathbf{n}}\right] = 0 \quad \text{along } \Gamma \times (0, T], \tag{1.1.3}$$

where $[v]$ denotes the jump of a quantity across the interface Γ, i.e. $[v](x) = v_1|_\Gamma - v_2|_\Gamma$ with $v_i(x) = v(x)|_{\Omega_i}$, $i = 1, 2$ and $\left[\epsilon \frac{\partial u'}{\partial \mathbf{n}} + \beta \frac{\partial u}{\partial \mathbf{n}}\right] := \epsilon_1 \frac{\partial u_1'}{\partial \mathbf{n}_1} + \epsilon_2 \frac{\partial u_2'}{\partial \mathbf{n}_2} + \beta_1 \frac{\partial u_1}{\partial \mathbf{n}_1} + \beta_2 \frac{\partial u_2}{\partial \mathbf{n}_2}$ with $\frac{\partial}{\partial \mathbf{n}_i}$ denotes the outer normal derivative with respect to Ω_i, $i = 1,\ 2$.

TH-2392_146123010

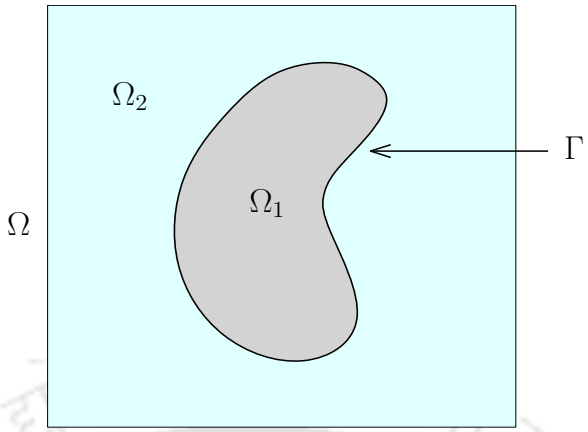

Figure 1.2: Domain Ω and its sub domains Ω_1, Ω_2 with interface Γ.

The electrical properties of biological tissues and cell suspensions have been of interest for over a century for many reasons (*cf.* [12, 97, 99, 111, 119]). In [99, 119], a biological tissue is described as having a permittivity and a conductivity, and current flow through the biological medium is discussed in [12, 97, 111]. To analyze the response of a tissue to external electric field, we need adequate mathematical models that characterize field distributions in biological systems. Exposure of cells to an external electric field induces a voltage on the cell membrane called the transmembrane voltage (*cf.* [62, 77]). The electric interface model problem (1.1.1)-(1.1.3) describes the voltage potential of a biological tissue under the influence of a pulsed electric field. The value and the spatial distribution of the transmembrane voltage are of significant interest in the electroporation of the cell membrane. Once the required voltage of electroporation is achieved the lipid bilayer molecules of the membrane rearrange themselves and form pores in the membrane through which ions and impermeable molecules can pass and enter the cytoplasm [136]. Electroporation is gaining increased importance because of its clinical applications in gene therapy and drug delivery as a method to introduce new DNA and drugs into a cell in order to change its function [11]. Several electrical models have been developed for biological cells exposed to an external electric field to obtain the distribution of the transmembrane voltage in [117].

Non-Fourier bio heat model problem. Let Ω be a bounded domain in $\mathbb{R}^d (d = 2,\ 3)$ with Lipschitz boundary $\partial\Omega$ and $\Omega_1 \subset \Omega$ is an open domain with C^2 smooth boundary $\Gamma = \partial\Omega_1$ and $\Omega_2 = \Omega \backslash \Omega_1$(see, Figure 1.2). In Ω, we consider the following non-Fourier bio heat transfer model in multi-layered media (*cf.* [33, 76, 121, 137] and references

TH-2392_146123010

therein)

$$u'' + \sigma u' - \nabla \cdot (\beta \nabla u) = f \quad \text{in } \Omega \times (0, T],\ T < \infty, \tag{1.1.4}$$

with initial and boundary conditions

$$u(x, 0) = u_0, \quad u'(x, 0) = v_0 \ \text{ in } \Omega \ \ \& \ \ u(x, t) = 0 \quad \text{on } \partial\Omega \times (0, T]. \tag{1.1.5}$$

Here, $\sigma = \sigma(x)$ and $\beta = \beta(x)$ are non-negative real-valued functions, and f denotes the source. Further, u' and u'' denotes the first and second order time differentiation of u, respectively.

Equation (1.1.4) is also known as hyperbolic heat equation/Maxwell-Cattaneo (MC) equation/damped wave equation. As a model, we consider bio heat transfer model in non-homogeneous media. With advances in laser, microwave, radio-frequency and similar technologies, a variety of thermal methods have been proposed to analyze the bio heat transfer in living tissue (*e.g.* [33, 76, 95, 100, 103, 121, 137]) since the landmark paper by Pennes [110]. But, due to simplicity, Pennes' bio heat transfer equation is used most commonly for simulation of thermal data. Pennes' bio heat transfer equation is based on classical Fourier's law. Pennes' model assumes that any temperature disturbance produced at a certain location will be felt through out the medium at that instant. However, in applications involving samples with non-homogeneous internal structures, *e.g.* biological samples, it has been experimentally demonstrated that the Fourier law of heat conduction cannot accurately predict the thermal response of such samples (*e.g.* [33, 72, 76, 100, 103, 133, 137]). Biological tissue, along with a number of other common materials, exhibits a relaxation time. Relaxation time reflects the time between phonon collisions or it represents a time lag between the imposition of a temperature gradient and the creation of a thermal flux. Skin tissue has a "lengthy" relaxation time, which means it is desirable to develop a computational approach to examine the non-Fourier heat transfer process. For details, we refer to Xu *et al.* [138]. Due to implication of such relaxation time, heat conduction in biological media is generally not described by Fourier's law, but rather by the Maxwell-Cattaneo law [130]. Thermal behavior or heat transfer in biological media is mainly a heat conduction process and since the thermal properties of biological media vary between different layers, so, it is natural to have heterogeneity in the underlying media. In particular, media parameters are discontinuous and piecewise constants in Ω (see, Figure 1.2). We write

$$(\sigma, \beta) = \begin{cases} (\sigma_1, \beta_1) & \text{in } \Omega_1, \\ (\sigma_2, \beta_2) & \text{in } \Omega_2. \end{cases}$$

TH-2392_146123010

The interfacial continuity conditions between layers are given by (*cf.* [33])

$$[u] = 0, \quad \left[\beta \frac{\partial u}{\partial \mathbf{n}}\right] = 0 \quad \text{along } \Gamma \times (0, T], \tag{1.1.6}$$

where the symbols $[v]$ and $\mathbf{n}$ are defined as before. The present work regards the temperature and the heat flux at the interface of two regions is continuous. In other words, the heat contact resistance at the interface between the two different media is neglected.

Dual-phase-lag (DPL) bio heat model problem. Let Ω be a bounded domain in $\mathbb{R}^d (d = 2,\ 3)$ with Lipschitz boundary $\partial\Omega$ and $\Omega_1 \subset \Omega$ is an open domain with C^2 smooth boundary $\Gamma = \partial\Omega_1$ and $\Omega_2 = \Omega \backslash \Omega_1$ (see, Figure 1.2). In Ω, we consider the DPL bio heat transfer model (*cf.* [94, 103, 128, 129, 130, 137, 138] and references therein) in multi-layered media

$$u'' + \sigma u' + \delta u - \nabla \cdot (\epsilon \nabla u') - \nabla \cdot (\beta \nabla u) = f \quad \text{in } \Omega \times (0, T],\ T < \infty, \tag{1.1.7}$$

with initial and boundary conditions

$$u(x, 0) = u_0 \ \ \& \ \ u'(x, 0) = v_0 \ \text{ in } \Omega; \ \ u(x, t) = 0 \quad \text{on } \partial\Omega \times (0, T]. \tag{1.1.8}$$

Here, $\sigma = \sigma(x),\ \delta = \delta(x),\ \epsilon = \epsilon(x)$ and $\beta = \beta(x)$ are non-negative real valued functions, and f denotes the source. Further, u' and u'' denotes the first and second order time differentiation of u, respectively.

Equation (1.1.7) is also known as general linear second order hyperbolic equation, which has received a great deal of attention within the context of viscous wave equation, networks of linked beams, hybrid chimney, bio heat transfer etc. Although Maxwell-Cattaneo model has taken care of thermal relaxation time, the validity of the thermal wave model becomes debatable in view of the fast-transient response with microstructural interaction effects [129]. In order to consider the effect of micro-structural interaction in the fast transient process of heat transport, a phase lag for temperature gradient, τ_T, which is absent in the Maxwell-Cattaneo model, has been introduced in [94, 128, 129, 137, 138]. The corresponding model is called the dual-phase-lag (DPL) model. Mathematically, DPL model is described by a time-dependent equation [137, 138]

$$\begin{aligned} \tau_q \rho c \frac{\partial^2 T}{\partial t^2} \ &= \ k\nabla^2 T + \tau_T k \nabla^2 \frac{\partial T}{\partial t} - \omega_b \rho_b c_b T - (\tau_q \omega_b \rho_b c_b + \rho c) \frac{\partial T}{\partial t} \\ &\quad + \big(\omega_b \rho_b c_b T_a + q_{\text{met}} + q_{\text{ext}} + \tau_q \frac{\partial q_{\text{met}}}{\partial t} + \tau_q \frac{\partial q_{\text{ext}}}{\partial t}\big), \end{aligned}$$

where ρ, c, k are the density, specific heat and thermal conductivity of skin tissue, respectively; ρ_b, c_b are the density and specific heat of blood, ω_b is the blood perfusion

TH-2392_146123010

rate; T_a and T are the temperatures of arterial blood and skin tissue respectively; q_{met} is the metabolic heat generation in the skin tissue and q_{ext} is the heat source due to external heating, and τ_q is defined as the thermal relaxation time. Due to heterogeneity in the underlying media, the thermal properties of biological media vary between different layers. In $\Omega = \Omega_1 \cup \Omega_2 \cup \Gamma$ (see, Figure 1.2), we assume that the physical coefficients are discontinuous and piecewise constants. We write

$$(\sigma, \delta, \epsilon, \beta) = \begin{cases} (\sigma_1, \delta_1, \epsilon_1, \beta_1) & \text{in } \Omega_1, \\ (\sigma_2, \delta_2, \epsilon_2, \beta_2) & \text{in } \Omega_2. \end{cases}$$

The problem (1.1.7)-(1.1.8) is completed with the following physical interface conditions (*cf.* [94])

$$[u] = 0, \quad \left[\epsilon(x)\frac{\partial u'}{\partial \mathbf{n}} + \beta(x)\frac{\partial u}{\partial \mathbf{n}}\right] = 0 \quad \text{along } \Gamma \times (0, T], \tag{1.1.9}$$

where the symbols $[v]$ and $\mathbf{n}$ are defined as before.

1.2 Notations and Preliminaries

In this section, we shall introduce some basic notations, function spaces and preliminary materials to be used in this thesis. All functions considered here are real valued. For the purpose of introducing notations, we assume Ω to be a convex polygonal domain in $\mathbb{R}^d$ (d-dimensional Euclidean space) and $\partial\Omega$ denote the boundary of Ω. For $x = (x_1, x_2, \ldots, x_d) \in \Omega$, set $dx = dx_1 \ldots dx_d$. Further, let $\alpha = (\alpha_1, \ldots, \alpha_d)$ be an d-tuple with nonnegative integer component and denote the order of α as $|\alpha| = \alpha_1 + \alpha_2 + \ldots + \alpha_d$. Then, by $D^\alpha\phi$, we shall mean the αth derivative of ϕ defined by

$$D^\alpha\phi = \frac{\partial^{|\alpha|}\phi}{\partial {x_1}^{\alpha_1} \ldots \partial {x_n}^{\alpha_d}}$$

By support of a function ϕ, denoted by $\text{supp}(\phi)$, we mean the closure of all points x with $\phi(x) \neq 0$, i.e.,

$$\text{supp}(\phi) = \overline{\{x \in \Omega : \phi(x) \neq 0\}}.$$

For any nonnegative integer m, $C^m(\overline{\Omega})$ denotes the space of functions with continuous derivatives upto and including order m in $\overline{\Omega}$. $C_0^m(\Omega)$ is the space of all $C^m(\Omega)$ functions with compact support in Ω and $C_0^\infty(\Omega)$ is the space of all infinitely differentiable functions with compact support in Ω.

Now we introduce the following function spaces which we shall refer frequently. For any domain $\mathcal{M} \subseteq \Omega \subset \mathbb{R}^d$, $d = 2,\ 3$, with $1 \leq p \leq \infty$, $L^p(\mathcal{M})$ denotes the linear space

TH-2392_146123010

of equivalence classes of measurable functions ϕ on Ω such that $\|\phi\|_{L^p(\mathcal{M})} < \infty$, where

$$\begin{aligned} \|\phi\|_{L^p(\mathcal{M})} &:= \left(\int_{\mathcal{M}} |\phi(x)|^p dx \right)^{\frac{1}{p}}, \quad 1 \le p < \infty, \\ \|\phi\|_{L^\infty(\mathcal{M})} &:= \operatorname*{ess\,sup}_{x \in \mathcal{M}} |\phi(x)| < \infty. \end{aligned}$$

When $p = 2$, $L^2(\mathcal{M})$ is a Hilbert space with respect to the inner product

$$(\phi, \psi)_{\mathcal{M}} = \int_{\mathcal{M}} \phi(x)\psi(x)dx.$$

For simplicity of notation, we write the norm $\|\cdot\|_{L^2(\mathcal{M})}$ of $L^2(\mathcal{M})$ by $\|\cdot\|_{\mathcal{M}}$ and remove the subscript $\mathcal{M}$ whenever $\mathcal{M} = \Omega$.

We now introduce the notion of Sobolev spaces. For each integer $k \ge 0$ and real number p with $1 \le p \le \infty$, $W^{k,p}(\mathcal{M})$ denotes the standard Sobolev space of functions with their distributional derivatives of order up to k in the Lebesgue space $L^p(\mathcal{M})$, i.e.

$$W^{k,p}(\mathcal{M}) = \{\phi \in L^p(\mathcal{M}) : \ D^\alpha \phi \in L^p(\mathcal{M}) \text{ for } 0 \le |\alpha| \le k\}.$$

The spaces $W^{k,p}(\mathcal{M})$ are Banach spaces endowed with the norm

$$\begin{aligned} \|\phi\|_{k,p} &:= \left(\sum_{0 \le |\alpha| \le k} \|D^\alpha \phi\|^p_{L^p(\mathcal{M})} \right)^{\frac{1}{p}}, \quad 1 \le p < \infty, \\ \|\phi\|_{k,\infty} &:= \max_{0 \le |\alpha| \le k} \|D^\alpha \phi(x)\|_{L^\infty(\mathcal{M})}, \quad p = \infty, \end{aligned}$$

also, the semi-norm on $W^{k,p}(\mathcal{M})$ is defined as

$$|\phi|_{k,p,\mathcal{M}} := \sum_{|\alpha| = k} \|D^\alpha \phi\|_{L^p(\mathcal{M})}.$$

When $p = 2$, we write $H^k(\mathcal{M})$ for $W^{k,2}(\mathcal{M})$ with the norm $\|\cdot\|_{k,2,\mathcal{M}} = \|\cdot\|_{k,\mathcal{M}}$ and the semi-norm $|\cdot|_{k,2,\mathcal{M}} = |\cdot|_{k,\mathcal{M}}$. For simplicity of notation, we skip the subscript $\mathcal{M}$ in the norm and inner product notation when $\mathcal{M} = \Omega$.

The space $H^k(\mathcal{M})$ is a Hilbert space with natural inner product defined by

$$(\phi, \psi)_{k,\mathcal{M}} = \sum_{0 \le |\alpha| \le k} \int_{\mathcal{M}} D^\alpha \phi D^\alpha \psi dx, \quad \phi, \psi \in H^k(\mathcal{M}).$$

The Sobolev space $H^k_0(\Omega)$ is defined as the closure of $C^\infty_0(\Omega)$ with respect to the norm $\|\phi\|_k = \|\phi\|_{k,2}$. This result is true under some smoothness assumption on the boundary $\partial\Omega$. For a complete discussion on Sobolev spaces, see Adams and Fournier [1].

TH-2392_146123010

We shall also use the following space-time function spaces in our error analysis. For $1 \leq p \leq \infty$, we also define the standard Bôchner spaces $L^p(J;\mathcal{B})$, where $\mathcal{B}$ is a real Banach space with norm $\|\cdot\|_{\mathcal{B}}$ and $J = [0,T]$, consisting of all measurable functions $\phi : J \to \mathcal{B}$ for which

$$\begin{aligned} \|\phi\|_{L^p(0,T;\mathcal{B})} &= \Big(\int_0^T \|\phi(t)\|_{\mathcal{B}}^p dt\Big)^{\frac{1}{p}} < \infty \quad \text{for } 1 \leq p < \infty, \\ \|\phi\|_{L^\infty(0,T;\mathcal{B})} &= \operatorname*{ess\,sup}_{t\in[0,T]} \|\phi(t)\|_{\mathcal{B}} < \infty \quad \text{for } p = \infty. \end{aligned}$$

We denote by $H^m(0,T;\mathcal{B})$, $1 \leq m < \infty$, the space of all measurable functions $\phi : J \to \mathcal{B}$ for which

$$\|\phi\|_{H^m(0,T;\mathcal{B})} = \left(\sum_{j=0}^{m} \int_0^T \left\|\frac{\partial^j \phi(t)}{\partial t^j}\right\|_{\mathcal{B}}^2 dt\right)^{\frac{1}{2}} < \infty.$$

When no risk of confusion exists, we shall write $L^2(\mathcal{B})$ for $L^2(J;\mathcal{B})$, $L^\infty(\mathcal{B})$ for $L^\infty(J;\mathcal{B})$ and $H^m(\mathcal{B})$ for $H^m(J;\mathcal{B})$. Furthermore, $C(0,T;\mathcal{B})$ is defined as the space of continuous functions $\phi : [0,T] \to \mathcal{B}$ with norm $\|\phi\|_{C(0,T;B)} := \max_{t\in[0,T]} |\phi(t)| < \infty$. For a complete discussion on Sobolev Spaces, one may refer to Adams and Fourier [1], Dautray and Lions [34] and Evans [49].

To deal with the interface problems, we introduce the following Banach spaces

$$\begin{aligned} \mathcal{Y} &:= H_0^1(\Omega) \cap H^2(\Omega_1) \cap H^2(\Omega_2), \\ \mathcal{X} &:= L^2(\Omega) \cap H^2(\Omega_1) \cap H^2(\Omega_2), \\ X &:= L^2(\Omega) \cap H^1(\Omega_1) \cap H^1(\Omega_2), \end{aligned}$$

equipped with the norms

$$\begin{aligned} \|u\|_{\mathcal{Y}} &:= \|u\|_{H^1(\Omega)} + \|u\|_{H^2(\Omega_1)} + \|u\|_{H^2(\Omega_2)}, \\ \|u\|_{\mathcal{X}} &:= \|u\|_{L^2(\Omega)} + \|u\|_{H^2(\Omega_1)} + \|u\|_{H^2(\Omega_2)}, \\ \|u\|_{X} &:= \|u\|_{L^2(\Omega)} + \|u\|_{H^1(\Omega_1)} + \|u\|_{H^1(\Omega_2)}, \end{aligned}$$

respectively. For the sake of brevity, we write $W = L^2(\Omega)$, $V = H_0^1(\Omega)$ with its dual space $V' = H^{-1}(\Omega)$. For our notational convenience, we will be using $\frac{\partial u}{\partial t}$ or u_t or u' interchangeably to denote the first order time derivative of u with respect to t. Similar notions are used for higher order time derivatives.

Now we shall recall some important inequalities for our subsequent use (see Hardy *et al.* [58]):

TH-2392_146123010

Young's inequality. For $a, b \geq 0$ and $\mu > 0$, the following inequality holds

$$ab \leq \frac{a^2}{2\mu} + \frac{\mu b^2}{2}.$$

An important consequence of the Young's inequality is the Hölder's inequality. The discrete version of Hölder's inequality is stated below.

Hölder's inequality: Let $p > 1$ and q be such that $\frac{1}{p} + \frac{1}{q} = 1$. Then, for any real numbers $a_i, b_i \in \mathbb{R}, i = 1, 2, \cdots, d$,

$$\sum_{i=1}^{d} |a_i b_i| \leq \left(\sum_{i=1}^{d} |a_i|^p \right)^{\frac{1}{p}} \left(\sum_{i=1}^{d} |b_i|^q \right)^{\frac{1}{q}}.$$

In particular, for $p = q = 2$, the above inequality is known as the *Cauchy-Schwarz inequality* in $\mathbb{R}^d$.

The integral analogue of Hölder's inequality is as follows: Let $p > 1$ and q be such that $\frac{1}{p} + \frac{1}{q} = 1$. Then, for any measurable functions $\phi, \psi : \Omega \to \mathbb{R}$

$$\|\phi\psi\|_{L^1(\Omega)} \leq \|\phi\|_{L^p(\Omega)} \|\psi\|_{L^q(\Omega)}.$$

For $p = q = 2$, the above inequality is known as the *Cauchy-Schwarz inequality.*

Poincaré inequality: Let Ω be a bounded open domain in $\mathbb{R}^d$. Then there exists a positive constant $C = C(\Omega)$ such that

$$\|\phi\| \leq C \|\nabla \phi\| \quad \forall \phi \in H_0^1(\Omega).$$

In view of the Poincaré inequality, $\|\nabla(\cdot)\|$ defines a norm on $H_0^1(\Omega)$.

Next we state without proof, the following continuous version of Grownwall's lemma. For a proof, see Rao [113].

Lemma 1.2.1 (Gronwall's lemma)**.** *Let $G(t)$ be a continuous function and $H(t)$ a non-negative continuous function on its interval $t_0 \leq t \leq t_0 + a$. If a continuous function $F(t)$ has the property*

$$F(t) \leq G(t) + \int_{t_0}^{t} F(s) H(s) ds \quad \text{for } t \in [t_0, t_0 + a],$$

then

$$F(t) \leq G(t) + \int_{t_0}^{t} G(s) H(s) exp\left[\int_{s}^{t} H(\tau) d\tau \right] ds \quad \text{for } t \in [t_0, t_0 + a].$$

In particular, when $G(t) = C$ a nonnegative constant, we have

$$F(t) \leq C exp\left[\int_{t_0}^{t} H(s) ds \right] \quad \text{for } t \in [t_0, t_0 + a].$$

TH-2392_146123010

For the purpose of finite element approximation, we introduce bilinear maps associated with the general linear hyperbolic equation (1.1.7). Let $\mathcal{A}_\epsilon(\cdot,\cdot)$ and $\mathcal{A}_\beta(\cdot,\cdot)$ be two bilinear maps defined on V as follows

$$\mathcal{A}_\epsilon(w,v) = \int_\Omega \epsilon \nabla w \cdot \nabla v dx = \mathcal{A}_\epsilon^1(w,v) + \mathcal{A}_\epsilon^2(w,v) \;\; \forall w, v \in V$$

and

$$\mathcal{A}_\beta(w,v) = \int_\Omega \beta \nabla w \cdot \nabla v dx = \mathcal{A}_\beta^1(w,v) + \mathcal{A}_\beta^2(w,v) \;\; \forall w, v \in V.$$

Here, $\mathcal{A}_\epsilon^l,\ \mathcal{A}_\beta^l : H^1(\Omega_l) \times H^1(\Omega_l) \to \mathbb{R},\ l = 1,\ 2$, are the local bilinear forms defined by

$$\mathcal{A}_\epsilon^l(w,v) = \int_{\Omega_l} \epsilon_l \nabla w \cdot \nabla v dx \;\; \& \;\; \mathcal{A}_\beta^l(w,v) = \int_{\Omega_l} \beta_l \nabla w \cdot \nabla v dx \;\; \forall w, v \in H^1(\Omega_l).$$

Further, we define bilinear forms $\mathcal{B}_\sigma(\cdot,\cdot),\ \mathcal{B}_\delta(\cdot,\cdot) : L^2(\Omega) \times L^2(\Omega) \to \mathbb{R}$ as

$$\mathcal{B}_\sigma(w,v) = \int_\Omega \sigma w v dx \;\; \& \;\; \mathcal{B}_\delta(w,v) = \int_\Omega \delta w v dx \;\; \forall w, v \in L^2(\Omega).$$

We now turn our discussion towards the discretization of domain Ω. Throughout this work, we will follow the same discretization. We assume that Ω is a convex polygon (if $d = 2$) or a convex polyhedral (if $d = 3$). The following discussion is borrowed from [8]. We assume that the family of triangulation $\{\mathcal{T}_h\}_{h\in(0,h_0)}$, for some fixed $h_0 > 0$, is quasi-uniform. By a quasi-uniform mesh, we mean [85]

$$c_0 h \le h_K \le c_1 h \quad \forall K \in \mathcal{T}_h,\ h \in (0, h_0) \text{ for some } c_0,\ c_1 > 0, \tag{1.2.1}$$

where $h_K := \frac{1}{2}\text{diam}(K) = \frac{1}{2}\sup\{\|x-y\| : x, y \in K\}$ and $h := \min_{K\in\mathcal{T}_h} \rho_K$ with ρ_K being the maximal radius such that $B_{\rho_K}(b_K) \subset K$. Here, $B_{\rho_K}(b_K)$ denotes the closed ball of radius ρ_K centered at the barycenter b_K of the element K. We first approximate the domain Ω_1 by a polyhedral domain $\Omega_{1,h}$ using a quasi-uniform mesh $\mathcal{T}_h^1$ such that all the boundary vertices of $\Omega_{1,h}$ lie on the boundary of Ω_1. Let $\Omega_{2,h}$ be the approximation for the domain Ω_2 due to a quasi-uniform triangulation $\mathcal{T}_h^2$ with simplicial elements of size h and we define $\Gamma_h = \bar{\Omega}_{1,h} \cap \bar{\Omega}_{2,h}$. The triangulation $\mathcal{T}_h^2$ is done such that all the vertices of the outer polyhedral boundary $\partial\Omega$ are also the vertices of $\Omega_{2,h}$, while all the vertices on the inner boundary of $\Omega_{2,h}$ match the boundary vertices of $\Omega_{1,h}$. More precisely, the triangulation $\mathcal{T}_h := \mathcal{T}_h^1 \cup \mathcal{T}_h^2$ satisfies the following conditions:

($\mathcal{A}1$) $\overline{\Omega} = \cup_{K\in T_h} K$,

($\mathcal{A}2$) if $K_1, K_2 \in \mathcal{T}_h$ and $K_1 \neq K_2$, then either $K_1 \cap K_2 = \emptyset$ or $K_1 \cap K_2$ is a common vertex, an edge or a face,

TH-2392_146123010

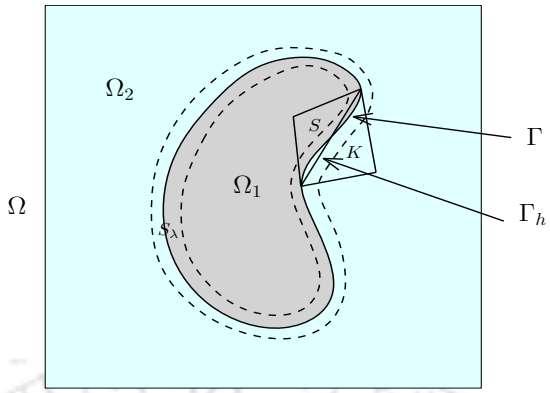

Figure 1.3: An illustrative example of interface triangles K and S with λ-strip S_λ.

($\mathcal{A}3$) for each K, all its vertices are completely contained in either $\overline{\Omega}_1$ or $\overline{\Omega}_2$.

Let V_h be the finite dimensional subspace of $H_0^1(\Omega)$ defined on $\mathcal{T}_h$ consisting of piecewise linear functions vanishing on the boundary $\partial\Omega$. We now define a tubular neighborhood S_λ of Γ by

$$S_\lambda = \{x \in \Omega : \ \text{dist}(x, \Gamma) < \lambda\}$$

for some $\lambda > 0$ with $\lambda = \mathrm{O}(h^2)$ (*cf.* [85]). Existence of such λ is possible due to the fact that interface Γ is of class C^2. A typical λ-strip is presented in Figure 1.3. In fact the mesh $\mathcal{T}_h$ can be decomposed into three disjoint subsets $\mathcal{T}_h = \dot{\mathcal{T}}_h^1 \cup \dot{\mathcal{T}}_h^2 \cup \mathcal{T}_\star$, where

$$\dot{\mathcal{T}}_h^i = \{K \in \mathcal{T}_h : \ K \subset \overline{\Omega}_i \backslash S_\lambda\}, \ i = 1, \ 2,$$

and $\mathcal{T}_\star = \mathcal{T}_h \backslash (\dot{\mathcal{T}}_h^1 \cup \dot{\mathcal{T}}_h^2)$. An element $K \in \mathcal{T}_*$ is called an interface element and $K \in \mathcal{T}_h \backslash \mathcal{T}_*$ is called a non-interface element. Further, for $i = 1, \ 2$, we define following disjoint collections of interface elements

$$\mathcal{T}_\star^i := \{K \in \mathcal{T}_\star : \ K \subset \bar{\Omega}_i \cup S_\lambda\}.$$

With above notations, we have

$$\Omega_{i,h} = \cup\{\overline{K} : \ K \in \dot{\mathcal{T}}_h^i \cup \mathcal{T}_*^i\},$$

so that for any $K \in \mathcal{T}_h$, either $K \subseteq \Omega_{1,h}$ or $K \subseteq \Omega_{2,h}$.

In order to approximate $\mathcal{A}_\epsilon(\cdot,\cdot)$, $\mathcal{A}_\beta(\cdot,\cdot)$, we now introduce approximate bilinear maps $\mathcal{A}_{\epsilon h}, \mathcal{A}_{\beta h} : H^1(\Omega) \times H^1(\Omega) \to \mathbb{R}$ defined as

$$\mathcal{A}_{\epsilon h}(w, v) = \sum_{K \in \mathcal{T}_h} \int_K \epsilon_K(x) \nabla w \cdot \nabla v dx \ \ \forall w, v \in H^1(\Omega),$$

$$\mathcal{A}_{\beta h}(w, v) = \sum_{K \in \mathcal{T}_h} \int_K \beta_K(x) \nabla w \cdot \nabla v dx \ \ \forall w, v \in H^1(\Omega),$$

TH-2392_146123010

with $\epsilon_K(x) = \epsilon_i$ and $\beta_K(x) = \beta_i$ if $K \subset \Omega_{i,h},\ i = 1, 2$.

Next, we approximate the bilinear maps $\mathcal{B}_\sigma(\cdot,\cdot)$, $\mathcal{B}_\delta(\cdot,\cdot)$ by $\mathcal{B}_{\sigma h}(\cdot,\cdot)$ and $\mathcal{B}_{\delta h}(\cdot,\cdot)$ respectively, defined as

$$\mathcal{B}_{\sigma h}(w, v) = \sum_{K\in\mathcal{T}_h} \int_K \sigma_K(x) wv dx \ \ \forall w, v \in L^2(\Omega),$$

$$\mathcal{B}_{\delta h}(w, v) = \sum_{K\in\mathcal{T}_h} \int_K \delta_K(x) wv dx \ \ \forall w, v \in L^2(\Omega),$$

with $\sigma_K(x) = \sigma_i$ and $\delta_K(x) = \delta_i$ if $K \subset \Omega_{i,h},\ i = 1, 2$.

For the simplicity of the exposition, we write $\mathcal{A}$ for $\mathcal{A}_\epsilon$ (or $\mathcal{A}_\beta$) and $\mathcal{A}_h$ for $\mathcal{A}_{\epsilon h}$ (or $\mathcal{A}_{\beta h}$), respectively. Similarly, we write $\mathcal{B}$ for $\mathcal{B}_\sigma$ (or $\mathcal{B}_\delta$) and $\mathcal{B}_h$ for $\mathcal{B}_{\sigma h}$ (or $\mathcal{B}_{\delta h}$), respectively.

We now state following approximation results near interface which will be frequently used in our later analysis. For a proof, we refer to [8, 85].

Lemma 1.2.2. *For $w,\ v \in H^1(\Omega)$, the form $\mathcal{A}^\Delta_{\epsilon h}(w, v) = \mathcal{A}_\epsilon(w, v) - \mathcal{A}_{\epsilon h}(w, v)$ satisfies*

$$|\mathcal{A}^\Delta_{\epsilon h}(w, v)| \le C|w|_{1,S_\lambda}|v|_{1,S_\lambda}.$$

Similar result also holds true for the operator $\mathcal{A}_\beta$.

Lemma 1.2.3. *For any $v \in H^1_0(\Omega)$, we have*

$$\|v\|^2_{S_\lambda} \le C\lambda\|v\|^2_1.$$

Moreover, for any $v \in \mathcal{Y}$, we have

$$|v|^2_{1,S_\lambda} \le C\lambda\|v\|^2_{\mathcal{Y}}.$$

Lemma 1.2.4. *There exists a positive constant μ independent of h such that*

$$\|v_h\|_{1,S_\lambda} \le C\sqrt{\frac{\lambda}{h}}\|v_h\|_{1,S_{\mu h}} \ \forall v_h \in V_h.$$

Throughout this thesis, C is a positive generic constant independent of the mesh parameters h and τ, and not necessarily the same at each occurrences.

1.3 A Brief Survey on Numerical Methods

This section presents a brief survey of the relevant literature concerning interface problems and their numerical solutions. Solving interface problems efficiently and accurately is still a challenge because of many irregularities associated with them. Many numerical methods designed for interface problems do not work or work poorly. Thus, the numerical solution to the interface problem is challenging as well as interesting also.

TH-2392_146123010

Interface problems are frequently encountered in scientific computing and many applied sciences. The typical mathematical models are the heat or wave type equations with discontinuous coefficients, which arise when the physical processes involve two or more materials or media with non-identical properties. Owing to its mathematical complexity and essential importance in a number of application areas, the study of interface problems has evolved into a well defined field in applied and computational mathematics. The past few decades have witnessed intensive research activity in interface problems. Finite element method (FEM) is an another class of important approaches for interface problems and a wide variety of FEM approaches have been proposed in the literature. There are two major classes of FEM depending on the choice of the discretization, namely, interface fitted FEMs and unfitted FEMs. In fitted FEMs, the discretization is made in such a way that the grid line is either follow the actual interface or an approximation of the smooth interface. In unfitted FEMs, the discretization is independent of the location of the interface. There are several finite element algorithms in the literature designed for the interface problems. Numerical methods applied for interface problems based on finite element framework can be mainly grouped by conforming FEM, Mixed FEM, Discontinuous Galerkin (DG) and Immersed FEMs. More recently, weak Galerkin (WG) FEMs with polygonal meshes are applied to interface problems. We now present a brief account of the literature concerning the FEMs for interface problems.

To begin with, we first present a brief account of the literature on interface fitted FEMs for the elliptic interface problems. Conforming finite element methods for interface problems are mainly based on the interface fitted discretization. The *a priori* error analysis of elliptic interface problems can be traced back to the work of Babuška in [14]. Since then, elliptic interface problems have attracted extensive effort in the FEM community as well (*e.g.*, [17, 31, 35, 85, 105] and reference therein). In [14], the author has formulated the problem as an equivalent minimization problem and then finite element methods are used to solve the minimization problem. Under some approximation assumptions on finite element spaces, Babuška has obtained sub-optimal order error estimate in H^1 norm. The algorithm in [14] requires the exact evaluation of line integrals on the boundary of the domain and on the interface, and exact integrals on the interface finite elements are also needed. The word "optimal order" refers to the classical terminology in the approximation theory (see, [126]). Then, assuming continuity of both the solution and the normal derivative of the solution along the interface, and fourth order differentiable on each subdomain, Barrett and Elliott in [17] have shown the convergence of finite element solution to the true solution at an optimal rate in both H^1 and

TH-2392_146123010

L^2 norms on each individual subdomain. Under practical regularity assumptions on the true solution, the convergence of finite element method is studied in [31, 35, 85, 105]. The authors of [31] have obtained almost optimal order convergence in both H^1 and L^2 norms. In [105], Nielsen has proved optimal order convergence in the H^1 norm for the elliptic interface problem in the presence of arbitrary small ellipticity. While deriving the estimates, the author has assumed that the interface triangles follow exactly the interface Γ. In practice, the integrals appearing in finite element approximation are evaluated numerically by using some well known quadrature schemes. The effect of the numerical quadrature on the finite element approximation to the exact solution of elliptic interface problem is studied in [35] and has derived optimal order error estimates in L^2 and H^1 norms. The performance of conforming FEMs based on interface fitted discretization depends not only on the quality of underlying finite element partition but also on the variational formulation of the problem. While the flux discontinuity of the solution can be captured in a variational formulation, the discontinuity of the solutions neither fit in the variational formulation nor satisfied in classical FEM solution spaces. Thus, conforming FEMs for interface problems assume continuity of the solutions along interfaces. The discontinuous Galerkin FEMs for interface fitted discretization can be found in [21, 24, 26, 55]. Surprisingly, there has been considerably less work on the mixed finite element methods for interface problems with non-homogeneous jump conditions (see [20, 27, 142]). In fact, convergence analysis of mixed finite element methods for time dependent interface problems is still open. In developing numerical methods for interface problems, higher order of convergence is always one of the major research goals, because high order methods are more accurate and cost efficient. It is challenging to obtain high order convergence when the interface geometries are arbitrarily complex. In [85], the authors provide a complete optimal error analysis of conforming higher order finite element methods of order p for elliptic interface problems with sufficiently smooth interfaces. The focus is especially on the case in which the interface is not resolved exactly but approximated with splines of order m and assuming continuity of the solution along the interface. The material interfaces in real applications can be geometrically complicated and very irregular. In some extreme cases with nonsmooth interfaces or interfaces with Lipschitz continuity, geometric singularities, such as sharp edges, cusps and tips, could be encountered.To achieve a higher order of convergence in the body fitted FEMs, in which unstructured meshes conform to the interfaces, a proper variational formulation that handles jumps in solution and flux is indispensable. By using super parametric elements at the interface, the hybridizable DG method [64] is able to deliver the optimal order of $p+1$ in the L^2 norm for several polynomial orders of p. A weak

TH-2392_146123010

Galerkin (WG) method is introduced in [102] for the elliptic interface problem. The WG method in [102] has many new features including symmetric positive definite formulation, fewer unknowns and, more importantly, allowing the use of general meshes such as hybrid meshes, polygonal and polyhedral meshes and meshes with hanging nodes. These features make the new WG-FEM more flexible in handling complicated interface geometries. Then the author in [37] provides an optimal combination for the polynomial spaces that minimize the number of unknowns in the WG scheme without affecting the accuracy of the numerical approximation. We now turn to the finite element Galerkin approximation to parabolic interface problems. The first contribution in this direction is given by Chen and Zou in [31]. For the backward Euler time discretization, Chen and Zou [31] have studied the convergence of fully discrete solution to the exact solution using fitted finite element methods. They have proved almost optimal error estimates in $L^2(L^2)$ and $L^2(H^1)$ norms. Then optimal order error estimates in the $L^2(H^1)$ and $L^2(L^2)$ norms have derived by Sinha and Deka in [122]. Both the spatially discrete and the fully discrete backward Euler approximations are analyzed. Later, the same authors have extended their work to obtain optimal order convergence in the $L^\infty(L^2)$ and $L^\infty(H^1)$ norms in [45]. Unlike the conforming Galerkin methods which need special treatment for the discontinuity across interface, the local discontinuous Galerkin (LDG) methods provide a natural framework to enforce the discontinuities in both the potential and the flux weakly in the discrete formulation based on fitted mesh (*cf.* [10]). And the LDG scheme for the non-homogeneous interface problem can also be written in the standard discrete formulation provided that we introduce a special choice of numerical fluxes. Theoretical convergence analysis of the LDG method for parabolic interface problems is still open. For other works dealing with parabolic interface problems with non-homogeneous jump conditions, we refer to [43, 124] and references therein. Numerical solutions of wave equation with interfaces via fitted finite element algorithm are carried out in [36, 38, 39]. For homogeneous wave equation with homogeneous jump conditions, optimal error estimates in $L^\infty(L^2)$ and $L^\infty(H^1)$ norms are established for continuous time discretization in Deka and Ahmed [39]. Further, a fully discrete scheme based on a symmetric difference approximation is considered and optimal order convergence in $L^\infty(H^1)$ norm has been established. Recently, for an implicit fully discrete scheme, optimal *a priori* and *a posteriori* error estimates in the $L^\infty(L^2)$ norm have derived in [36, 38].

Many efforts have been made to develop alternative finite element methods based on unfitted meshes for solving interface problems. The numerical solution for elliptic interface problems by means of unfitted finite element methods are investigated by sev-

TH-2392_146123010

eral authors in [17, 46, 57, 61, 82, 83, 88, 98, 123]. The authors of [17] have studied the unfitted finite element method for elliptic interface problem via a related penalized problem and have shown that a weaker result on the convergence holds if the penalty parameter is chosen appropriately. Optimal error estimates in H^1 and L^2 norms, for unfitted finite element discretization, is due to Hansbo *et al.* [57]. The method allows for discontinuities, internal to the elements, in the approximation across the interface. Then the work of Hansbo *et al.* [57] has extended by Massjung in [98] for *hp* version of discontinuous Galerkin method. Massjung [98] proposes and analyzes an unfitted discontinuous Galerkin (DG) method to discretize elliptic interface problems. The method is based on the symmetric interior penalty DG method and follows some ideas from [57]. In the numerical analysis the author has established *hp*-error estimates in the energy and L^2 norms. These estimates are optimal in h and suboptimal in p. Hou *et al.* [61] propose a new formulation and further study of the second order accurate numerical method for elliptic interface problems with general matrix coefficients. The approach relies on the decomposition of the solution into two parts, a singular part and a regular part. The singular part is constructed explicitly in terms of the interface conditions and/or the regular part only locally near the interface. One key advantage of using a weak formulation is that one can avoid assuming/using more regularity than necessary of the solution and the interface. Conforming unfitted FEM is proposed and analysed for linear elliptic interface problems by Sinha and Deka [123]. It has established error estimates of optimal order in the H^1 norm and almost optimal order in the L^2 norm. In the context of unfitted finite element discretizations, the realization of high order methods is challenging due to the fact that the geometry approximation has to be sufficiently accurate. Recently, a high-order unfitted finite element method for elliptic interface problem is introduced by Lehrenfeld *et al.* [82]. The analysis reveals optimal order error bounds in discrete energy norm for arbitrary high-order discretization. Subsequently, L^2 norm error analysis has discussed in [83] for elliptic interface problems. A hybridizable discontinuous Galerkin method present and analyse in [46]. Rigorous error analysis to show that the scheme can achieve a second order convergence rate for the approximation of the solution and its gradient. The work has extended in [23]. The authors propose a new hybrid higher order method to solve elliptic interface problems. The method works with very general unfitted meshes that satisfy a set of regularity conditions. However, in this type of methods, mesh generation and refinement can be a technically demanding and computationally time consuming process. To avoid the complicated mesh generation process, immersed FEMs have been proposed to allow the interface to cut through elements so that simple structured Cartesian meshes can be employed. This renders

TH-2392_146123010

immersed FEMs great popularity in solving a variety of interface problems, such as elliptic interface problem [28, 29, 32, 50, 56, 65, 66, 67, 68, 84, 86, 87, 88, 90, 143] to name only a few. In fact, immersed FEMs can be regarded as the Galerkin formulations of finite difference based interface schemes. It is not surprised that key ideas of many immersed FEMs actually come from the corresponding finite-difference based interface schemes. More recently, a unified work for developing and analyzing a group of immersed finite element spaces that use interface independent meshes, such as highly structured Cartesian meshes, to solve elliptic interface problem is presented in [53]. For higher order immersed finite element methods, we refer to [4, 5]. Discontinuous Galerkin FEM for elliptic interface problem, based on structured Cartesian meshes, is proposed in [19]. Essential boundary conditions are imposed weakly via the DG formulation. This method offers a discretization where the number of unknowns is independent of the complexity of the domain. Convergence rates for different polynomial degrees are studied. Further, combining immersed FEMs and DG methods (DG-IFE) together to solve elliptic interface problems has been proposed in [59, 92]. Subsequently it has been extended to stoke interface problems [2, 3], parabolic interface problems [60, 91, 140], hyperbolic interface problems [6, 7, 73].

1.4 Motivation and Objectives

This section elucidates our contributions and motivation for the present study. In science and engineering, many physical phenomenons can be described by interface problems. Hence, solving interface problems accurately and efficiently is of great importance and has been studied for decades. Due to the inherent complexity of these problems and low global regularity of solutions, the convergence analysis (both *a priori* and *a posteriori* error analysis) of these problems has remained a major part of the mathematical study up to the present day. In the present work, we have used conforming fitted finite element methods to study the convergence of finite element solutions to the exact solutions of some interface problems arising in biological media.

The equation (1.1.1) is numerically interesting as it does not belong to the well-studied classes of time-dependent equations. One of the first finite element methods treating electric interface problem has been studied by Ammari *et al.* in [8]. Well-posedness of the model interface problem and the regularity of its solutions have been established. A fully discrete finite element scheme based on backward Euler discretization has been proposed for the numerical approximation of the potential distribution. Optimal convergence order in both $L^2(H^1)$ and $L^2(L^2)$ norms have been obtained with homogeneous jump conditions. In [8], authors have used fitted finite element discretiza-

TH-2392_146123010

tion. More recently, a fully discrete approximation based on backward Euler scheme is analyzed in [44] for nonhomogeneous jump conditions. Then optimal error estimates are derived in $L^\infty(H^1)$-norm and $L^\infty(L^2)$-norm. As far as we know, the other classes of finite element methods which are developed for interface problems yet to be discussed for the electric interface model. In this thesis, a fitted finite element method is proposed and analyzed for the electric interface model (1.1.1)-(1.1.3). Typical semidiscrete and fully discrete schemes are presented, and analyzed. The fully discrete space-time finite element discretization are based on the Crank-Nicolson approximations. Optimal *a priori* error estimates for both semidiscrete and fully discrete schemes are proved in $L^\infty(H^1)$ and $L^\infty(L^2)$ norms. Numerical solutions of electric interface model (1.1.1)-(1.1.3) draw significant attention in a variety of fields such as neural activation during deep brain simulations [25, 52], debacterization of liquids, food processing [139], biofouling prevention [118], selective spectroscopic imaging of the electrical properties of biological media [9].

The equation (1.1.4) is a mixture of the second order in time wave equation and the first order in time advection equation. When $\sigma = 0$, equation (1.1.4) represents wave equation with interface. Hyperbolic equations with discontinuous coefficients are used in many applications such as ocean acoustics, elasticity and seismology to model the propagation of small disturbances in fluids or solids. In the study of wave equations for some physical problems, such as acoustic or elastic waves traveling through heterogeneous media, there can be discontinuities in the coefficients of the equation (*e.g.*, [36, 39, 78, 134, 141] and references therein). It has long been established that body temperature is an indicator of health. Abnormalities in local body surface temperature have been recognized as a sign of disease for centuries. The modeling of heat related phenomena such as bio heat transfer is of great importance for the development of biomedical technologies, such as thermotherapy in treating diseases like tumor and injury involving skin tissue. Heating to the temperatures higher than that required to treat the diseased tissue can result in inadmissible damage to the adjoining healthy regions and insufficient heating can lead to under-treatment. Numerical study of non-Fourier bio heat model (1.1.4) is especially relevant to the field of thermal medicine, since experimental temperature data is not extensively available. Surprisingly, there has been considerably less work on the finite element methods for interface problems (1.1.4)-(1.1.6), despite the substantial amount of research in the design of finite difference methods for the hyperbolic heat equation with discontinuous coefficients (see, [33, 76, 100, 108, 121, 138] and references therein). The main contribution of the current work is to derive optimal order of convergence in time and space for the finite element

TH-2392_146123010

solution to the BVP (1.1.4)-(1.1.6). More precisely, optimal error estimate is derived in the L^∞-in-time/L^2-in-space norm. The fully discrete scheme can be reinterpreted as the Crank-Nicolson discretization of the reformulation of the governing equation in the first-order system, as in Baker [15]. In fact time discretization method is the well-known Newmark method for wave equation when we adopt the particular choice for the parameters in the Newmark scheme (*cf.* [51, 104]). It is noteworthy that convergence of finite element method based on Newmark scheme for the wave equations with interfaces has not been studied earlier. For the fully discrete method based on Backward Euler scheme, we refer to [36]. Further, current study could provide scope for generalization to the higher order finite element methods for different classes of time dependent interface problems (see, Remak 3.5.1 in Chapter 3). To the best of our knowledge optimal *a priori* error estimates of conforming finite element methods for parabolic interface problems based on Crank-Nicolson scheme is missing. The error bounds discussed in [54] is second order in time and almost optimal order in space in the $L^\infty(L^2)$-norm. The new results and finite element schemes can be applied to solve a wide variety of physical models in the fields of engineering, medicine and biotechnology with non-homogeneous inner structures.

Next, we have made an attempt to extend the convergence analysis to the general linear second order hyperbolic equation (1.1.7) with interfaces. Convergence analysis, without the interface, for the general linear second order hyperbolic equation via finite element algorithm has been well studied in literature (*cf.* [18, 74, 81, 109] just to name a few). More recently, the spatial discretization of Westervelt's quasi-linear strongly damped wave equation by piecewise linear finite elements has been discussed in [107]. *A priori* error analysis in [107] heavily depends on general linear wave model with time dependent coefficients. Optimal convergence in $L^\infty(L^2)$ norm is obtained for sufficiently smooth solution. Fully discrete error analysis is still open for such problems. However, to the best of our knowledge, finite element analysis for the general linear second order hyperbolic equation with discontinuous coefficients has not been studied earlier. In this work, we are providing both mathematical and numerical framework for the study of BVP (1.1.7)-(1.1.9). Well-posedness of the model interface problem and *a priori* estimates of its solutions are established. Optimal *a priori* error estimates for both semidiscrete and fully discrete schemes are proved in $L^\infty(L^2)$ norm. The fully discrete space-time finite element discretizations is based on second order in time Newmark scheme. Our results are intended to enhance the numerical analysis of strongly damped linear wave equations where physical domain consists of heterogenous media.

TH-2392_146123010

1.5 Organization of the thesis

This thesis consists of six chapters, and is organized as follows.

Chapter 1 contains the description of the problems, notations and preliminary materials to be used in the thesis. It also provides a brief survey on the relevant literature concerning the problems and their numerical solutions. Further, motivations for the present study is discussed.

Chapter 2 is devoted to the study of *a priori* error analysis for the electric interface problem (1.1.1)-(1.1.3). Optimal order of convergence in $L^\infty(L^2)$, $H^1(L^2)$ and $L^\infty(H^1)$ norms are established for the semidiscrete solution. We have also studied stability of the semidiscrete solution and derived some estimates which are very crucial for the fully discrete error analysis. A discrete in time scheme based on Crank-Nicolson scheme is considered and analyzed for the fully discrete solution. Optimal *a priori* error estimates in $L^\infty(L^2)$ and $L^\infty(H^1)$ norms are derived for the fully discrete solution. Further, numerical results are discussed to validate our theoretical findings. Results and findings of this Chapter are published in [40, 48].

In Chapter 3, we study *a priori* error analysis for hyperbolic heat conduction model problem (1.1.4)-(1.1.6). We have established some new error estimates for the elliptic projection operator which are crucial for the argument of convergence. Optimal order of convergence in $L^\infty(L^2)$ and $L^\infty(H^1)$ norms are established for the semidiscrete solution. The fully discrete scheme can be interpreted as the well-known Newmark method for wave equation. Optimal order of convergence in $L^\infty(L^2)$ and $L^\infty(H^1)$ norms are established. Finally, numerical results are presented to consolidates our theoretical findings. Results and findings of this Chapter are published in [41, 42].

Chapter 4 presents *a priori* error estimates for the spatially semidiscrete scheme for the Dual-phase-lag (DPL) bio heat model problem (1.1.7)-(1.1.9). Optimal order of convergence in $L^\infty(L^2)$ and $L^\infty(H^1)$ norms are established. The derivation of the *a priori* error bound heavily depends on the approximation properties of a newly introduced non-standard elliptic type projection operator along with some new analytical tools and techniques, including a λ-strip argument for quantifying the relation of error near the interface in terms of the mismatch parameter λ.

In Chapter 5, we extend the spatially discrete *a priori* error analysis to the fully discrete approximation for the Dual-phase-lag (DPL) bio heat model problem (1.1.7)-(1.1.9). The fully discrete scheme discussed is similar to the one in Chapter 3. Optimal *a priori* error estimates in $L^\infty(L^2)$ and $L^\infty(H^1)$ norms are derived for the fully discrete solution. Further, numerical results are presented to validate our theoretical findings.

TH-2392_146123010

Results and findings of Chapter 4 and Chapter 5 are communicated in [47].

Finally in Chapter 6, we discuss the critical evaluation of the results presented in this thesis. This chapter concludes with a brief discussion on the possible extensions and future work.

For clarity of presentation we have repeatedly mentioned the problems and relevant preliminary materials at the beginning of each chapter.

TH-2392_146123010

TH-2392_146123010

2

Convergence of FEMs for Electric Interface Problem

In this chapter, we study *a priori* error estimates for the spatially semidiscrete scheme for the electric interface problem (1.1.1)-(1.1.3). Optimal order of convergence for $L^\infty(L^2)$ and $L^\infty(H^1)$ norms are established when the global regularity of the solution is low on the entire domain. In fact, pointwise-in-time error estimates in L^2 norm error analysis is based on the newly established optimal error estimates for $H^1(L^2)$ norm. We have also established some *a priori* estimates for the semidiscrete solution which are very crucial to prove optimal convergence rate of the fully discrete solution.

2.1 Introduction

To begin with, let us first recall the electric interface interface problem of the form

$$-\nabla \cdot \big(\epsilon \nabla u' + \beta \nabla u\big) = f \ \text{ in } \Omega \times (0,T],\ T < \infty, \tag{2.1.1}$$

with initial and boundary conditions

$$u(x,0) = u_0 \ \text{ in } \Omega; \ \ u(x,t) = 0 \ \ \text{ on } \partial\Omega \times (0,T] \tag{2.1.2}$$

and jump conditions on the interface

$$[u] = 0, \ \ \Big[\epsilon \frac{\partial u'}{\partial \mathbf{n}} + \beta \frac{\partial u}{\partial \mathbf{n}}\Big] = 0 \ \ \text{ along } \Gamma \times (0,T], \tag{2.1.3}$$

where Ω is a bounded domain in $\mathbb{R}^d (d = 2,\ 3)$ with Lipschitz boundary $\partial\Omega$ and $\Omega_1 \subset \Omega$ is an open domain with C^2 smooth boundary $\Gamma = \partial\Omega_1$ and $\Omega_2 = \Omega \backslash \Omega_1$. Other symbols are as defined in Chapter 1. We assume that the physical coefficients are discontinuous

Published online in *Appl. Anal., doi.org/10.1080/00036811.2019.1643010 and Math. Methods Appl. Sci., 43 (2020), 4598-4613*

TH-2392_146123010

along interface Γ and piecewise positive constants. We write

$$(\epsilon, \beta) = \begin{cases} (\epsilon_1, \beta_1) & \text{in } \Omega_1, \\ (\epsilon_2, \beta_2) & \text{in } \Omega_2. \end{cases}$$

Further, initial data u_0 and source f are real valued functions in Ω, and assumed to be sufficiently smooth.

Well-posedness of the model interface problem and the regularity of its solutions have been established by Ammari *et al.* in [8]. In [8], authors have used fitted finite element discretization with homogeneous jump conditions. Optimal order of convergence in both $L^2(H^1)$ and $L^2(L^2)$ norms have been derived for semidiscrete and fully discrete schemes. Fully discrete scheme is based on backward Euler time discretization. More recently, a fully discrete approximation based on backward Euler scheme is analyzed in [44] for nonhomogeneous jump conditions. Then optimal error estimates are derived in $L^\infty(H^1)$ and $L^\infty(L^2)$ norms for weak Galerkin method. In this chapter, a fitted finite element method is proposed and analyzed for the electric interface model (2.1.1)-(2.1.3). Optimal *a priori* error estimates for semidiscrete solution are proved in both $L^\infty(H^1)$ and $L^\infty(L^2)$ norms. In fact, $L^\infty(L^2)$ norm error analysis is based on a newly established optimal error estimates for $H^1(L^2)$ norm (see, Theorem 2.3.2). A fully discrete finite element approximation based on Crank-Nicolson scheme is proposed and have derived optimal error estimates for the fully discrete solution in both $L^\infty(H^1)$ and $L^\infty(L^2)$ norms. The achieved estimates are analogous to the error estimates for parabolic interface problems (*cf.* [45]). It is worth to note that equation (2.1.1) does not belong to the well-studied classes of parabolic problems. Present analysis provides a scope for the generalization of these works to higher order finite element methods by combining the theory in this work with the analysis in [85].

The rest of this chapter is organized as follows: Section 2.2 introduces the existence, uniqueness and regularity of the weak solution. Further, we recall some basic approximation properties associated with the finite element spaces. Optimal *a priori* error estimates for the semidiscrete solution are derived in Section 2.3. In Section 2.4, Crank-Nicolson scheme is described along with *a priori* error bounds in $L^\infty(H^1)$ and $L^\infty(L^2)$ norms. Finally, numerical results are presented in Section 2.5.

Throughout this chapter, C is a positive generic constant independent of the mesh parameters h and τ, and not necessarily the same at each occurrences.

TH-2392_146123010

2.2 Preliminaries and Auxiliary Results

In this section, well-posedness of the model interface problem (2.1.1)-(2.1.3) and the regularity of its solutions are discussed. Further, we recall some basic approximation properties associated with some auxiliary projections.

The weak formulation of the interface problem (2.1.1)-(2.1.3) is stated as follows: Find $u \in H^1(0,T;H_0^1(\Omega))$ such that

$$\mathcal{A}_\epsilon(u',v) + \mathcal{A}_\beta(u,v) = (f,v) \quad \forall v \in H_0^1(\Omega). \tag{2.2.1}$$

Operators $\mathcal{A}_\epsilon$ and $\mathcal{A}_\beta$ are as discussed in Chapter 1.

Due to the presence of discontinuous coefficients the solution u, in general, does not belong to $H^2(\Omega)$. But one can expect higher local regularity of the solution when the coefficients are more smooth locally (*cf.* [8]). Concerning the problem (2.1.1)-(2.1.3), we have the following regularity result. For a proof, we refer to Ammari *et al.* [8].

Theorem 2.2.1. *Let $f \in L^2(J;L^2(\Omega))$ and $u_0 \in \mathcal{Y}$. Then the problem (2.1.1)-(2.1.3) has a unique solution $u \in H^1(J;\mathcal{Y})$ and u satisfies a priori estimate*

$$\|u\|_{H^1(J;\mathcal{Y})} \leq C\left(\|f\|_{L^2(J;L^2(\Omega))} + \|u_0\|_{\mathcal{Y}}\right).$$

Let $\mathcal{T}_h$ be the fitted triangulation of Ω as described in Chapter 1. Let $V_h \subset H_0^1(\Omega)$ be the finite element space, based on the triangulation $\mathcal{T}_h$, consisting of piecewise linear functions vanishing on the boundary $\partial\Omega$. Now, we recall following approximated bilinear maps $\mathcal{A}_{\epsilon h}(\cdot,\cdot)$ and $\mathcal{A}_{\beta h}(\cdot,\cdot)$ defined as

$$\mathcal{A}_{\epsilon h}(w,v) = \sum_{K\in\mathcal{T}_h}\int_K \epsilon_K(x)\nabla w\cdot\nabla v dx \quad \forall w,v \in H^1(\Omega) \tag{2.2.2}$$

$$\mathcal{A}_{\beta h}(w,v) = \sum_{K\in\mathcal{T}_h}\int_K \beta_K(x)\nabla w\cdot\nabla v dx \quad \forall w,v \in H^1(\Omega), \tag{2.2.3}$$

with $\epsilon_K(x) = \epsilon_i$ and $\beta_K(x) = \beta_i$ if $K \subset \Omega_{i,h}$, $i = 1,2$.

To derive optimal error bounds, we introduce the elliptic projection operators $\mathcal{Q}_h^i : \mathcal{Y} \to V_h$, $i = 1, 2$. For each $v \in \mathcal{Y}$, let $f_1^* = -\beta_i\Delta v_i$ in Ω_i, $i = 1,2$ and $g_1^* = \left[\beta\frac{\partial v}{\partial \mathbf{n}}\right]$. Clearly, $f_1^* \in L^2(\Omega)$ and $g_1^* \in L^2(\Gamma)$. With this f_1^* and g_1^*, we define $\mathcal{Q}_h^1 : \mathcal{Y} \to V_h$ by

$$\mathcal{A}_{\beta h}(\mathcal{Q}_h^1 v, v_h) = (f_1^*, v_h) + \langle g_1^*, v_h\rangle \quad \forall v_h \in V_h,$$

where $\langle\cdot,\cdot\rangle$ denotes the scaler product in $L^2(\Gamma)$.

In a similar way, we define our second elliptic projection operator $\mathcal{Q}_h^2 : \mathcal{Y} \to V_h$ by

$$\mathcal{A}_{\epsilon h}(\mathcal{Q}_h^2 v, v_h) = (f_2^*, v_h) + \langle g_2^*, v_h\rangle \ \forall v_h \in V_h,$$

TH-2392_146123010

where $f_2^* = -\epsilon_i \Delta u_i,\ i = 1,\ 2$ and $g_2^* = \left[\epsilon \frac{\partial u}{\partial \mathbf{n}}\right]$.

By the definitions of the projection operators, it is easy to notice that

$$\mathcal{A}_{\beta h}(\mathcal{Q}_h^1 v, v_h) = \mathcal{A}_\beta(v, v_h)\ \forall v_h \in V_h,\ v \in \mathcal{Y}\ \& \tag{2.2.4}$$

$$\mathcal{A}_{\epsilon h}(\mathcal{Q}_h^2 v, v_h) = \mathcal{A}_\epsilon(v, v_h)\ \forall v_h \in V_h,\ v \in \mathcal{Y}, \tag{2.2.5}$$

and hence, using the coercivity and continuity of the bilinear forms, we obtain

$$\|\mathcal{Q}_h^i v\|_1 \leq \|v\|_1\ \forall v \in \mathcal{Y},\ i = 1,\ 2. \tag{2.2.6}$$

To simplify the notation, in the future, we will not distinguish between $\mathcal{Q}_h^1$ and $\mathcal{Q}_h^2$, and we write $\mathcal{Q}_h$ for $\mathcal{Q}_h^1$ or $\mathcal{Q}_h^2$. Regarding the approximation properties of the elliptic projection operator defined in ((2.2.4)(or (2.2.5)), we have the following approximation result.

Lemma 2.2.1. *Let $\mathcal{Q}_h$ be defined by (2.2.4)(or (2.2.5)), then for any $v \in \mathcal{Y}$ there is a positive constant C such that (cf. [45, 85])*

$$\|v - \mathcal{Q}_h v\| + h\|v - \mathcal{Q}_h v\|_1 \leq Ch^2 \|v\|_{\mathcal{Y}}.$$

Remark 2.2.1. *The newly defined projection operator $\mathcal{Q}_h$ is very important for our later analysis. In Section 2.4, we will see that it enables us to establish optimal $H^1(L^2)$-norm a priori error estimates and generalize the results of [8]. The regularity assumptions for the solutions are as in [8].*

2.3 Spatially Semidiscrete Error Analysis

This section deals with the pointwise-in-time error analysis for the spatially discrete scheme. First we derive stability results for the semidiscrete solution at the initial stage. Optimal order of convergence for $L^\infty(L^2)$ and $L^\infty(H^1)$ norms are established when the global regularity of the solution is low on the entire domain. In fact, $L^\infty(L^2)$ norm error analysis is based on the newly established optimal error estimates for $H^1(L^2)$ norm.

The continuous time Galerkin finite element approximation to (2.2.1) is stated as follows: Find $u_h : [0, T] \to V_h$ such that

$$\mathcal{A}_{\epsilon h}(u_h'(t), v_h) + \mathcal{A}_{\beta h}(u_h(t), v_h) = (f, v_h)\ \forall v_h \in V_h \tag{2.3.1}$$

with $u_h(0) = \mathcal{Q}_h^1 u_0$.

Choose $v_h = u_h'$ in (2.3.1) to have

$$\mathcal{A}_{\epsilon h}(u_h', u_h') = (f, u_h') - \mathcal{A}_{\beta h}(u_h, u_h'). \tag{2.3.2}$$

TH-2392_146123010

Letting $t \to 0$ and coercivity of $\mathcal{A}_{\epsilon h}$ along with Cauchy-Schwartz inequality on the right hand side yields

$$\begin{aligned} \|u_h'(0)\|_1^2 &\leq C(\|f(0)\|\|u_h'(0)\| + \|u_h(0)\|_1\|u_h'(0)\|_1) \\ &\leq C(\|f\|_{H^1(J;L^2(\Omega))}\|u_h'(0)\| + \|u_h(0)\|_1\|u_h'(0)\|_1). \end{aligned} \tag{2.3.3}$$

In the previous inequality, we have used the fact that

$$\sup_{0\leq t\leq T} \|f(t)\| \leq C\|f\|_{H^1(J;L^2(\Omega))}.$$

In fact, for any Banach space $\mathcal{B}$, we know that (*cf.* [116], Proposition 7.1)

$$\sup_{0\leq t\leq T} \|v(t)\|_{\mathcal{B}} \leq C\|v\|_{H^1(J;\mathcal{B})} \quad \forall v \in H^1(J;\mathcal{B}). \tag{2.3.4}$$

For suitable $\mu > 0$, we apply Young's inequality in (2.3.3) to obtain

$$\|u_h'(0)\|_1^2 \leq C(\mu)(\|f\|^2_{H^1(J;L^2(\Omega))} + \|\mathcal{Q}_h u_0\|_1^2) + \mu\|u_h'(0)\|_1^2.$$

Setting $\mu > 0$ appropriately so that $1 - \mu > 0$ and use estimate (2.2.6) to obtain

$$\|u_h'(0)\|_1 \leq C(\|f\|_{H^1(J;L^2(\Omega))} + \|u_0\|_1). \tag{2.3.5}$$

Proceeding in a similar fashion and using (2.3.4), we obtain following stability result at initial stage and therefore the proof is omitted.

Lemma 2.3.1. *Let u_h be the solution of (2.3.1). Then, for $f \in H^i(J;L^2(\Omega))$, we have*

$$\|u_h^{(i)}(0)\|_1 \leq C(\|f\|_{H^i(J;L^2(\Omega))} + \|u_0\|_1), \quad i = 1,2,3,$$

where $u_h^{(i)}(0) = \partial^i u_h(t)/\partial t^i\Big|_{t=0}$.

Further, choosing $v_h = u_h$ in (2.3.1) and then integrating the resultant from 0 to t, we obtain

$$\begin{aligned} &\frac{1}{2}\mathcal{A}_{\epsilon h}(u_h(t),u_h(t)) + \int_0^t \mathcal{A}_{\beta h}(u_h(s),u_h(s))ds \\ &= \frac{1}{2}\mathcal{A}_{\epsilon h}(u_h(0),u_h(0)) + \int_0^t (f(s),u_h(s))ds, \end{aligned}$$

which, together with (2.2.6), leads to

$$\begin{aligned} \|u_h(t)\|_1^2 + \int_0^t \|u_h(s)\|_1^2 ds &\leq C\Big(\|u_h(0)\|_1^2 + \int_0^t \|f(s)\|^2 ds\Big) \\ &\leq C\Big(\|u_0\|_1^2 + \|f\|^2_{L^2(0,t;L^2(\Omega))}\Big). \end{aligned} \tag{2.3.6}$$

TH-2392_146123010

Now, differentiate (2.3.1) with respect to t and choose $v_h = u_h'$ in the resulting equation to have

$$\frac{1}{2}\frac{d}{dt}\mathcal{A}_{\epsilon h}(u_h', u_h') + \mathcal{A}_{\beta h}(u_h', u_h') = (f', u_h').$$

Now, integrate above relation in $[0, t]$ and use standard arguments to have

$$\begin{aligned}\|u_h'(t)\|_1^2 + \int_0^t \|u_h'(s)\|_1^2 ds &\leq C\Big(\|u_h'(0)\|_1^2 + \int_0^t \|f'(s)\|^2 ds\Big) \\ &\leq C\Big(\|u_0\|_1^2 + \|f\|^2_{H^1(0,t;L^2(\Omega))}\Big). \end{aligned} \tag{2.3.7}$$

In the last inequality, we have used Lemma 2.3.1.

For higher order derivatives, we differentiate (2.3.1) twice with respect to t and choose $v_h = u_h''$ in the resulting equation to have

$$\frac{1}{2}\frac{d}{dt}\mathcal{A}_{\epsilon h}(u_h'', u_h'') + \mathcal{A}_{\beta h}(u_h'', u_h'') = (f'', u_h'')$$

Integrating from 0 to t, we have

$$\begin{aligned}\frac{1}{2}\mathcal{A}_{\epsilon h}(u_h''(t), u_h''(t)) + \int_0^t \mathcal{A}_{\beta h}(u_h''(s), u_h''(s))ds &= \frac{1}{2}\mathcal{A}_{\epsilon h}(u_h''(0), u_h''(0)) \\ &+ \int_0^t (f''(s), u_h''(s))ds.\end{aligned}$$

Now, standard arguments lead to

$$\|u_h''(t)\|_1^2 + \int_0^t \|u_h''(s)\|_1^2 ds \leq C\Big(\|u_h''(0)\|_1^2 + \int_0^t \|f''(s)\|^2 ds\Big).$$

This together with Lemma 2.3.1 leads to

$$\|u_h''(t)\|_1^2 + \int_0^t \|u_h''(s)\|_1^2 ds \leq C\Big(\|u_0\|_1^2 + \|f\|^2_{H^2(0,t;L^2(\Omega))}\Big). \tag{2.3.8}$$

Combining the estimates (2.3.6)-(2.3.8), we have the following stability results for the semidiscrete solution u_h satisfying equation (2.3.1).

Lemma 2.3.2. *Let u_h be the solution of (2.3.1). Then, for $f \in H^i(J; L^2(\Omega))$ $(i = 0, 1, 2, 3)$, we have*

$$\|u_h^{(i)}(t)\|_1^2 + \int_0^t \|u_h^{(i)}(s)\|_1^2 ds \leq C\Big(\|u_0\|_1^2 + \|f\|^2_{H^i(0,t;L^2(\Omega))}\Big),$$

where $u_h^{(i)}(t) = \partial^i u_h(t)/\partial t^i$.

TH-2392_146123010

Define the error $e(t)$ as $e(t) = u(t) - u_h(t)$ and further splitting $e(t)$ into standard ρ and θ arguments, we obtain

$$e(t) = u(t) - u_h(t) = \rho(t) + \theta(t), \tag{2.3.9}$$

where $\rho(t) = u(t) - \mathcal{Q}_h^2 u(t)$ and $\theta(t) = \mathcal{Q}_h^2 u(t) - u_h(t)$. From Lemma 2.2.1, we already have a bound for $\rho(t)$. So, we only need to estimate $\theta(t)$.

Subtracting (2.3.1) from the weak formulation (2.2.1) and using the definition (2.2.5) of projection operator $\mathcal{Q}_h^2$, it is easy to verify that $\theta(t)$ satisfy the following error equation

$$\begin{aligned} \mathcal{A}_{\epsilon h}(\theta'(t), v_h) + \mathcal{A}_{\beta h}(\theta(t), v_h) &= \mathcal{A}_{\epsilon h}(\rho'(t), v_h) + \mathcal{A}_{\beta h}(\rho(t), v_h) - \mathcal{A}^{\Delta}_{\epsilon h}(u'(t), v_h) \\ &\quad - \mathcal{A}^{\Delta}_{\beta h}(u(t), v_h) \ \ \forall\, v_h \in V_h. \end{aligned} \tag{2.3.10}$$

Set $v_h = \theta(t)$ in (2.3.10) and then integrate the resulting equation from 0 to t to obtain

$$\begin{aligned} \|\theta(t)\|_1^2 + \int_0^t \|\theta(s)\|_1^2 ds &\leq C \int_0^t |\mathcal{A}_{\epsilon h}(\rho'(s), \theta(s)) + \mathcal{A}_{\beta h}(\rho(s), \theta(s))| ds \\ &\quad + C \int_0^t |\mathcal{A}^{\Delta}_{\epsilon h}(u'(s), \theta(s)) + \mathcal{A}^{\Delta}_{\beta h}(u(s), \theta(s))| ds \\ &\quad + C\|\theta(0)\|_1^2 \\ &:= I_1 + I_2 + I_3. \end{aligned} \tag{2.3.11}$$

For I_1, apply continuity of $\mathcal{A}_{\epsilon h}$ and $\mathcal{A}_{\beta h}$ to have

$$\begin{aligned} I_1 &\leq C \int_0^t \|\rho'(s)\|_1 \|\theta(s)\|_1 ds + C \int_0^t \|\rho(s)\|_1 \|\theta(s)\|_1 ds \\ &\leq C(\mu) \int_0^t \left\{ \|\rho'(s)\|_1^2 + \|\rho(s)\|_1^2 \right\} ds + C_\mu \int_0^t \|\theta(s)\|_1^2 ds. \end{aligned}$$

In the last inequality we used the Young's inequality for some $\mu > 0$. Then apply Lemma 2.2.1 to obtain

$$I_1 \leq C(\mu) h^2 \|u\|^2_{H^1(J;\mathcal{Y})} + C_\mu \int_0^t \|\theta(s)\|_1^2 ds. \tag{2.3.12}$$

To estimate I_2, we apply Lemma 1.2.2 and Lemma 1.2.4 to have

$$I_2 \leq C \int_0^t \{|u(s)|_{1,S_\lambda} + |u'(s)|_{1,S_\lambda}\} \sqrt{\frac{\lambda}{h}} \|\theta(s)\|_1 ds.$$

Now, using Young's inequality and then apply Lemma 1.2.3 to obtain

$$I_2 \leq C(\mu) \frac{\lambda^2}{h} \|u\|^2_{H^1(J;\mathcal{Y})} + C(\mu) \int_0^t \|\theta(s)\|_1^2 ds. \tag{2.3.13}$$

TH-2392_146123010

Combining estimates (2.3.11)-(2.3.13), it now leads to

$$\int_0^t \|\theta(s)\|_1^2 ds + \|\theta(t)\|_1^2 \leq C\|\theta(0)\|_1^2 + C\left(h^2 + \frac{\lambda^2}{h}\right)\|u\|^2_{H^1(J;\mathcal{Y})} + C\int_0^t \|\theta(s)\|_1^2 ds.$$

Finally, an application of Lemma 2.2.1 and regularity result Theorem 2.2.1, and the fact that $\lambda \in \mathrm{O}(h^2)$ and $\|\theta(0)\| \in \mathrm{O}(h^2)$ leads to the following optimal H^1-norm error estimate.

Theorem 2.3.1. *Let u and u_h be the solutions to the problem (2.2.1) and (2.3.1), respectively. Then, for $u_0 \in \mathcal{Y}$ and $f \in L^2(J; L^2(\Omega))$, we have*

$$\|u - u_h\|_{L^\infty(J;H^1(\Omega))} \leq Ch(\|f\|_{L^2(J;L^2(\Omega))} + \|u_0\|_{\mathcal{Y}}).$$

Now, before proving the $L^\infty(L^2)$-norm error estimate, we shall prove an optimal $H^1(L^2)$-norm error estimate. The basic technique used here is analogous to the technique used in [8].

Theorem 2.3.2. *Under the assumptions of Theorem 2.3.1, we have the following estimate*

$$\|u - u_h\|_{H^1(J;L^2(\Omega))} \leq Ch^2(\|f\|_{L^2(J;L^2(\Omega))} + \|u_0\|_{\mathcal{Y}}).$$

Proof. We use parabolic duality argument. We define $w \in H^1(J; \mathcal{Y})$ and $w_h \in H^1(J; V_h)$ such that for *a.e.* $t \in J$

$$\mathcal{A}_\beta(w(t), v) - \mathcal{A}_\epsilon(w'(t), v) = (u'(t) - u_h'(t), v) \ \ \forall v \in H_0^1(\Omega), \tag{2.3.14}$$

$$\mathcal{A}_\beta(w_h(t), v_h) - \mathcal{A}_\epsilon(w_h'(t), v_h) = (u'(t) - u_h'(t), v_h) \ \ \forall v_h \in V_h, \tag{2.3.15}$$

with $w(T) = w_h(T) = 0$. Then $\tilde{w}(t) = w(T - t)$ is the weak solution of (2.1.1)-(2.1.3) with initial value $\tilde{w}(0) = 0$ and $f(t) = u'(t) - u_h'(t)$. Then Theorem 2.2.1 implies that

$$\|w\|_{H^1(J;\mathcal{Y})} \leq C\|u' - u_h'\|_{L^2(J;L^2(\Omega))}. \tag{2.3.16}$$

TH-2392_146123010

Now, we have

$$\begin{aligned}
&\|w - w_h\|^2_{H^1(J;H^1(\Omega))} \\
&= \int_0^T \|w(t) - w_h(t)\|_1^2 dt + \int_0^T \|w'(t) - w_h'(t)\|_1^2 dt \\
&\leq \int_0^T \Big(\|w - \mathcal{Q}_h w\|_1^2 + \|\mathcal{Q}_h w - w_h\|_1^2\Big) dt \\
&+ \int_0^T \Big(\|w' - \mathcal{Q}_h w'\|_1^2 + \|\mathcal{Q}_h w' - w_h'\|_1^2\Big) dt \\
&= \int_0^T \Big(\|w - \mathcal{Q}_h w\|_1^2 + \|w' - \mathcal{Q}_h w'\|_1^2\Big) dt \\
&+ \int_0^T \Big(\|\mathcal{Q}_h w - w_h\|_1^2 + \|\mathcal{Q}_h w' - w_h'\|_1^2\Big) dt \\
&= I_4 + I_5. \qquad (2.3.17)
\end{aligned}$$

Using Lemma 2.2.1 and (2.3.16), we obtain

$$I_4 \leq Ch^2 \|w\|^2_{H^1(J;\mathcal{Y})} \leq Ch^2 \|u' - u_h'\|^2_{L^2(J;L^2(\Omega))}. \qquad (2.3.18)$$

Subtracting (2.3.14) from (2.3.15) and setting $\tilde{w} = w_h - \mathcal{Q}_h w$, we obtain

$$\mathcal{A}_\beta(\tilde{w}(t), v_h) - \mathcal{A}_\epsilon(\tilde{w}'(t), v_h) = \langle F(t), v_h \rangle_{H^{-1}(\Omega)\times H_0^1(\Omega)},$$

where $F(t) \in H^{-1}(\Omega)$ for $t \in J$ defined by

$$\begin{aligned}
\langle F(t), v \rangle_{H^{-1}(\Omega)\times H_0^1(\Omega)} &= \mathcal{A}_\beta(w(t) - \mathcal{Q}_h w(t), v) \\
&\quad - \mathcal{A}_\epsilon(w'(t) - \mathcal{Q}_h w'(t), v) \quad \forall v \in H_0^1(\Omega).
\end{aligned}$$

Then, using Theorem 3.1 of [8], we obtain

$$\|\tilde{w}\|_{H^1(J;H^1(\Omega))} \leq C \|F(t)\|_{L^2(J;H^{-1}(\Omega))}.$$

Now,

$$\langle F(t), v \rangle_{H^{-1}(\Omega)\times H_0^1(\Omega)} \leq C\Big(\|w - \mathcal{Q}_h w\|_1 \|v\|_1 + \|w' - \mathcal{Q}_h w'\|_1 \|v\|_1\Big).$$

Using Lemma 2.2.1, we have

$$\|F(t)\|_{L^2(J;H^{-1}(\Omega))} \leq Ch \|w\|_{H^1(J;\mathcal{Y})}.$$

Hence,

$$\begin{aligned}
I_5 = \|\tilde{w}\|^2_{H^1(J;H^1(\Omega))} &\leq Ch^2 \|w\|^2_{H^1(J;\mathcal{Y})} \\
&\leq Ch^2 \|u' - u_h'\|^2_{L^2(J;L^2(\Omega))}. \qquad (2.3.19)
\end{aligned}$$

TH-2392_146123010

Using estimates (2.3.18)-(2.3.19) in (2.3.17), we obtain

$$\|w - w_h\|_{H^1(J;H^1(\Omega))} \leq Ch\|u' - u_h'\|_{L^2(J;L^2(\Omega))}. \tag{2.3.20}$$

Next, we set $v = u'(t) - u_h'(t)$ in (2.3.14) to get

$$\begin{aligned}\|u'(t) - u_h'(t)\|^2 &= \mathcal{A}_\beta(u'(t) - \mathcal{Q}_h^1 u'(t), w(t) - w_h(t)) \\ &\quad -\mathcal{A}_\epsilon(u'(t) - \mathcal{Q}_h^1 u'(t), w'(t) - w_h'(t)) \\ &\quad +\mathcal{A}_\beta(w_h(t), u'(t) - u_h'(t)) - \mathcal{A}_\epsilon(w_h'(t), u'(t) - u_h'(t)) \\ &\quad +\mathcal{A}_\beta(\mathcal{Q}_h^1 u'(t) - u_h'(t), w(t) - w_h(t)) \\ &\quad -\mathcal{A}_\epsilon(\mathcal{Q}_h^1 u'(t) - u_h'(t), w'(t) - w_h'(t)).\end{aligned} \tag{2.3.21}$$

Now, subtract (2.3.15) from (2.3.14) and then set $v_h = \mathcal{Q}_h^1 u'(t) - u_h'(t)$ to obtain

$$\mathcal{A}_\beta(w - w_h, \mathcal{Q}_h^1 u' - u_h') - \mathcal{A}_\epsilon(w' - w_h', \mathcal{Q}_h^1 u' - u_h') = 0. \tag{2.3.22}$$

Using (2.3.22) in (2.3.21) and then integrating the resultant from 0 to T, we have

$$\begin{aligned}\int_0^T \|u'(t) - u_h'(t)\|^2 dt &= \int_0^T \Big\{\mathcal{A}_\beta(u'(t) - \mathcal{Q}_h^1 u'(t), w(t) - w_h(t)) \\ &\quad -\mathcal{A}_\epsilon(u'(t) - \mathcal{Q}_h^1 u'(t), w'(t) - w_h'(t))\Big\} dt \\ &\quad + \int_0^T \Big\{\mathcal{A}_\beta(w_h(t), u'(t) - u_h'(t)) \\ &\quad -\mathcal{A}_\epsilon(w_h'(t), u'(t) - u_h'(t))\Big\} dt \\ &:= J_1 + J_2.\end{aligned} \tag{2.3.23}$$

For J_1, we have

$$\begin{aligned}J_1 &\leq C\|u - \mathcal{Q}_h^1 u\|_{H^1(J;H^1(\Omega))}\|w - w_h\|_{H^1(J;H^1(\Omega))} \\ &\leq Ch^2\|u\|_{H^1(J;\mathcal{Y})}\|u' - u_h'\|_{L^2(J;L^2(\Omega))}.\end{aligned} \tag{2.3.24}$$

In the last inequality, we have used (2.3.20) and Lemma 2.2.1.

To estimate J_2, we first observe that

$$\begin{aligned}\int_0^T \mathcal{A}_\beta(w_h(t), u'(t) - u_h'(t)) dt &= -\mathcal{A}_\beta(w_h(0), u(0) - u_h(0)) \\ &\quad - \int_0^T \mathcal{A}_\beta(w_h'(t), u(t) - u_h(t)) dt\end{aligned} \tag{2.3.25}$$

and

$$\begin{aligned}&\mathcal{A}_\beta(w_h'(t), u(t) - u_h(t)) + \mathcal{A}_\epsilon(w_h'(t), u'(t) - u_h'(t)) \\ &= \mathcal{A}_{\beta h}^\Delta(u_h(t), w_h'(t)) + \mathcal{A}_{\epsilon h}^\Delta(u_h'(t), w_h'(t)).\end{aligned} \tag{2.3.26}$$

TH-2392_146123010

Above relation is a consequence of (2.2.1) and (2.3.1). Now, combine (2.3.25)-(2.3.26) to have

$$\begin{aligned} J_2 &= \int_0^T \Big\{\mathcal{A}^{\Delta}_{\beta h}(u_h(t), w_h'(t)) + \mathcal{A}^{\Delta}_{\epsilon h}(u_h'(t), w_h'(t))\Big\}dt \\ &\quad -\mathcal{A}_{\beta}(w_h(0), u_0 - \mathcal{Q}_h^1 u_0) \\ &= \int_0^T \Big\{\mathcal{A}^{\Delta}_{\beta h}(u_h(t), w_h'(t)) + \mathcal{A}^{\Delta}_{\epsilon h}(u_h'(t), w_h'(t))\Big\}dt \\ &\quad +\{\mathcal{A}_{\beta}(w_h(0), \mathcal{Q}_h^1 u_0) - \mathcal{A}_{\beta h}(w_h(0), \mathcal{Q}_h^1 u_0)\} \\ &:= T_1 + T_2. \end{aligned} \tag{2.3.27}$$

Here, we have used the definition (2.2.4) of the projection operator Q_h^1. We estimate T_1 and T_2 separately. For T_1, use Lemma 1.2.2 and Cauchy-Schwartz inequality to obtain

$$T_1 \leq C|u_h|_{H^1(J;H^1(S_\lambda))}|w_h|_{H^1(J;H^1(S_\lambda))}. \tag{2.3.28}$$

Applying Lemma 1.2.3 and Theorem 4.1 in [8], we have

$$\begin{aligned} |u_h|_{H^1(J;H^1(S_\lambda))} &\leq |u_h - u|_{H^1(J;H^1(S_\lambda))} + |u|_{H^1(J;H^1(S_\lambda))} \\ &\leq C\Big(\|u_h - u\|_{H^1(J;H^1(S_\lambda))} + \sqrt{\lambda}\|u\|_{H^1(J;\mathcal{Y})}\Big) \\ &\leq C\Big(h\|u\|_{H^1(J;\mathcal{Y})} + \sqrt{\lambda}\|u\|_{H^1(J;\mathcal{Y})}\Big) \\ &\leq C(h + \sqrt{\lambda})\|u\|_{H^1(J;\mathcal{Y})}. \end{aligned}$$

Using Lemma 1.2.3 and estimates (2.3.16)-(2.3.20), we have

$$|w_h|_{H^1(J;H^1(S_\lambda))} \leq C(h + \sqrt{\lambda})\|u' - u_h'\|_{L^2(J;L^2(\Omega))}.$$

Use above estimates in (2.3.28) to have

$$T_1 \leq C(\lambda + h\sqrt{\lambda})\|u\|_{H^1(J;\mathcal{Y})}\|u' - u_h'\|_{L^2(J;L^2(\Omega))}. \tag{2.3.29}$$

Finally, for the term T_2 use Lemma 2.2.1 and Lemma 1.2.2 to have

$$T_2 \leq C|w_h(0)|_{1,S_\lambda}|\mathcal{Q}_h^1 u(0)|_{1,S_\lambda}. \tag{2.3.30}$$

Simple use of Lemma 2.2.1 and Lemma 1.2.3 yields

$$\begin{aligned} |\mathcal{Q}_h^1 u_0|_{1,S_\lambda} &\leq |\mathcal{Q}_h^1 u_0 - u_0|_{1,S_\lambda} + |u_0|_{1,S_\lambda} \\ &\leq C(\sqrt{\lambda} + h)\|u_0\|_{\mathcal{Y}} \end{aligned}$$

TH-2392_146123010

On the other hand, using estimate (2.3.4), triangle inequality and Lemma 1.2.3, we obtain

$$\begin{aligned}|w_h(0)|_{1,S_\lambda} \leq \sup_{0\leq t\leq T}\|w_h(t)\|_{1,S_\lambda} &\leq C\|w_h\|_{H^1(J;H^1(S_\lambda))}\\ &\leq C\|w_h-w\|_{H^1(J;H^1(\Omega))}+C\|w\|_{H^1(J;H^1(S_\lambda))}\\ &\leq C(h+\sqrt{\lambda})\|w\|_{H^1(J;\mathcal{Y})}\\ &\leq C(h+\sqrt{\lambda})\|u'-u_h'\|_{L^2(J;L^2(\Omega))}.\end{aligned}$$

In the last inequality, we have used (2.3.16). Using the above estimates in (2.3.30), we have

$$T_2 \leq C(\lambda+h^2)\|u_0\|_{\mathcal{Y}}\|u'-u_h'\|_{L^2(J;L^2(\Omega))}.$$

This together with (2.3.29) yields

$$J_2 \leq C(\lambda+h^2)(\|u\|_{H^1(J;\mathcal{Y})}+\|u_0\|_{\mathcal{Y}})\|u'-u_h'\|_{L^2(J;L^2(\Omega))}. \tag{2.3.31}$$

Summarizing the estimates (2.3.23), (2.3.24) and (2.3.31), we obtain

$$\begin{aligned}\|u'-u_h'\|_{L^2(J;L^2(\Omega))} &\leq C(\lambda+h^2)(\|u\|_{H^1(J;\mathcal{Y})}+\|u_0\|_{\mathcal{Y}})\\ &\leq Ch^2(\|f\|_{L^2(J;L^2(\Omega))}+\|u_0\|_{\mathcal{Y}}).\end{aligned} \tag{2.3.32}$$

In the last inequality, we have used the fact that $\lambda = \mathrm{O}(h^2)$ and Theorem 2.2.1. Finally Theorem 4.2 in [8] leads to the desired result. □

Remark 2.3.1. *In Theorem 2.3.2, we have assumed $u_h(0) = \mathcal{Q}_h^1 u_0$ for our convenience. Optimal error bounds in Theorem 2.3.2 can also be easily established for the other choice $u_h(0) = \mathcal{Q}_h^2 u_0$.*

Now, we are in a position to derive the $L^\infty(L^2)$-norm error estimate for the semidiscrete scheme in the following theorem.

Theorem 2.3.3. *Under the assumptions of Theorem 2.3.1, we have*

$$\|u-u_h\|_{L^\infty(J;L^2(\Omega))} \leq Ch^2(\|f\|_{L^2(J;L^2(\Omega))}+\|u_0\|_{\mathcal{Y}}).$$

Proof. Similar to Theorem 2.3.2, we use parabolic duality argument. We define $w \in H^1(J;\mathcal{Y})$ and $w_h \in H^1(J;V_h)$ such that for *a.e.* $t \in J$

$$\mathcal{A}_\beta(w(t),v)-\mathcal{A}_\epsilon(w'(t),v) = (u(t)-u_h(t),v)\ \forall v\in H_0^1(\Omega), \tag{2.3.33}$$

$$\mathcal{A}_\beta(w_h(t),v_h)-\mathcal{A}_\epsilon(w_h'(t),v_h) = (u(t)-u_h(t),v_h)\ \forall v_h\in V_h, \tag{2.3.34}$$

TH-2392_146123010

with $w(T) = w_h(T) = 0$ and

$$\left[\beta\frac{\partial w}{\partial \mathbf{n}} - \epsilon\frac{\partial w}{\partial \mathbf{n}}\right] = 0 \text{ on } \Gamma \times (0,T]. \tag{2.3.35}$$

Then $w \in H^1(J;\mathcal{Y})$ satisfies following *a priori* estimate (*cf.* [8])

$$\|w\|_{H^1(J;\mathcal{Y})} \leq C\|u - u_h\|_{L^2(J;L^2(\Omega))}. \tag{2.3.36}$$

Set $v = u'(t) - u_h'(t)$ in (2.3.33) and then integrate the resulting equation from 0 to t to obtain

$$\begin{aligned}&\frac{1}{2}\|u(t) - u_h(t)\|^2 - \frac{1}{2}\|u(0) - u_h(0)\|^2\\ &= \int_0^t \Big\{\mathcal{A}_\beta(w(s), u'(s) - u_h'(s)) - \mathcal{A}_\epsilon(w'(s), u'(s) - u_h'(s))\Big\}ds.\end{aligned}$$

A simple use of Green's formula and identity (2.3.35) leads to

$$\begin{aligned}&\frac{1}{2}\|u(t) - u_h(t)\|^2 - \frac{1}{2}\|u_0 - \mathcal{Q}_h^1 u_0\|^2\\ &= \int_0^t \Big\{ - (\nabla\cdot(\beta\nabla w(s)), u'(s) - u_h'(s)) + (\nabla\cdot(\epsilon\nabla w'(s)), u'(s) - u_h'(s))\Big\}ds.\end{aligned}$$

Then by Cauchy-Schwartz inequality, we obtain

$$\begin{aligned}\|u(t) - u_h(t)\|^2 - \|u_0 - \mathcal{Q}_h^1 u_0\|^2 &\leq C\|w\|_{H^1(J;\mathcal{Y})}\|u' - u_h'\|_{L^2(J;L^2(\Omega))}\\ &\leq C\|u - u_h\|^2_{H^1(J;L^2(\Omega))}\\ &\leq Ch^4(\|f\|_{L^2(J;L^2(\Omega))} + \|u_0\|_{\mathcal{Y}})^2,\end{aligned}$$

where we have employed Theorem 2.3.2 and (2.3.36). Combining this inequality with $\|u_0 - \mathcal{Q}_h^1 u_0\|^2 \in \mathrm{O}(h^4)$ completes the proof of Theorem 2.3.3 $\square$

2.4 Fully Discrete Error Analysis

In this section, we are now going to formulate a fully discrete finite element scheme to approximate the solution of the interface problem (2.1.1)-(2.1.3). A discrete in time scheme based on Crank-Nicolson scheme is considered and analyzed in this section. Optimal *a priori* error estimate in $L^\infty(L^2)$ and $L^\infty(H^1)$ norms are derived.

We first divide the time interval $[0,T]$ into M equally-spaced subintervals by the following points

$$0 = t_0 < t_1 < \ldots < t_M = T,$$

TH-2392_146123010

with $t_n = n\tau$, $\tau = \frac{T}{M}$ being the time step. Let, $I_n = (t_{n-1}, t_n]$ be the n-th subinterval. For any given sequence $\{\phi^n\}_{n=1}^M \subset L^2(\Omega)$ and a function $g \in C(J; L^2(\Omega))$, we define

$$\bar{\partial}\phi^n = \frac{\phi^n - \phi^{n-1}}{\tau}, \quad g^n(.) = g(., t_n), \quad n = 1, 2, \ldots, M.$$

Let V_h be the finite dimensional subspace of $H_0^1(\Omega)$ defined on $\mathcal{T}_h$ consisting of piecewise linear functions vanishing on the boundary $\partial\Omega$. The assumptions on the triangulation $\mathcal{T}_h$ are detailed in Chapter 1.

Then the fully discrete finite element approximations to the problem (2.1.1)-(2.1.3) is defined as follows: For each $n = 1, 2, \ldots, M$, find $U^n \in V_h$ such that

$$\mathcal{A}_{\epsilon h}\big(\bar{\partial}U^n, v_h\big) + \mathcal{A}_{\beta h}\Big(\frac{U^n + U^{n-1}}{2}, v_h\Big) = \Big(\frac{f^n + f^{n-1}}{2}, v_h\Big) \ \forall v_h \in V_h, \tag{2.4.1}$$

with $U^0 = \mathcal{Q}_h^1 u_0$.

The existence and uniqueness follows immediately from the Lax-Milgram theorem. Next, we define the error e^n as $e^n = u^n - U^n$ and using the semidiscrete solution u_h as the intermediate operator, we obtain

$$e^n = (u^n - u_h(t_n)) + (u_h(t_n) - U^n) := \rho^n + \theta^n,$$

where $\rho^n = u^n - u_h(t_n)$ and $\theta^n = u_h(t_n) - U^n$.

From Theorem 2.3.3, we already have a bound for ρ^n. So, we only need to estimate θ^n. For that we have the following result.

Lemma 2.4.1. *Let U^n and u_h be the solutions to the problem (2.4.1) and (2.3.1), respectively. Then, we have*

$$\|\nabla\theta^n\| \le C\tau^2 \int_0^T \|\nabla u_h'''\| ds.$$

Proof. To analyze θ^n, we substitute $t = t_k$ and $t = t_{k-1}$ in (2.3.1) and then add to obtain

$$\begin{aligned}
&\mathcal{A}_{\epsilon h}\Big(\frac{u_h(t_k) - u_h(t_{k-1})}{\tau}, v_h\Big) + \mathcal{A}_{\beta h}\Big(\frac{u_h(t_k) + u_h(t_{k-1})}{2}, v_h\Big) \\
&= \Big(\frac{f^k + f^{k-1}}{2}, v_h\Big) + \mathcal{A}_{\epsilon h}\Big(\frac{u_h(t_k) - u_h(t_{k-1})}{\tau}, v_h\Big) \\
&\quad -\mathcal{A}_{\epsilon h}\Big(\frac{u_h'(t_k) + u_h'(t_{k-1})}{2}, v_h\Big) \ \forall v_h \in V_h
\end{aligned} \tag{2.4.2}$$

Now, subtracting (2.4.1) from (2.4.2) and making some arrangements, we have

$$\mathcal{A}_{\beta h}\Big(\frac{\theta^k + \theta^{k-1}}{2}, v_h\Big) + \mathcal{A}_{\epsilon h}\Big(\frac{\theta^k - \theta^{k-1}}{\tau}, v_h\Big) = \mathcal{A}_{\epsilon h}(\sigma^k, v_h), \tag{2.4.3}$$

TH-2392_146123010

where

$$\sigma^k = \frac{u_h(t_k) - u_h(t_{k-1})}{\tau} - \frac{u_h'(t_k) + u_h'(t_{k-1})}{2}.$$

Choose $v_h = \frac{\theta^k + \theta^{k-1}}{2}$ in (2.4.3) to have

$$\mathcal{A}_{\epsilon h}(\theta^k, \theta^k) - \mathcal{A}_{\epsilon h}(\theta^{k-1}, \theta^{k-1}) \leq C\tau \mathcal{A}_{\epsilon h}(\sigma^k, \theta^k + \theta^{k-1}). \tag{2.4.4}$$

Now, it follows from (2.2.2) that

$$\mathcal{A}_{\epsilon h}(w, w) = \sum_{i=1}^{2} \int_{\Omega_{i,h}} \epsilon_i \nabla w \cdot \nabla w dx = \int_{\Omega} \epsilon_h \nabla w \cdot \nabla w dx, \tag{2.4.5}$$

where $\epsilon_h = \epsilon_i$ in $\Omega_{i,h}$ $(i = 1,\ 2)$. Using equation (2.4.5) in (2.4.4), we obtain

$$\|\epsilon_h^{\frac{1}{2}} \nabla \theta^k\|^2 - \|\epsilon_h^{\frac{1}{2}} \nabla \theta^{k-1}\|^2 \leq C\tau \|\epsilon_h^{\frac{1}{2}} \nabla \sigma^k\| (\|\epsilon_h^{\frac{1}{2}} \nabla \theta^k\| + \|\epsilon_h^{\frac{1}{2}} \nabla \theta^{k-1}\|),$$

so that

$$\|\epsilon_h^{\frac{1}{2}} \nabla \theta^k\| - \|\epsilon_h^{\frac{1}{2}} \nabla \theta^{k-1}\| \leq C\tau \|\epsilon_h^{\frac{1}{2}} \nabla \sigma^k\|. \tag{2.4.6}$$

Summing both sides in (2.4.6) over $k = 1, 2, \ldots, n$ and observing that $\theta^0 = 0$ leads to

$$\|\epsilon_h^{\frac{1}{2}} \nabla \theta^n\| \leq C\tau \sum_{k=1}^{n} \|\epsilon_h^{\frac{1}{2}} \nabla \sigma^k\|. \tag{2.4.7}$$

Now, it remains to determine estimates for σ^k. To find an estimate for σ^k, we consider the following two parts separately

$$\begin{aligned} \sigma_1^k &:= \frac{u_h(t_k) - u_h(t_{k-1})}{\tau} - u_h'\Big(t_{k-1} + \frac{\tau}{2}\Big), \\ \sigma_2^k &:= u_h'\Big(t_{k-1} + \frac{\tau}{2}\Big) - \frac{u_h'(t_k) + u_h'(t_{k-1})}{2}. \end{aligned}$$

First we estimate σ_1^k. Using the Taylor's expansion, we obtain

$$\begin{aligned} \frac{u_h(t_k) - u_h(t_{k-1})}{\tau} - u_h'\Big(t_{k-1} + \frac{\tau}{2}\Big) &= \frac{1}{\tau} \int_{t_{k-1}+\frac{\tau}{2}}^{t_k} (t_k - s)^2 u_h'''(s) ds \\ &\quad + \frac{1}{\tau} \int_{t_{k-1}}^{t_{k-1}+\frac{\tau}{2}} (t_{k-1} - s)^2 u_h'''(s) ds. \end{aligned}$$

Then the standard analysis from Thomée [126] leads to

$$\begin{aligned} \|\nabla \sigma_1^k\| &= \Big\| \nabla \Big(\frac{u_h(t_k) - u_h(t_{k-1})}{\tau} - u_h'\Big(t_{k-1} + \frac{\tau}{2}\Big) \Big) \Big\| \\ &\leq C\tau \int_{t_{k-1}}^{t_k} \|\nabla u_h'''\| ds. \end{aligned} \tag{2.4.8}$$

TH-2392_146123010

Following the same arguments as for σ_1^k, we obtain

$$\|\nabla\sigma_2^k\| \leq C\tau \int_{t_{k-1}}^{t_k} \|\nabla u_h'''\| ds. \tag{2.4.9}$$

Use (2.4.8) and (2.4.9) in (2.4.7) to get the desired result.

Finally, from Lemma 2.3.2, Lemma 2.4.1 and Theorem 2.3.1, Theorem 2.3.3 the following results follows immediately.

Theorem 2.4.1. *Let u and U^n be the solutions of (2.1.1)-(2.1.3) and (2.4.1), respectively, then for $f \in H^3(J; L^2(\Omega))$, the following estimates hold*

$$\begin{aligned} \|u^n - U^n\|_1 &\leq C(h+\tau^2)\Big(\|f\|_{H^3(J;L^2(\Omega))} + \|u_0\|_{\mathcal{Y}}\Big), \\ \|u^n - U^n\| &\leq C(h^2+\tau^2)\Big(\|f\|_{H^3(J;L^2(\Omega))} + \|u_0\|_{\mathcal{Y}}\Big). \end{aligned}$$

Remark 2.4.1. *To derive $O(h^m)$ $(m \geq 0)$ error estimates for non-interface time dependent problems in the literature generally require $u \in L^2(0,T; H^{m+1}(\Omega)) \cap H^1(0,T; H^{m-1}(\Omega))$, see [126]. Because of the low global regularity of the true solution of interface problem it is not straight forward to apply the standard finite element error analysis technique of non-interface problems to interface problems. The present work generalize the results of [8] under the same regularity assumptions of the true solution. To the best of our knowledge, optimal pointwise-in-time error estimates for the electric interface problems have not been established earlier for conforming finite element methods.*

Remark 2.4.2. *The proposed fully discrete finite element scheme can be easily extended for the numerical approximation of the solutions to the IBVP (2.1.1)-(2.1.2) coupled with the following jump conditions*

$$[u] = 0, \quad \left[\epsilon\frac{\partial u'}{\partial \mathbf{n}} + \beta\frac{\partial u}{\partial \mathbf{n}}\right] = g \quad along\, \Gamma \times (0,T]. \tag{2.4.10}$$

For numerical validation, we refer to numerical Examples 2.5.1-2.5.3. For backward Euler time discretization, we refer to Dutta et al. [48].

2.5 Numerical Results

In this section, we present some numerical experiments to validate the theoretical findings presented in the previous section. To illustrate the flexibility of the method, different forms of interfaces along with a large scale of variation in the physical coefficients are considered. For our first two numerical experiment, globally continuous piecewise linear

TH-2392_146123010

finite elements ($\mathbb{P}_1$) based on fitted triangulations of Ω_i, $i = 1, 2$ are used. The nodes of the triangulations of Ω_1 and Ω_2 coincide on the interface Γ as stated in Chapter 1. A higher order fitted finite element approximation has been carried out in Example 2.3. All the numerical computations are done in the time interval $J = (0, 1]$.

Our main emphasis here is to understand the behavior of the true errors obtained in Theorem 2.4.1 on fitted meshes with uniform time steps. For each quantities of interest we observe its experimental order of convergence (EOC). For a given finite sequence of successive runs (indexed by i), let

- $e(i)$ = the error corresponding to the L^2 and H^1-norms on the $i-$th iteration and
- $h(i)$ = the mesh size of the run i .

Then the experimental order of convergence (EOC) is computed by

$$\mathrm{EOC}(i+1) = \frac{\log(e(i+1)/e(i))}{\log(h(i+1)/h(i))}.$$

Example 2.5.1. For our first numerical example, we consider the two dimensional domain $\Omega = (-1, 1) \times (-1, 1)$ and the interface Γ is taken to be the circle $x^2 + y^2 = r^2 = 1/4$. The source function f is taken as

$$f(x,y,t) = \begin{cases} 4(\sigma_1 t + \epsilon_1) & \text{if } r^2 \le \frac{1}{4}, \\ \big\{(\sigma_2 t + \epsilon_2)\sin(\pi x)\sin(\pi y)(2\pi^2(\frac{1}{4} - r^2) & \\ \quad + 4\sin(\pi x)\sin(\pi y)) + 4\pi x \sin(\pi y)\cos(\pi x) & \\ \quad + 4\pi y \cos(\pi y)\sin(\pi x)\big\} & \text{if } r^2 > \frac{1}{4}. \end{cases}$$

And the exact solution of the problem is given by

$$u(x,y,t) = \begin{cases} t(\frac{1}{4} - r^2) & \text{if } r^2 \le \frac{1}{4}, \\ t(\frac{1}{4} - r^2)\sin(\pi x)\sin(\pi y) & \text{if } r^2 > \frac{1}{4}. \end{cases}$$

The Dirichlet boundary condition, initial data and interface function are calculated from the exact solution. To mark the significance of the interface model problem (2.1.1), we take a specific thermal parameters from the paper by Rems *et al.* [114] given as

$$\sigma = \begin{cases} \sigma_1 = 0.25 & \text{if } r^2 \le \frac{1}{4}, \\ \sigma_2 = 5 \times 10^{-7} & \text{if } r^2 > \frac{1}{4}, \end{cases} \quad \& \quad \epsilon = \begin{cases} \epsilon_1 = 70 & \text{if } r^2 \le \frac{1}{4}, \\ \epsilon_2 = 4.5 & \text{if } r^2 > \frac{1}{4}. \end{cases}$$

TH-2392_146123010

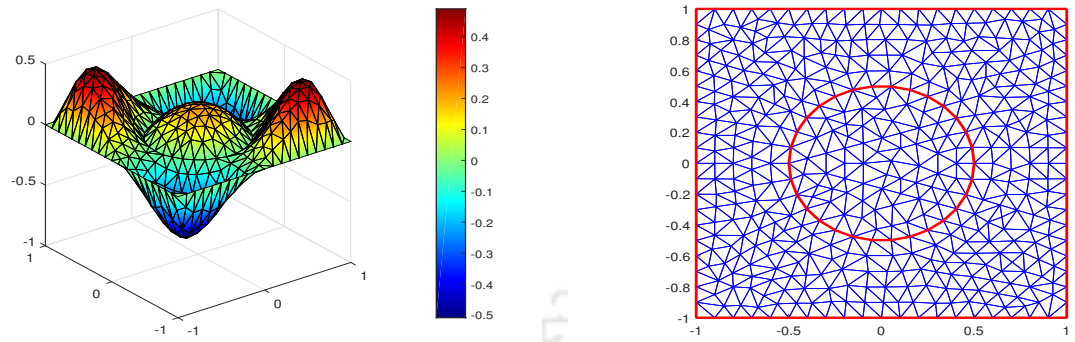

Figure 2.1: Exact solution (left) and triangulation (right) of Ω for $h = 0.167378$ with circular interface (Test Example 2.5.1).

In Figure 2.1, we show the exact solution and triangulation of the domain Ω with mesh size $h = 0.167378$ at final time step. Table 2.1 represents the numerical solution errors and convergence rates in both L^2-norm and H^1-norm for the Crank-Nicolson scheme. It is clear from Table 2.1 that the Crank-Nicolson scheme, for linear finite element solution, gives optimal order of convergence for $\tau = h$ in both L^2 and H^1 norms which confirm the theoretical prediction as proved in the Theorem 2.4.1.

Table 2.1: L^2 and H^1 norms error analysis with time step $\tau = h$

h	$\tau \approx h$	$\|u - u_h\|_{L^2(\Omega)}$	EOC	$\|u - u_h\|_{H^1(\Omega)}$	EOC
0.3050910	0.30	3.68502e-01	-	6.97774	-
0.1673780	0.16	9.78080e-02	2.0648	3.58550	0.9648
0.0828717	0.08	2.64808e-02	1.9537	1.82200	1.0122
0.0420952	0.04	7.43036e-03	1.9911	9.0403e-01	1.0980

Example 2.5.2. For our second numerical example, we take the computational domain $\Omega = (-1, 1) \times (-1, 1)$ and the interface Γ is the ellipse given by $4x^2 + 16y^2 = r^2 = 1$. We select the data in (2.1.1)-(2.1.2) and (2.4.10) such that the exact solution is given by

$$u(x, y, t) = \begin{cases} 5(1 - r^2) \sin t & \text{if } r^2 \leq 1, \\ t(1 - r^2)(x^2 - 1)(y^2 - 1) & \text{if } r^2 > 1, \end{cases}$$

with $\sigma_1 = \epsilon_1 = 1$ and $\sigma_2 = \epsilon_2 = 10$.

TH-2392_146123010

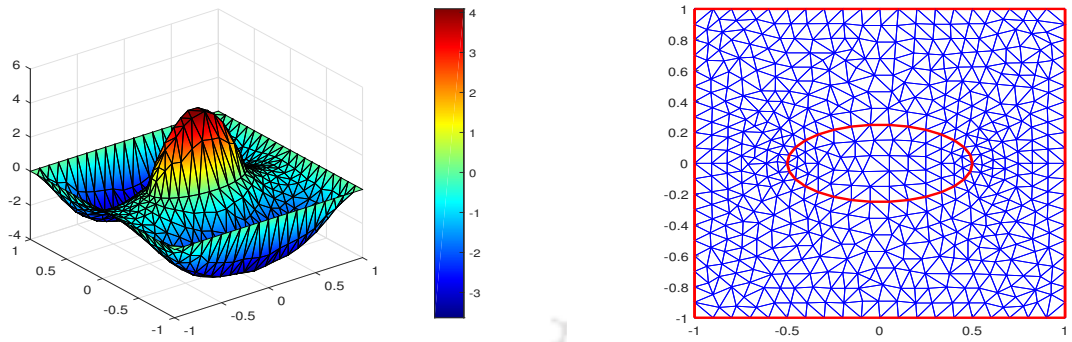

Figure 2.2: Exact solution (left) and triangulation (right) of Ω for $h = 0.152069$ with elliptic interface (Test Example 2.5.2).

In Figure 2.2, we show the exact solution and triangulation of the domain Ω with mesh size $h = 0.152069$ at final time step. By successive mesh refinements using piecewise linear finite elements, the convergence behavior of the solution with respect to the L^2-norm and H^1-norm are listed in Table 2.2. It is evident from Table 2.2 that we have achieved optimal first order of convergence in H^1-norm and optimal second order of convergence in L^2-norm for the coupling $\tau = h$ which confirm the theoretical prediction as proved in the Theorem 2.4.1.

Table 2.2: L^2 and H^1 norms error analysis with time step $\tau = h$

h	$\tau \approx h$	$\|u - u_h\|_{L^2(\Omega)}$	EOC	$\|u - u_h\|_{H^1(\Omega)}$	EOC
0.1520690	0.15	2.46751e-01	-	8.71344	-
0.0779091	0.07	6.11024e-02	2.0871	4.36022	1.0352
0.0411529	0.04	1.58101e-02	2.1181	2.17988	1.0862
0.0247278	0.02	3.98563e-03	2.1792	1.07225	1.1221

Example 2.5.3. For our final numerical example, we consider the two dimensional domain $\Omega = (-1, 1) \times (-1, 1)$ and take line interface $x = 0$. The exact solution of the problem is given by

$$u(x, y, t) = \begin{cases} t \sin(\pi x) \sin(\pi y) & \text{if } x \leq 0, \\ t \sin(2\pi x) \sin(\pi y) & \text{if } x > 0. \end{cases}$$

TH-2392_146123010

The value of coefficients σ and ϵ are same with example 2.1. The source function f, Dirichlet boundary condition, initial data and interface function are calculated from the exact solution.

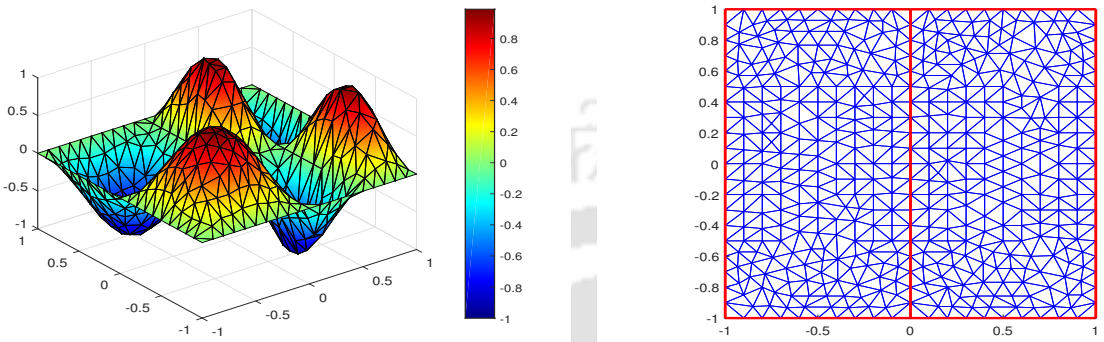

Figure 2.3: Exact solution (left) and triangulation (right) of Ω for $h = 0.125$ with line interface (Test Example 2.5.3).

In Figure 2.3, we show the exact solution and triangulation of the domain Ω with mesh size $h = 0.125$ at final time step. Figure 2.4 (a) shows the convergence behavior of the P_1 elements. We note that the linear finite element (P_1) solution gives the optimal first order convergence in the H^1-norm and second order convergence in the L^2-norm. Due to poor approximation of the interface it is not always possible to get higher order approximation using Galerkin finite element methods. However one may expect higher convergence result depending on how well the mesh resolves the interface. It is clear from Figure 2.4 (b)-(c) that we have achieved optimal order of convergence in both H^1-norm and L^2-norm for quadratic finite element and cubic finite element respectively.

TH-2392_146123010

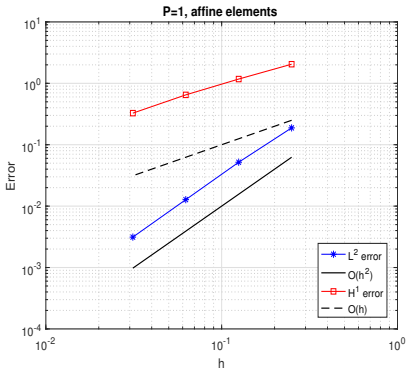

(a)

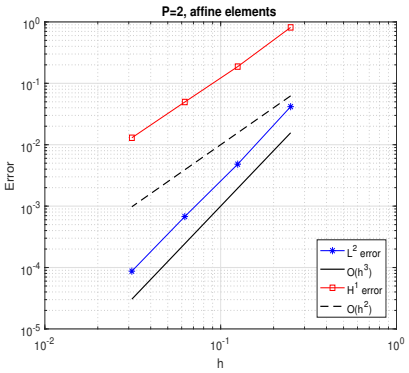

(b)

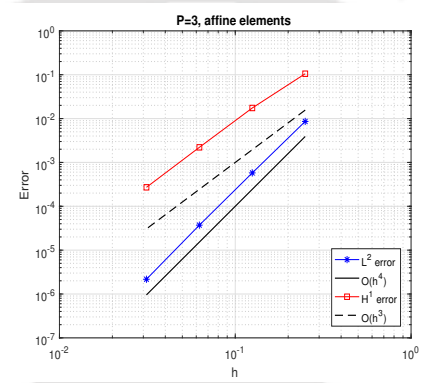

(c)

Figure 2.4: Convergence of P_1, P_2 and P_3 elements in Example 2.5.3

TH-2392_146123010

TH-2392_146123010

3

Convergence of FEMs for Hyperbolic Heat Equation with Interface

This chapter is devoted to the *a priori* error analysis in finite element methods for the hyperbolic heat conduction model problem (1.1.4)-(1.1.6). Typical semidiscrete and fully discrete schemes are presented for a fitted finite element discretization with straight interface triangles. The fully discrete space-time finite element discretizations is based on second order in time Newmark scheme. Optimal *a priori* error estimates for both semidiscrete and fully discrete schemes are proved in $L^\infty(L^2)$ norm. Numerical experiments are reported for several test cases to confirm our theoretical convergence rate.

3.1 Introduction

To start with, we first rewrite the Non-Fourier bio heat transfer model problem of the form

$$u'' + \sigma u' - \nabla \cdot (\beta \nabla u) = f \quad \text{in } \Omega \times (0, T],\ T < \infty, \tag{3.1.1}$$

with initial and boundary conditions

$$u(x,0) = u_0,\ \ u'(x,0) = v_0 \ \text{ in } \Omega \ \ \& \ \ u(x,t) = 0 \quad \text{on } \partial\Omega \times (0,T] \tag{3.1.2}$$

and jump conditions on the interface

$$[u] = 0, \quad \left[\beta \frac{\partial u}{\partial \mathbf{n}}\right] = 0 \quad \text{along } \Gamma \times (0,T], \tag{3.1.3}$$

Some parts of this chapter published online in *Comput. Math. Appl., 79(2020), 3139–3159 and J. Appl. Math. Comput. 62 (2020), 701–724*

TH-2392_146123010

where Ω is a bounded domain in $\mathbb{R}^d (d = 2,\ 3)$ with Lipschitz boundary $\partial\Omega$ and $\Omega_1 \subset \Omega$ is an open domain with C^2 smooth boundary $\Gamma = \partial\Omega_1$ and $\Omega_2 = \Omega \backslash \Omega_1$. Other symbols are as defined in Chapter 1. We assume that the physical coefficients are discontinuous along interface Γ and piecewise positive constants. We write

$$(\sigma, \beta) = \begin{cases} (\sigma_1, \beta_1) & \text{in } \Omega_1, \\ (\sigma_2, \beta_2) & \text{in } \Omega_2. \end{cases}$$

Further, initial data (u_0, v_0) and external force f are real valued functions and assumed to be sufficiently smooth.

In the last few years, demand for reliable and efficient numerical algorithms for partial differential equations with interfaces has increased. Due to the discontinuity of coefficients along the interface, the solution of such problem has low regularity on the whole physical domain which makes it very challenging to construct a stable and accurate numerical scheme with the classical finite element/finite difference methods. However, one can expect higher local regularity of the solution of the interface problem when the interface is smooth enough [31, 79]. Although there are substantial amount of research in the design of finite difference methods for the hyperbolic heat equation with discontinuous coefficients (see, [33, 76, 100, 108, 121, 138] and references therein), there are considerably less work on the finite element methods for interface problem (3.1.1)-(3.1.3). In this chapter, we propose a fitted finite element method for the hyperbolic heat equation with discontinuous coefficients. The finite element solution, for the spatially discrete scheme, converges to the true solution with an optimal order in $L^\infty(L^2)$ and $L^\infty(H^1)$ norms. For the temporal discretization, Crank-Nicolson scheme is applied after rewriting the governing equation in the first-order system, as in Baker [15]. Optimal order of convergence in $L^\infty(L^2)$ norm is derived for the fully discrete solution. The derivation of the error bounds in present work are based on some new analytical tools and techniques, including a λ-strip argument for quantifying the relation of error near the interface in terms of the mismatch parameter λ. Finite element algorithm presented here can be used to solve a wide variety of hyperbolic heat conduction models arising in science, engineering and biomedical technologies.

The rest of this chapter is organized as follows: Section 3.2 concerns well-posedness of the model problem. In Section 3.3, we derive some error estimates for newly introduced operators, involving λ-strip. Optimal *a priori* error estimates for the semidiscrete solution in $L^\infty(L^2)$ and $L^\infty(H^1)$ norms are derived in Section 3.4. Error estimates for the fully discrete scheme are discussed in Section 3.5. Finally, Section 3.6 focuses on numerical experiments.

TH-2392_146123010

3.2 Preliminaries

In this section, well-posedness of the model interface problem (3.1.1)-(3.1.3) and the regularity of its solution are discussed. For our convenience, we use spaces W, V and V' for $L^2(\Omega)$, $H_0^1(\Omega)$ and $H^{-1}(\Omega)$, respectively. Further, we recall global bilinear maps $\mathcal{A}_\beta(\cdot,\cdot) : H^1(\Omega) \times H^1(\Omega) \to \mathbb{R}$ and $\mathcal{B}_\sigma(\cdot,\cdot) : L^2(\Omega) \times L^2(\Omega) \to \mathbb{R}$ defined by

$$\begin{aligned} \mathcal{A}_\beta(w,v) &= \int_\Omega \beta(x)\nabla w \cdot \nabla v dx = \mathcal{A}_\beta^1(w,v) + \mathcal{A}_\beta^2(w,v) \ \ \forall\ w,\ v \in V, \\ \mathcal{B}_\sigma(w,v) &= \int_\Omega \sigma(x) w v dx \quad \forall\ w, v \in L^2(\Omega) \ \ \forall\ w,\ v \in W. \end{aligned}$$

Local bilinear maps $\mathcal{A}_\beta^l : H^1(\Omega_l) \times H^1(\Omega_l) \to \mathbb{R}$, $l = 1,\ 2$, are as defined in Chapter 1.

Next, we define the weak and strong solutions to the equation (3.1.1). We adapt following notion of weak solution to the model interface problem (see, for instance, [8, 18]).

Definition 3.2.1. *Let $u_0 \in V$, $v_0 \in W$ and $f \in L^2(V')$. A function $u \in L^2(V) \cap H^1(W) \cap H^2(W)$ is called a weak solution of (3.1.1)-(3.1.2) if $u(0) = u_0$ and $u_t(0) = v_0$, and it satisfies following weak formulation*

$$(u'', v) + \mathcal{B}_\sigma(u', v) + \mathcal{A}_\beta(u, v) = \langle f(t,\cdot), v\rangle_{V'\times V}, \tag{3.2.1}$$

for all $v \in H_0^1(\Omega)$ and a.e. $t \in (0,T]$. Here, $\langle\cdot,\cdot\rangle_{V'\times V}$ denotes the standard duality product.

Existence and uniqueness of a solution to the variational problem (3.2.1) is proved in [120, 132]. We refer to ([132], Theorem 2) for the sufficient conditions under which problem (3.2.1) has a unique solution such that $u \in L^2(H_0^1(\Omega)) \cap H^2(L^2(\Omega))$. It is wroth to note that formulation (3.2.1) also arises in the modeling of acoustic wave equation with absorbing boundary condition, in which physical quantities are allowed to be discontinuous at the interface (*cf.* [16] and references therein).

Definition 3.2.2. *Let $u_0 \in \mathcal{Y}$, $v_0 \in W$ and $f \in L^2(W)$. A function $u \in L^2(\mathcal{Y}) \cap H^1(W) \cap H^2(W)$ is called a strong solution of (3.1.1)-(3.1.3) if $u(0) = u_0$ and $u'(0) = v_0$ with jump conditions (3.1.3), and the relation*

$$u''(x,t) + \sigma(x)u'(x,t) - \nabla\cdot(\beta(x)\nabla u(x,t)) = f(x,t) \tag{3.2.2}$$

holds for a.e. $t \in (0,T]$ and a.e. $x \in \Omega_i$ $(i = 1,\ 2)$.

TH-2392_146123010

Now, we prove the following result which is crucial to prove the existence of a strong solution to the interface problem.

Lemma 3.2.1. *Let u be the weak solution of (3.1.1)-(3.1.2). Assume that $u_0 \in \mathcal{Y}$, $v_0 \in W$, $f \in L^2(W)$ and $u \in L^2(\mathcal{Y}) \cap H^1(W) \cap H^2(W)$. Then u is a strong solution for (3.1.1)-(3.1.3).*

Proof. For $u \in L^2(\mathcal{Y}) \cap H^1(W) \cap H^2(W)$ and *a.e.* $t \in (0, T]$, upon integration by parts, we obtain

$$\begin{aligned} \int_{\Omega_i} -\nabla \cdot (\beta_i \nabla u) v dx &= \int_{\Omega_i} \beta_i \nabla u \cdot \nabla v dx \\ &= (f - u'' - \sigma_i u', v)_{\Omega_i} \quad \forall v \in H_0^1(\Omega_i), \end{aligned} \tag{3.2.3}$$

which implies that

$$-\nabla \cdot (\beta_i \nabla u(x,t)) = f(x,t) - u''(x,t) - \sigma_i u'(x,t)$$

holds for *a.e.* $t \in (0, T]$ and *a.e.* $x \in \Omega_i$ $(i = 1,\ 2)$. Next we show that the weak solution also satisfies the jump conditions (3.1.3). Applying integration by parts, for *a.e.* $t \in (0, T]$, we have

$$\begin{aligned} 0 &= \sum_{i=1}^{2} \int_{\Omega_i} (u'' + \sigma_i u' - f) v dx + \sum_{i=1}^{2} \int_{\Omega_i} -\nabla \cdot (\beta_i \nabla u) v dx \\ &= \sum_{i=1}^{2} \int_{\Omega_i} (u'' + \sigma_i u' - f) v dx + \sum_{i=1}^{2} \int_{\Omega_i} \beta_i \nabla u \cdot \nabla v dx \\ &\quad - \int_{\Gamma} \beta_1 \frac{\partial u}{\partial \mathbf{n}} v ds + \int_{\Gamma} \beta_2 \frac{\partial u}{\partial \mathbf{n}} v ds \\ &= \sum_{i=1}^{2} \int_{\Omega_i} (u'' + \sigma_i u' - f) v dx + \sum_{i=1}^{2} \int_{\Omega_i} \beta_i \nabla u \cdot \nabla v dx - \int_{\Gamma} \left[\beta \frac{\partial u}{\partial \mathbf{n}} \right] v ds \\ &= \sum_{i=1}^{2} (u'' + \sigma_i u' - f, v)_{\Omega_i} + \sum_{i=1}^{2} \mathcal{A}_{\beta}^{i}(u, v) - \int_{\Gamma} \left[\beta \frac{\partial u}{\partial \mathbf{n}} \right] v ds \quad \forall v \in V. \end{aligned} \tag{3.2.4}$$

Above relation together with the definition of weak solution it follows that

$$\int_{\Gamma} \left[\beta \frac{\partial u}{\partial \mathbf{n}} \right] v ds = 0 \quad \forall v \in V.$$

The arbitrariness of v shows that u satisfies the second jump condition in (3.1.3) (for instance, see [8]).

TH-2392_146123010

The first condition in (3.1.3) is a direct consequence of the fact that $u \in L^2(V)$. For instance, if γ_Γ designates the trace operator on Γ, it is well known [22] that

$$u_1|_\Gamma - u_2|_\Gamma = \gamma_\Gamma u_1 - \gamma_\Gamma u_2 = \gamma_\Gamma u - \gamma_\Gamma u = 0.$$

This completes the proof. □

The next result is concerned on the existence of a strong solution to interface problem (3.1.1)-(3.1.3).

Theorem 3.2.1. *Let $u_0 \in \mathcal{Y}$, $v_0 \in V$ and $f \in L^2(W)$, then the interface problem (3.1.1)-(3.1.3) admits a unique strong solution.*

Proof. Let u be a weak solution to the interface problem (3.1.1)-(3.1.3) satisfying (3.2.1). For *a.e.* $t \in (0, T]$, we consider following auxiliary problem: Find $w(t) \in V$ such that

$$\mathcal{A}_\beta(w, v) = (f - u'' - \sigma u', v) \quad \forall v \in V, \tag{3.2.5}$$

with $[w] = 0$ & $\left[\beta \frac{\partial w}{\partial \mathbf{n}}\right] = 0$ across the interface Γ. From the regularity estimate for elliptic interface problem (*cf.* [31]), it follows that $w \in \mathcal{Y}$.

Now, subtracting (3.2.5) from (3.2.1), we have

$$\mathcal{A}_\beta(u - w, v) = 0 \quad \forall v \in V,$$

which implies that $u(x,t) = w(x,t)$ for *a.e.* $t \in (0, T]$ and *a.e.* $x \in \Omega$. Therefore, $u \in L^2(\mathcal{Y})$ and due to Lemma 3.2.1 it is a strong solution to the interface problem (3.1.1)-(3.1.3).

Uniqueness follows from the fact that the problem: Find $w : [0, T] \to H_0^1(\Omega)$ such that

$$(w'', v) + \mathcal{B}_\sigma(w', v) + \mathcal{A}_\beta(w, v) = 0 \ \ \forall v \in H_0^1(\Omega),$$

with $w(x, 0) = 0 = w'(x, 0)$ has only trivial solution in $\Omega \times [0, T]$. □

Remark 3.2.1. *Due to the presence of discontinuous coefficients the solution to the time-dependent interface problem, in general, does not belong to $H^1(H^2(\Omega))$. However, the solution to the interface problem can be proved to be sufficiently smooth in each individual subdomain Ω_1 and Ω_2 for smooth data. As we are not aware of proofs of such local regularities for the interface problem (3.1.1)-(3.1.3) in literature, we will assume additional regularity of u which guarantee the convergence results. In this work, it is implicitly assumed that initial data (u_0, v_0) and the source function f are sufficiently smooth so that solution belongs to desired Sobolev spaces.*

TH-2392_146123010

We assume $u''' \in L^2(0,T;L^2(\Omega))$ *and then map the solution* u *to*

$$w \in L^2(0,T;\mathcal{Y}) \cap H^1(0,T;H^2(\Omega_1)\cap H^2(\Omega_2)) \cap H^2(0,T;H^1(\Omega_1)\cap H^1(\Omega_2)),$$

which satisfies following wave equation (cf. [36], Theorem 2.1.1)

$$w'' - \nabla\cdot(\beta\nabla w) = f - \sigma u' \quad in\ \Omega\times(0,T],$$

with initial and boundary conditions

$$w(x,0) = u_0 \ \ \&\ \ w'(x,0) = v_0 \ \ in\ \Omega;\ \ w(x,t) = 0 \quad on\ \partial\Omega\times(0,T]$$

and jump conditions on the interface

$$[w] = 0, \quad \left[\beta\frac{\partial w}{\partial \mathbf{n}}\right] = 0 \quad along\ \Gamma\times(0,T].$$

It is easy to verify that $u(x,t) = w(x,t)$ *for a.e.* $t\in(0,T]$ *and a.e.* $x\in\Omega$, *and* u *satisfies following a priori estimate (cf. [36], Theorem 2.1.1)*

$$\begin{aligned}
&\sum_{i=1}^{2}\left\{\|u\|^2_{H^2(H^1(\Omega_i))} + \|u\|^2_{H^1(H^2(\Omega_i))}\right\}\\
&\le C\Big(\|w'''(0)\|^2 + \sum_{i=1}^{2}\|w''(0)\|^2_{H^1(\Omega_i)} + \|f\|^2_{H^2(L^2(\Omega))} + \|u'''\|^2_{L^2(L^2(\Omega))}\Big)\\
&\le C\Big(\|u_0\|^2_{H^3(\Omega)} + \|v_0\|^2_{H^2(\Omega)} + \|f\|^2_{H^2(H^1)} + \|u'''\|^2_{L^2(L^2(\Omega))}\Big). \qquad (3.2.6)
\end{aligned}$$

Thus, if $u\in H^3(0,T;L^2(\Omega))$, *we find that* $u(t)$ *and* $u'(t)$ *are smooth in each subdoman* Ω_1 *and* Ω_2 *for a.e.* $t\in(0,T]$ *when initial data* $u_0\in H^3(\Omega)$ *and* $v_0\in H^2(\Omega)$, *and source function* $f\in H^2(H^1(\Omega))$. *In fact, such smoothness for* (u_0,v_0) *and* f *should be sufficient to ensure* $u\in H^3(0,T;L^2(\Omega))$ *(cf. Remark 3.4.1).*

3.3 Auxiliary Projections

In this section, we introduce some auxiliary projections and prove their approximation properties for the fitted finite element triangulations $\mathcal{T}_h$ as discussed in Chapter 1.

As it may be computationally inconvenient to evaluate the integrals appearing in finite element approximations exactly, we use approximations of the original bilinear maps $\mathcal{A}_\beta(\cdot,\cdot)$ and $\mathcal{B}_\sigma(\cdot,\cdot)$. For our convenience, we now recall approximated bilinear maps $\mathcal{A}_{\beta h}(\cdot,\cdot)$ and $\mathcal{B}_{\sigma h}(\cdot,\cdot)$ from Chapter 1 defined as

$$\begin{aligned}
\mathcal{A}_{\beta h}(w,v) &= \sum_{K\in\mathcal{T}_h}\int_K \beta_K(x)\nabla w\cdot\nabla v dx \ \ \forall w,v\in H^1(\Omega),\\
\mathcal{B}_{\sigma h}(w,v) &= \sum_{K\in\mathcal{T}_h}\int_K \sigma_K(x) wv dx \ \ \forall w,v\in L^2(\Omega).
\end{aligned}$$

TH-2392_146123010

Here, $\beta_K(x) = \beta_i$ and $\sigma_K(x) = \sigma_i$ if $K \subset \Omega_{i,h},\ i = 1, 2$.

Analogue to Lemma 1.2.2, for the difference between the bilinear form $\mathcal{B}_\sigma(\cdot,\cdot)$ and its approximated bilinear form $\mathcal{B}_{\sigma h}(\cdot,\cdot)$, we have the following result

Lemma 3.3.1. *For $z \in H^1(\Omega)$, we have*

$$|\mathcal{B}_\sigma(z, v_h) - \mathcal{B}_{\sigma h}(z, v_h)| \leq Ch^2\|z\|_1\|v_h\|_1 \ \ \forall\ v_h \in V_h. \tag{3.3.1}$$

Furthermore, for $z \in \mathcal{X}$ and $v_h \in V_h$ there holds

$$|\mathcal{B}_\sigma(z, v_h) - \mathcal{B}_{\sigma h}(z, v_h)| \leq C(h^2 + \lambda)\|z\|_{\mathcal{X}}\|v_h\|. \tag{3.3.2}$$

Proof. We define

$$\tilde{K} = \begin{cases} K \cap \Omega_1 & \text{if } K \in \mathcal{T}_*^2, \\ K \cap \Omega_2 & \text{if } K \in \mathcal{T}_*^1. \end{cases} \tag{3.3.3}$$

Clearly, $\tilde{K} \subset S_\lambda \cap \Omega_i,\ i = 1, 2$. Then we get

$$|\mathcal{B}_\sigma(z, v_h) - \mathcal{B}_{\sigma h}(z, v_h)| \leq \sum_{K \in \mathcal{T}_*} \left| \Big((\sigma - \sigma_K) z, v_h \Big)_{\tilde{K}} \right| \leq C \sum_{K \in \mathcal{T}_*} \|z\|_{\tilde{K}} \|v_h\|_{\tilde{K}}. \tag{3.3.4}$$

Now, using Hölder's inequality, we obtain

$$\|z\|_{\tilde{K}} \leq Ch^{\frac{3(p-2)}{2p}} \|z\|_{L^p(\tilde{K})} \ \ \forall\ p > 2. \tag{3.3.5}$$

We now recall Sobolev embedding inequality for two dimensions (*cf.* Ren and Wei [115])

$$\|w\|_{L^p(\mathcal{M})} \leq Cp^{\frac{1}{2}} \|w\|_{1,\mathcal{M}} \ \ \forall w \in H^1(\mathcal{M}),\ \ p > 2. \tag{3.3.6}$$

Now, setting $p = 6$ in (3.3.5) and then using the Sobolev embedding inequality (3.3.6), we obtain

$$\|z\|_{\tilde{K}} \leq Ch\|z\|_{1,K}. \tag{3.3.7}$$

Proceeding in a similar way, we obtain

$$\|v_h\|_{\tilde{K}} \leq Ch\|v_h\|_{1,K}. \tag{3.3.8}$$

Using estimates (3.3.7)-(3.3.8) in (3.3.4), we obtain the first inequality.

For the second inequality, let $p \to \infty$ in (3.3.5) to have

$$\|z\|_{\tilde{K}} \leq Ch^{\frac{3}{2}} \|z\|_{L^\infty(\tilde{K})} \leq Ch^{\frac{3}{2}} \sum_{i=1}^{2} \|z\|_{L^\infty(\Omega_i)} \leq Ch^{\frac{3}{2}} \|z\|_{2,\Omega_i}. \tag{3.3.9}$$

TH-2392_146123010

Here, we have used Sobolev embedding inequality $\|z\|_{L^\infty(\Omega_i)} \leq C\|z\|_{2,\Omega_i}$. From Lemma 2.1 in [85] we then infer

$$\|z\|^2_{S_\lambda \cap \Omega_i} \leq C\lambda \|z\|_{\Omega_i}\|z\|_{1,\Omega_i}, \ i = 1, 2. \tag{3.3.10}$$

Finally, Poincaŕe inequality, standard inverse estimate $\|\nabla v_h\| \leq Ch^{-1}\|v_h\|$ together with (3.3.9)-(3.3.10) and (3.3.4) leads to

$$\begin{aligned}
|\mathcal{B}_\sigma(z, v_h) - \mathcal{B}_{\sigma h}(z, v_h)| &\leq Ch^{\frac{3}{2}}\|z\|_{\mathcal{X}}\Big(\sum_{K\in\mathcal{T}_*}\|v_h\|^2_{\tilde{K}}\Big)^{\frac{1}{2}} \\
&\leq Ch^{\frac{3}{2}}\|z\|_{\mathcal{X}}\Big(\sum_{i=1}^{2}\|v_h\|^2_{S_\lambda\cap\Omega_i}\Big)^{\frac{1}{2}} \\
&\leq Ch^{\frac{3}{2}}\|z\|_{\mathcal{X}}\Big(\sum_{i=1}^{2}\lambda\|v_h\|_{\Omega_i}\|v_h\|_{1,\Omega_i}\Big)^{\frac{1}{2}} \\
&\leq Ch^{\frac{3}{2}}\|z\|_{\mathcal{X}}\sqrt{\lambda}\|v_h\|^{\frac{1}{2}}\|v_h\|_1^{\frac{1}{2}} \\
&\leq Ch\sqrt{\lambda}\|z\|_{\mathcal{X}}\|v_h\| \leq C(h^2+\lambda)\|z\|_{\mathcal{X}}\|v_h\|.
\end{aligned}$$

This completes the rest of the proof. □

Let $\tilde{\mathcal{X}} = \{v \in \mathcal{X} : [v] = 0$ and $[\beta\partial v/\partial \mathbf{n}] = 0$ along Γ with $v = 0$ on $\partial\Omega\}$. Since Γ is of class C^2, thus $v_i = v|_{\Omega_i} \in H^2(\Omega_i), \ \ i = 1, \ 2$ can be extended to $\mathcal{E}_i v \in H^2(\Omega)$ such that

$$\mathcal{E}_i v = v \ \ a.e. \text{ in } \Omega_i \text{ and } \|\mathcal{E}_i v\|_2 \leq C\|v\|_{2,\Omega_i}. \tag{3.3.11}$$

For the existence of such extension, we refer to Stein [125].

Let $\Pi_h : C(\bar{\Omega}) \to V_h$ be the standard Lagrange interpolation operator. Then for $K \in \mathcal{T}_h$ and $v \in \tilde{\mathcal{X}}$, we define our new interpolation operator such that

$$v_I = \begin{cases} \Pi_h\mathcal{E}_1 v & \text{if } K \subset \Omega_{1,h}, \\ \Pi_h\mathcal{E}_2 v & \text{if } K \subset \Omega_{2,h}. \end{cases} \tag{3.3.12}$$

Next, we derive an important lemma to be used in proving the convergence of the new interpolation operator v_I.

Lemma 3.3.2. *Let $v \in \tilde{\mathcal{X}}$, then, for $l = 1, \ 2$, we have*

(a) $\displaystyle\sum_{K\in\mathcal{T}_*^l}\|\mathcal{E}_l v\|_{1,\tilde{K}} \leq C\sqrt{\lambda}\|v\|_{2,\Omega_l}$,

(b) $\displaystyle\sum_{K\in\mathcal{T}_*^l}\|v\|_{1,\tilde{K}} \leq C\sqrt{\lambda}\|v\|_{2,\Omega_{l'}}, \ l' = 2, \ \text{when } l = 1 \text{ and } l' = 1, \ \text{when } l = 2,$

where $\tilde{K}$ is as defined in (3.3.3).

TH-2392_146123010

Proof. For the first inequality, we observe

$$\cup_{K\in\mathcal{T}_*^1}\tilde{K} = \cup_{K\in\mathcal{T}_*^1}(K\cap\Omega_2) \subset S_\lambda^2 \subset \Omega_2, \quad S_\lambda^i = S_\lambda \cap \Omega_i,\ i=1,2.$$

Hence, it follows immediately that

$$\sum_{K\in\mathcal{T}_*^1} \|\mathcal{E}_1 v\|_{1,\tilde{K}} = \sum_{K\in\mathcal{T}_*^1} \|\mathcal{E}_1 v\|_{1,K\cap\Omega_2} \le \|\mathcal{E}_1 v\|_{1,S_\lambda^2}.$$

Now, using (3.3.10), we obtain

$$\|\mathcal{E}_1 v\|_{1,S_\lambda^2} \le C\sqrt{\lambda}\|\mathcal{E}_1 v\|_{2,\Omega_2} \le C\sqrt{\lambda}\|\mathcal{E}_1 v\|_2.$$

Finally, equation (3.3.11) leads to the part (a).

The proof of the second inequality is analogous to the above proof and hence we omit the details. □

Based on previous lemma and techniques used in [36], we have the following approximation result for v_I.

Lemma 3.3.3. *For any $v \in \tilde{\mathcal{X}}$, we have*

$$\|v - v_I\|_{1,\Omega_1} + \|v - v_I\|_{1,\Omega_2} \le C(h+\sqrt{\lambda})(\|v\|_{2,\Omega_1} + \|v\|_{2,\Omega_2}).$$

Proof. For the H^1-norm estimate, we have

$$\begin{aligned}
&\|v - v_I\|_{1,\Omega_1} + \|v - v_I\|_{1,\Omega_2} \\
&\le \sum_{K\in\mathcal{T}_h\setminus\mathcal{T}_*} \|v - v_I\|_{1,K} + \sum_{K\in\mathcal{T}_*} \|v - v_I\|_{1,K} \\
&\le Ch(\|v\|_{2,\Omega_1} + \|v\|_{2,\Omega_2}) + \sum_{K\in\mathcal{T}_*^1} \|v - v_I\|_{1,K} + \sum_{K\in\mathcal{T}_*^2} \|v - v_I\|_{1,K} \\
&:= Ch(\|v\|_{2,\Omega_1} + \|v\|_{2,\Omega_2}) + J_1 + J_2. \qquad (3.3.13)
\end{aligned}$$

First, we estimate the term J_1 as follows

$$J_1 \le \sum_{K\in\mathcal{T}_*^1} \|v - v_I\|_{1,K\cap\Omega_1} + \sum_{K\in\mathcal{T}_*^1} \|v - v_I\|_{1,K\cap\Omega_2}. \qquad (3.3.14)$$

For any interface element $K \in \mathcal{T}_*^1$, we have $K \subset \Omega_{1,h}$. Also, using the continuity property of the extension operator $\mathcal{E}_1$ and noting the fact that $\cup_{K\in\mathcal{T}_*^1} K\cap\Omega_1 \subset \Omega_1$ yields

$$\begin{aligned}
\sum_{K\in\mathcal{T}_*^1} \|v - v_I\|_{1,K\cap\Omega_1} &= \sum_{K\in\mathcal{T}_*^1} \|\mathcal{E}_1 v - \Pi_h\mathcal{E}_1 v\|_{1,K\cap\Omega_1} \\
&\le \|\mathcal{E}_1 v - \Pi_h\mathcal{E}_1 v\|_{1,\Omega_1} \le Ch\|\mathcal{E}_1 v\|_2 \le Ch\|v\|_{2,\Omega_1}.
\end{aligned}$$

TH-2392_146123010

For the second term in right hand side of (3.3.14), we observe that

$$\begin{aligned}
&\sum_{K\in\mathcal{T}_*^1} \|v - v_I\|_{1,K\cap\Omega_2} \\
&\leq \sum_{K\in\mathcal{T}_*^1} \|\mathcal{E}_2 v - \mathcal{E}_1 v\|_{1,K\cap\Omega_2} + \sum_{K\in\mathcal{T}_*^1} \|\mathcal{E}_1 v - \Pi_h \mathcal{E}_1 v\|_{1,K\cap\Omega_2} \\
&\leq C\sqrt{\lambda}(\|v\|_{2,\Omega_1} + \|v\|_{2,\Omega_2}) + \|\mathcal{E}_1 v - \Pi_h \mathcal{E}_1 v\|_1 \\
&\leq C\sqrt{\lambda}(\|v\|_{2,\Omega_1} + \|v\|_{2,\Omega_2}) + Ch\|\mathcal{E}_1 v\|_2 \\
&\leq C(\sqrt{\lambda} + h)(\|v\|_{2,\Omega_1} + \|v\|_{2,\Omega_2}).
\end{aligned}$$

Here, we have used the continuity of extension operators $\mathcal{E}_l,\ l = 1,\ 2$ and Lemma 3.3.2. Using both estimates in (3.3.14), we obtain

$$J_1 \leq C(h + \sqrt{\lambda})(\|v\|_{2,\Omega_1} + \|v\|_{2,\Omega_2}).$$

Proceeding in a similar way, we derive

$$J_2 \leq C(h + \sqrt{\lambda})(\|v\|_{2,\Omega_1} + \|v\|_{2,\Omega_2}).$$

This completes the rest of the proof. □

Now, we are in a position to define our elliptic projection operator. We define $\mathcal{Q}_h : \tilde{\mathcal{X}} \to V_h$ by

$$\mathcal{A}_{\beta h}(\mathcal{Q}_h v, v_h) = \mathcal{A}_\beta^1(v, v_h) + \mathcal{A}_\beta^2(v, v_h). \tag{3.3.15}$$

Regarding the approximation properties of $\mathcal{Q}_h$ operator defined by (3.3.15), we have the following results. For a proof see Appendix A in Dutta *et al.* [41].

Lemma 3.3.4. *Let $\mathcal{Q}_h$ be defined by (3.3.15), then for any $v \in \tilde{\mathcal{X}}$ there is a positive constant C independent of the mesh parameter h such that*

a. $\|\mathcal{Q}_h v - v\|_{1,\Omega_1} + \|\mathcal{Q}_h v - v\|_{1,\Omega_2} \leq C\Big(h + \sqrt{\lambda} + \dfrac{\lambda}{h}\Big)(\|v\|_{2,\Omega_1} + \|v\|_{2,\Omega_2}),$

b. $\|\mathcal{Q}_h v - v\| \leq C\left(h + \sqrt{\lambda} + \dfrac{\lambda}{h}\right)^2 (\|v\|_{2,\Omega_1} + \|v\|_{2,\Omega_2}).$

Let $\mathcal{L}_h : L^2(\Omega) \to V_h$ be the standard L^2 projection defined by

$$(\mathcal{L}_h v, \phi) = (v, \phi) \ \ \forall \phi \in V_h, \ \ v \in L^2(\Omega). \tag{3.3.16}$$

Previous result along with definition of L^2 projection leads to the following error estimate.

TH-2392_146123010

Lemma 3.3.5. *Let $\mathcal{L}_h$ be defined by (3.3.16), then for any $v \in \tilde{\mathcal{X}}$ there is a positive constant C independent of the mesh size parameter h such that*

$$\|\mathcal{L}_h v - v\| \leq C\left(h + \sqrt{\lambda} + \frac{\lambda}{h}\right)^2 (\|v\|_{2,\Omega_1} + \|v\|_{2,\Omega_2}).$$

For any $v \in H_0^1(\Omega)$, we know that there exists a unique solution $w \in \mathcal{Y}$ for the elliptic interface problem

$$\mathcal{A}_\beta(w, \phi) = (v - \mathcal{Q}_h v, \phi) \ \ \forall \phi \in H_0^1(\Omega). \tag{3.3.17}$$

Equation (3.3.17) together with (3.3.15) and Lemma 1.2.2 leads to

$$\begin{aligned} \|v - \mathcal{Q}_h v\|^2 &= \mathcal{A}_\beta(w - \mathcal{Q}_h w, v - \mathcal{Q}_h v) + \mathcal{A}_\beta(\mathcal{Q}_h w, v - \mathcal{Q}_h v) \\ &\leq C\|w - \mathcal{Q}_h w\|_1 \|v - \mathcal{Q}_h v\|_1 \\ &\quad + \mathcal{A}_{\beta h}(\mathcal{Q}_h v, \mathcal{Q}_h w) - \mathcal{A}_\beta(\mathcal{Q}_h v, \mathcal{Q}_h w) \\ &\leq Ch\|w\|_{\mathcal{Y}} \|v - \mathcal{Q}_h v\|_1 + Ch\|\mathcal{Q}_h v\|_1 \|\mathcal{Q}_h w\|_1 \\ &\leq Ch\|v - \mathcal{Q}_h v\| \|v\|_1. \end{aligned} \tag{3.3.18}$$

Here, we have used the fact that $\|w\|_{\mathcal{Y}} \leq C\|v - \mathcal{Q}_h v\|$ and stability of projection $\mathcal{Q}_h$.

We know $\mathcal{L}_h v$ is the best approximation of $v \in L^2(\Omega)$ with respect to L^2 norm. Thus

$$\|v - \mathcal{L}_h v\| \leq \|v - \mathcal{Q}_h v\| \leq Ch\|v\|_1 \ \forall v \in H_0^1(\Omega). \tag{3.3.19}$$

Now, estimates (3.3.18)-(3.3.19) together with standard inverse estimate $\|\nabla v_h\| \leq Ch^{-1}\|v_h\|$, for all $v \in H_0^1(\Omega)$, we obtain following H^1-stability for L^2 projection

$$\begin{aligned} \|\mathcal{L}_h v\|_1 &\leq \|\mathcal{L}_h v - \mathcal{Q}_h v\|_1 + \|\mathcal{Q}_h v\|_1 \\ &\leq Ch^{-1}\|\mathcal{L}_h v - \mathcal{Q}_h v\| + C\|v\|_1 \leq C\|v\|_1. \end{aligned} \tag{3.3.20}$$

Remark 3.3.1. *Using a similar argument employed for estimates (3.3.18)-(3.3.20) with a natural modification, for all $v \in X$ with $[v] = 0$ along Γ and $v = 0$ on $\partial\Omega$, we find that*

$$\|v - \mathcal{Q}_h v\| + \|v - \mathcal{L}_h v\| \leq Ch(\|v\|_{H^1(\Omega_1)} + \|v\|_{H^1(\Omega_2)}) \tag{3.3.21}$$

and $\|\mathcal{L}_h v\|_1 \leq C(\|v\|_{H^1(\Omega_1)} + \|v\|_{H^1(\Omega_2)})$.

Due to discontinuity of coefficients σ and β, $u''(0)$ satisfying

$$u''(0) = -\sigma v_0 + \nabla \cdot (\beta \nabla u_0) + f(0),$$

may not belongs to $H^1(\Omega)$ even $(u_0, v_0) \in H^3(\Omega) \times H^1(\Omega)$ and $f \in H^1(H^1(\Omega))$. But, for $u \in H^2(0, T; H^1(\Omega_1) \cap H^1(\Omega_2))$ with $[u] = 0$ along Γ and $u = 0$ on $\partial\Omega$, we obtain (cf. [63])

$$[u''] = 0 \text{ on } \Gamma \ \& \ u'' = 0 \text{ on } \partial\Omega.$$

TH-2392_146123010

This together with H^1-stability of L^2 projection yields

$$\begin{aligned}\|\mathcal{L}_h u''(0)\|_{H^1(\Omega)} &\leq C(\|u''(0)\|_{H^1(\Omega_1)} + \|u''(0)\|_{H^1(\Omega_2)}) \\ &\leq C(\|u_0\|_{H^3(\Omega)} + \|v_0\|_{H^1(\Omega)} + \|f\|_{H^1(H^1(\Omega))}). \end{aligned} \tag{3.3.22}$$

Similar argument leads to

$$\|\mathcal{L}_h u'''(0)\|_{H^1(\Omega)} \leq C(\|u_0\|_{H^3(\Omega)} + \|v_0\|_{H^3(\Omega)} + \|f\|_{H^2(H^1(\Omega))}). \tag{3.3.23}$$

3.4 Spatially Semidiscrete Error Estimate Analysis

This section deals with the pointwise-in-time error analysis for the spatially discrete scheme. First we derive stability results for the semidiscrete solution. Optimal order of convergence for $L^\infty(L^2)$ and $L^\infty(H^1)$ norms are established when the global regularity of the solution is low on the entire domain. The stability error analysis is very crucial to established optimal error estimates for fully discrete solution .

The continuous time Galerkin finite element approximation to (3.2.1) is stated as follows: Find $u_h : [0, T] \to V_h$ such that

$$(u_{htt}, v_h) + \mathcal{B}_{\sigma h}(u_{ht}, v_h) + \mathcal{A}_{\beta h}(u_h, v_h) = (f, v_h) \ \ \forall v_h \in V_h, \ t \in (0, T] \tag{3.4.1}$$

with $u_h(0) = \mathcal{Q}_h u_0$ and $u_{ht}(0) = \mathcal{Q}_h v_0$.

Regarding the stability of u_h at the initial stage, we have the following result.

Lemma 3.4.1. *Let u_h satisfy (3.4.1). For $i = 2, 3, 4$, we assume $u_0 \in H_0^1(\Omega) \cap H^i(\Omega)$, $v_0 \in H_0^1(\Omega) \cap H^{i-1}(\Omega)$ and $f \in H^{i-1}(H^1(\Omega))$. Then we have*

$$\|D_t^i u_h(0)\| + \|D_t^{i-1} u_h(0)\|_{H^1(\Omega)} \leq C\big(\|u_0\|_{H^i(\Omega)} + \|v_0\|_{H^{i-1}(\Omega)} + \|f\|_{H^{i-1}(H^1)}\big),$$

where $D_t^i = \frac{\partial^i}{\partial t^i}$.

Proof. Taking the limit as $t \to 0^+$ in (3.4.1) and then using definition of $\mathcal{Q}_h$ operator, we obtain

$$\begin{aligned}(u_{htt}(0), v_h) &= -\mathcal{B}_{\sigma h}(u_{ht}(0), v_h) - \mathcal{A}_{\beta h}(u_h(0), v_h) + (f(0), v_h) \\ &= -(\mathcal{Q}_h v_0, v_h) - \mathcal{A}_{\beta h}(\mathcal{Q}_h u_0, v_h) + (f(0), v_h) \\ &= -(\mathcal{Q}_h v_0, v_h) - \mathcal{A}_{\beta}(u_0, v_h) + (f(0), v_h). \end{aligned} \tag{3.4.2}$$

For the second term in (3.4.2), we use Green's formula and boundary condition to derive

$$\mathcal{A}_\beta(u_0, v_h) = -(\nabla \cdot (\beta \nabla u_0), v_h) \leq C\|u_0\|_{H^2(\Omega)}\|v_h\|. \tag{3.4.3}$$

TH-2392_146123010

Hence, (3.4.2) yields

$$\|u_{htt}(0)\| \leq C(\|u_0\|_{H^2(\Omega)} + \|v_0\|_{H^1(\Omega)} + \|f\|_{H^1(L^2)}). \tag{3.4.4}$$

In the previous estimate, we have used the fact that

$$\sup_{0\leq t\leq T} \|f(t)\| \leq C\|f\|_{H^1(J;W)}.$$

In fact, for any Banach space $\mathcal{B}$, we know that (*cf.* [116], Proposition 7.1)

$$\sup_{0\leq t\leq T} \|v(t)\|_{\mathcal{B}} \leq C\|v\|_{H^1(J;\mathcal{B})} \quad \forall v \in H^1(J;\mathcal{B}). \tag{3.4.5}$$

Again, we know $\mathcal{Q}_h$ is H^1-stable, so

$$\|u_{ht}(0)\|_{H^1(\Omega)} = \|\mathcal{Q}_h v_0\|_{H^1(\Omega)} \leq C\|v_0\|_{H^1(\Omega)}. \tag{3.4.6}$$

For $i = 3$, taking $t \to 0^+$ in (3.2.1) and using (3.4.1), we have

$$\begin{aligned}(u_{htt}(0) - u_{tt}(0), v_h) &= \mathcal{B}_\sigma(v_0, v_h) - \mathcal{B}_{\sigma h}(\mathcal{Q}_h v_0, v_h) + \mathcal{A}_\beta(u_0, v_h) - \mathcal{A}_{\beta h}(\mathcal{Q}_h u_0, v_h)\\ &= \mathcal{B}^{\Delta}_\sigma(v_0, v_h) + \mathcal{B}_{\sigma h}(v_0 - \mathcal{Q}_h v_0, v_h)\\ &\leq Ch\|v_0\|_{H^1(\Omega)}\|v_h\|. \end{aligned} \tag{3.4.7}$$

In the last inequality, we have used Lemma 3.3.1 and Lemma 3.3.4. Then use the definition of L^2 projection and (3.4.7) to obtain

$$\begin{aligned}(u_{htt}(0) - \mathcal{L}_h u_{tt}(0), v_h) &= (u_{htt}(0) - u_{tt}(0), v_h)\\ &\leq Ch\|v_0\|_{H^1(\Omega)}\|v_h\|, \end{aligned} \tag{3.4.8}$$

which imply

$$\|u_{htt}(0) - \mathcal{L}_h u_{tt}(0)\| \leq Ch\|v_0\|_{H^1(\Omega)}. \tag{3.4.9}$$

Estimate (3.4.9) together with inverse inequality and (3.3.22) yields

$$\begin{aligned}\|u_{htt}(0)\|_{H^1(\Omega)} &\leq Ch^{-1}\|u_{htt}(0) - L_h u_{tt}(0)\| + \|L_h u_{tt}(0)\|_{H^1(\Omega)}\\ &\leq C(\|u_0\|_{H^3(\Omega)} + \|v_0\|_{H^1(\Omega)} + \|f\|_{H^1(H^1)}). \end{aligned} \tag{3.4.10}$$

Next, we differentiate (3.4.1) with respect to t and then take $t \to 0^+$ to have

$$\begin{aligned}(u_{httt}(0), v_h) &= -\mathcal{B}_{\sigma h}(u_{htt}(0), v_h) - \mathcal{A}_{\beta h}(\mathcal{Q}_h v_0, v_h) + (f_t(0), v_h)\\ &= -\mathcal{B}_{\sigma h}(u_{htt}(0), v_h) - \mathcal{A}_\beta(v_0, v_h) + (f_t(0), v_h). \end{aligned} \tag{3.4.11}$$

TH-2392_146123010

Following the arguments as in (3.4.4), it is easy to establish that

$$\|u_{htttt}(0)\| \leq C\Big(\|u_0\|_{H^2(\Omega)} + \|v_0\|_{H^2(\Omega)} + \|f\|_{H^2(L^2)}\Big). \tag{3.4.12}$$

For $i = 4$, we first observe that

$$\begin{aligned}
(u_{htttt}(0), v_h) &= -\mathcal{B}_{\sigma h}(u_{httt}(0), v_h) - \mathcal{A}_{\beta h}(u_{htt}(0), v_h) + (f_{tt}(0), v_h) \\
&= -\mathcal{B}_{\sigma h}(u_{httt}(0), v_h) - \mathcal{A}_{\beta h}(u_{htt}(0) - \mathcal{Q}_h u_{tt}(0), v_h) \\
&\quad -\mathcal{A}_{\beta}(u_{tt}(0), v_h) + (f_{tt}(0), v_h) \\
&= -\mathcal{B}_{\sigma h}(u_{httt}(0), v_h) - \mathcal{A}_{\beta h}(u_{htt}(0) - \mathcal{Q}_h u_{tt}(0), v_h) \\
&\quad +(\nabla \cdot (\beta \nabla u_{tt}(0)), v_h) + (f_{tt}(0), v_h) \\
&\leq C\big(\|u_{httt}(0)\| + h^{-1}\|u_{htt}(0) - \mathcal{Q}_h u_{tt}(0)\|_{H^1(\Omega)} \\
&\qquad + \sum_{l=1}^{2} \|u_{tt}(0)\|_{H^2(\Omega_l)} + \|f\|_{H^3(L^2)}\big)\|v_h\|.
\end{aligned} \tag{3.4.13}$$

From (3.4.8), we have

$$\begin{aligned}
&\|u_{htt}(0) - \mathcal{Q}_h u_{tt}(0)\|_{H^1(\Omega)} \\
&\leq Ch^{-1}\|u_{htt}(0) - \mathcal{L}_h u_{tt}(0)\| + \|\mathcal{L}_h u_{tt}(0) - \mathcal{Q}_h u_{tt}(0)\|_{H^1(\Omega)} \\
&\leq Ch\|v_0\|_{H^2(\Omega)} + Ch\sum_{l=1}^{2} \|u_{tt}(0)\|_{H^2(\Omega_l)}.
\end{aligned} \tag{3.4.14}$$

In the last inequality, we have used equation (3.4.8), Lemma 3.3.4 and Lemma 3.3.5. Estimate (3.4.14) together with (3.4.12) and (3.4.13) leads to

$$\|u_{htttt}(0)\| \leq C\big(\|u_0\|_{H^4(\Omega)} + \|v_0\|_{H^2(\Omega)} + \|f\|_{H^3(H^2)}\big). \tag{3.4.15}$$

Now, using the same argument employed in (3.4.10), we obtain

$$\begin{aligned}
\|u_{httt}(0)\|_{H^1(\Omega)} &\leq Ch^{-1}\|u_{httt}(0) - \mathcal{L}_h u_{ttt}(0)\| + \|\mathcal{L}_h u_{ttt}(0)\|_{H^1(\Omega)} \\
&\leq C(\|u_0\|_{H^3(\Omega)} + \|v_0\|_{H^3(\Omega)} + \|f\|_{H^2(H^1)}).
\end{aligned} \tag{3.4.16}$$

This completes the rest of the proof. □

Differentiating (3.4.1) twice with respect to t and then substitute $v_h = u_{httt}$ to obtain

$$\frac{1}{2}\frac{d}{dt}\|u_{htt}\|^2 + \mathcal{B}_{\sigma h}(u_{htt}, u_{htt}) + \frac{1}{2}\frac{d}{dt}\mathcal{A}_{\beta h}(u_{ht}, u_{htt}) = (f_{tt}, u_{htt}). \tag{3.4.17}$$

Integrating (3.4.17) from 0 to t and Lemma 3.4.1 leads to

$$\begin{aligned}
&\|u_{htt}\|^2 + \int_0^t \|u_{htt}\|^2 ds + \|u_{ht}\|^2_{H^1(\Omega)} \\
&\leq C\Big(\|u_0\|^2_{H^3(\Omega)} + \|v_0\|^2_{H^2(\Omega)} + \|f\|^2_{H^2(H^1)}\Big).
\end{aligned}$$

TH-2392_146123010

Proceeding in a similar way and using Lemma 3.4.1, we obtain following stability results for the semidiscrete solution u_h satisfying equation (3.4.1).

Lemma 3.4.2. *Let u_h be the solution of (3.4.1), then for $i = 2, 3, 4$, we have*

$$\|D_t^i u_h\|^2_{L^2(L^2)} \leq C\Big(\|u_0\|^2_{H^i(\Omega)} + \|v_0\|^2_{H^{i-1}(\Omega)} + \|f\|^2_{H^{i-1}(H^1)}\Big). \tag{3.4.18}$$

Remark 3.4.1. *Analogue of Lemma 3.4.2, for $u \in H^i(0, T; X)$, we assume following a priori estimates for our solution u satisfying (3.1.1)-(3.1.3)*

$$\|D_t^i u\|^2_{L^2(L^2)} \leq C\Big(\|u_0\|^2_{H^i(\Omega)} + \|v_0\|^2_{H^{i-1}(\Omega)} + \|f\|^2_{H^{i-1}(H^1)}\Big), \quad i = 2, 3, 4.$$

Above a priori bounds together with estimates (3.2.6) and (3.4.5) yields

$$\begin{aligned}&\sum_{i=1}^{2} \left\{\|u\|^2_{H^2(H^1(\Omega_i))} + \|u\|^2_{H^1(H^2(\Omega_i))}\right\} + \sup_{t\in[0,T]} \|u(t)\|^2_{H^2(\Omega_i)} \\ &\leq C\Big(\|u_0\|^2_{H^3(\Omega)} + \|v_0\|^2_{H^2(\Omega)} + \|f\|^2_{H^2(H^1)}\Big).\end{aligned} \tag{3.4.19}$$

Now, we prove the convergence result for the semidiscrete scheme in $L^\infty(L^2)$-norm.

Theorem 3.4.1. *Let u and u_h be the solutions of the problem (3.1.1)-(3.1.3) and (3.4.1), respectively. Then, for $u_0 \in H^3(\Omega)\cap H_0^1(\Omega)$, $v_0 \in H^2(\Omega)\cap H_0^1(\Omega)$ and $f \in H^2(J; L^2(\Omega))\cap H^1(J; H^1(\Omega))$, we have*

$$\|u - u_h\|_{L^\infty(0,T;L^2(\Omega))} \leq C(u_0, v_0, f)\left(h + \sqrt{\lambda} + \frac{\lambda}{h}\right)^2,$$

where $C(u_0, v_0, f) := C\left\{\|u_0\|_3^2 + \|v_0\|_2^2 + \|f\|^2_{H^1(H^1)} + \|f\|^2_{H^2(L^2)}\right\}^{\frac{1}{2}}$.

Proof. Subtracting (3.2.1) from (3.4.1), we obtain

$$\begin{aligned}&(u_{htt} - u_{tt}, v_h) + \mathcal{B}_{\sigma h}(u_{ht} - u_t, v_h) + \mathcal{A}_{\beta h}(u_h - u, v_h) \\ &= \mathcal{B}_\sigma(u_t, v_h) - \mathcal{B}_{\sigma h}(u_t, v_h) + \mathcal{A}_\beta(u, v_h) - \mathcal{A}_{\beta h}(u, v_h)\ \forall v_h \in V_h.\end{aligned} \tag{3.4.20}$$

Define the error $e(t)$ as $e(t) := u_h(t) - u(t)$. Then we have the following error equation

$$\begin{aligned}(e_{tt}, v_h) + \mathcal{B}_{\sigma h}(e_t, v_h) + \mathcal{A}_{\beta h}(e, v_h) \;&=\; \mathcal{B}_\sigma(u_t, v_h) - \mathcal{B}_{\sigma h}(u_t, v_h) \\ &\quad + \mathcal{A}_\beta(u, v_h) - \mathcal{A}_{\beta h}(u, v_h)\ \forall v_h \in V_h.\end{aligned} \tag{3.4.21}$$

Further, splitting $e(t)$ into standard ρ and θ arguments, we obtain

$$e = \rho - \theta,\ \rho := u_h - \mathcal{Q}_h u,\ \theta := u - \mathcal{Q}_h u.$$

TH-2392_146123010

Then equation (3.4.21) reduces to

$$\begin{aligned}(e_{tt}, v_h) + \mathcal{B}_{\sigma h}(e_t, v_h) + \mathcal{A}_{\beta h}(\rho, v_h) &= \mathcal{B}_{\sigma}(u_t, v_h) - \mathcal{B}_{\sigma h}(u_t, v_h) + \mathcal{A}_{\beta h}(\theta, v_h) \\ &\quad + \mathcal{A}_{\beta}(u, v_h) - \mathcal{A}_{\beta h}(u, v_h)\ \forall v_h \in V_h. \quad (3.4.22)\end{aligned}$$

Using the definition of $\mathcal{Q}_h$, we observe that

$$\mathcal{A}_{\beta h}(\theta, v_h) = \mathcal{A}_{\beta h}(u, v_h) - \mathcal{A}_{\beta h}(\mathcal{Q}_h u, v_h) = \mathcal{A}_{\beta h}(u, v_h) - \mathcal{A}_{\beta}(u, v_h). \quad (3.4.23)$$

Above equation together with (3.4.22) leads to

$$(e_{tt}, v_h) + \mathcal{B}_{\sigma h}(e_t, v_h) + \mathcal{A}_{\beta h}(\rho, v_h) = \mathcal{B}_{\sigma}(u_t, v_h) - \mathcal{B}_{\sigma h}(u_t, v_h)\ \forall v_h \in V_h. \quad (3.4.24)$$

Following Baker [15], we define $\hat{\rho} : [0, T] \times \Omega \to \mathbb{R}$ as

$$\hat{\rho}(., t) = \int_t^{\xi} \rho(., s) ds\ , \quad 0 \le t \le T,$$

for some fixed $\xi \in [0, T]$. Then, clearly $\hat{\rho} \in V_h$ as $\rho = u_h - \mathcal{Q}_h u \in V_h$. Also, observe that

$$\hat{\rho}(., \xi) = 0 \ \text{ and } \ \hat{\rho}_t(., t) = -\rho(., t)\ , \ \ 0 \le t \le T. \quad (3.4.25)$$

Set $v_h = \hat{\rho}$ in (3.4.24), integrate between 0 to ξ with respect to the variable t and integrate by parts the first two terms on the left-hand side to obtain

$$\begin{aligned}&(e_t(\xi), \hat{\rho}(\xi)) - \int_0^{\xi} (e_t, \hat{\rho}_t) ds + \mathcal{B}_{\sigma h}(e(\xi), \hat{\rho}(\xi)) - \int_0^{\xi} \mathcal{B}_{\sigma h}(e, \hat{\rho}_t) ds + \int_0^{\xi} \mathcal{A}_{\beta h}(\rho, \hat{\rho}) ds \\ &= (e_t(0), \hat{\rho}(0)) + \mathcal{B}_{\sigma h}(e(0), \hat{\rho}(0)) + \int_0^{\xi} \big\{\mathcal{B}_{\sigma}(u_t, \hat{\rho}) - \mathcal{B}_{\sigma h}(u_t, \hat{\rho})\big\} ds. \quad (3.4.26)\end{aligned}$$

Now, using (3.4.25) in (3.4.26), we have

$$\begin{aligned}&\int_0^{\xi} \frac{1}{2} \frac{d}{dt} \|\rho\|^2 ds + \int_0^{\xi} \mathcal{B}_{\sigma h}(\rho, \rho) ds - \int_0^{\xi} \frac{1}{2} \frac{d}{dt} \mathcal{A}_{\beta h}(\hat{\rho}, \hat{\rho}) ds \\ &= (e_t(0), \hat{\rho}(0)) + \mathcal{B}_{\sigma h}(e(0), \hat{\rho}(0)) + \int_0^{\xi} (\theta_t, \rho) ds + \int_0^{\xi} \mathcal{B}_{\sigma h}(\theta, \rho) ds \\ &\quad + \int_0^{\xi} \big\{\mathcal{B}_{\sigma}(u_t, \hat{\rho}) - \mathcal{B}_{\sigma h}(u_t, \hat{\rho})\big\} ds,\end{aligned}$$

which yields

$$\begin{aligned}&\frac{1}{2} \|\rho(\xi)\|^2 - \frac{1}{2} \|\rho(0)\|^2 + \int_0^{\xi} \mathcal{B}_{\sigma h}(\rho, \rho) ds + \frac{1}{2} \mathcal{A}_{\beta h}(\hat{\rho}(0), \hat{\rho}(0)) \\ &= (e_t(0), \hat{\rho}(0)) + \mathcal{B}_{\sigma h}(e(0), \hat{\rho}(0)) + \int_0^{\xi} (\theta_t, \rho) ds + \int_0^{\xi} \mathcal{B}_{\sigma h}(\theta, \rho) ds \\ &\quad + \int_0^{\xi} \big\{\mathcal{B}_{\sigma}(u_t, \hat{\rho}) - \mathcal{B}_{\sigma h}(u_t, \hat{\rho})\big\} ds.\end{aligned}$$

TH-2392_146123010

Now, we use the fact that both $\mathcal{B}_\sigma$ and $\mathcal{B}_{\sigma h}$ are bounded, and then using Lemma 3.3.1 and Lemma 3.3.4 leads to

$$\begin{aligned}
&\frac{1}{2}\|\rho(\xi)\|^2 - \frac{1}{2}\|\rho(0)\|^2 + \int_0^\xi \mathcal{B}_{\sigma h}(\rho,\rho)ds + \frac{1}{2}\mathcal{A}_{\beta h}(\hat{\rho}(0),\hat{\rho}(0)) \\
&\leq C\Bigg(\|(e(0)+e_t(0))\|\|\hat{\rho}(0)\| + \left(h+\sqrt{\lambda}+\frac{\lambda}{h}\right)^2 \max_{0\leq t\leq T}\|\rho(t)\| \int_0^\xi \|u_t\|_{\mathcal{X}} ds \\
&\quad + \left(h+\sqrt{\lambda}+\frac{\lambda}{h}\right)^2 \max_{0\leq t\leq T}\|\rho(t)\| \int_0^\xi \|u\|_{\mathcal{X}} ds \\
&\quad + \left(h+\sqrt{\lambda}+\frac{\lambda}{h}\right)^2 \int_0^\xi \|u_t\|_{\mathcal{X}}\|\hat{\rho}\| ds \Bigg).
\end{aligned}$$

Since ρ is continuous in the time variable, we select ξ such that $\|\rho(\xi)\| = \max_{0\leq t\leq T}\|\rho(t)\|$. Then we observe that $\|\hat{\rho}(t)\| \leq C\|\rho(\xi)\|,\ (0 \leq t \leq T)$, which gives

$$\|\rho(\xi)\| \leq C\left(\|\rho(0)\| + \|e(0)\| + \left(h+\sqrt{\lambda}+\frac{\lambda}{h}\right)^2 \|u\|_{H^1(0,T;\mathcal{X})}\right). \tag{3.4.27}$$

This together with estimate (3.4.19) and Lemma 3.3.4 leads to Theorem 3.4.1. □

Standard inverse inequality, together with estimates (3.4.19) and (3.4.27), and Lemma 3.3.4 leads to following $L^\infty(H^1)$ norm error estimate

Theorem 3.4.2. *Let u and u_h be the solutions of the problem (3.1.1)-(3.1.3) and (3.4.1), respectively. Then, for $u_0 \in H^3(\Omega)\cap H_0^1(\Omega),\ v_0 \in H^2(\Omega)\cap H_0^1(\Omega)$ and $f \in H^2(J;L^2(\Omega))\cap H^1(J;H^1(\Omega))$, we have*

$$\|u-u_h\|_{L^\infty(0,T;H^1(\Omega))} \leq C(u_0,v_0,f)\left(h+\sqrt{\lambda}+\frac{\lambda}{h}\right),$$

where $C(u_0,v_0,f) := C\left\{\|u_0\|_3^2 + \|v_0\|_2^2 + \|f\|_{H^1(H^1)}^2 + \|f\|_{H^2(L^2)}^2\right\}^{\frac{1}{2}}$.

3.5 Fully Discrete Error Analysis

In this section, we extend the spatially discrete *a priori* error analysis to the fully discrete approximation for the hyperbolic heat conduction model problem (3.1.1)-(3.1.3). We consider discretizing the interface problem by rewriting the governing equation in the first-order system and then Crank-Nicolson scheme is applied, as in Baker [15]. Optimal order of convergence in $L^\infty(L^2)$ norm is derived for the fully discrete solution.

For the temporal discretization, we introduce an auxiliary unknown $v = u_t$ to reduce the model equation (3.1.1) as the following first-order in time system

$$\begin{cases} u_t - v = 0 & \text{in } \Omega\times(0,T], \\ v_t + \sigma u_t - \nabla\cdot(\beta\nabla u) = f & \text{in } \Omega\times(0,T]. \end{cases} \tag{3.5.1}$$

TH-2392_146123010

Next we divide time interval $J = [0, T]$ into N equally spaced subintervals $I_n = (t_{n-1}, t_n]$, $n = 1, 2, \ldots, N$ with $t_0 = 0$ and $t_N = T$, and $\tau = t_n - t_{n-1}$, the time step. For a sequence $\{v^n\}_{n=0}^N \subset L^2(\Omega)$, we define

$$\partial_\tau v^n = \frac{v^{n+1} - v^n}{\tau} \quad \text{and} \quad v^{n+\frac{1}{2}} = \frac{1}{2}(v^{n+1} + v^n), \;\; n = 0, 1, \ldots, N-1.$$

Also, for a continuous mapping $\phi : [0, T] \to L^2(\Omega)$, we define $\phi^n = \phi(., t_n)$, $0 \le n \le N$.

Now, applying Crank-Nicolson discretization to both equations in (3.5.1) we get a second order in time scheme. The fully discretized method is defined as follows: Compute $U^n, v^n \in V_h$ for $n = 0, 1, \ldots, N-1$ from the system

$$\begin{cases} \partial_\tau U^n = v^{n+\frac{1}{2}}, \\ (\partial_\tau v^n, \psi) + \mathcal{B}_{\sigma h}(v^{n+\frac{1}{2}}, \psi) + \mathcal{A}_{\beta h}(U^{n+\frac{1}{2}}, \psi) = (f^{n+\frac{1}{2}}, \psi) \;\; \forall\, \phi \in V_h, \end{cases} \tag{3.5.2}$$

with $U^0 = \mathcal{Q}_h u_0$ and $v^0 = \mathcal{Q}_h v_0$.

The following Lemma gives the existence and uniqueness of the fully discrete solution U^n of u.

Lemma 3.5.1. *There exists a unique sequence $\{U^n\}_{n=0}^N \subset V_h$ and a corresponding unique sequence $\{v^n\}_{n=0}^N \subset V_h$ satisfying (3.5.2).*

Proof. From (3.5.2), we have

$$U^{n+1} = \frac{\tau}{2}(v^{n+1} + v^n) + U^n \tag{3.5.3}$$

and

$$\begin{aligned} &(v^{n+1}, \psi) + \frac{\tau}{2}\mathcal{B}_{\sigma h}(v^{n+1}, \psi) + \frac{\tau^2}{4}\mathcal{A}_{\beta h}(v^{n+1}, \psi) \\ &= (v^n, \psi) - \frac{\tau}{2}\mathcal{B}_{\sigma h}(v^n, \psi) - \tau\mathcal{A}_{\beta h}(U^n, \psi) \\ &\quad - \frac{\tau^2}{4}\mathcal{A}_{\beta h}(v^n, \psi) + \tau(f^{n+\frac{1}{2}}, \psi) \; \forall \psi \in V_h. \end{aligned} \tag{3.5.4}$$

Due to the positivity of bilinear forms $\mathcal{B}_{\sigma h}$ and $\mathcal{A}_{\beta h}$, there exists uniquely defined $v^{n+1} \in V_h$ satisfying equation (3.5.4) and subsequently U^{n+1} exists uniquely for $n = 0, 1, \ldots, N-1$. □

Later on, we will be required the following result. The proof involves the use of Taylor's series and standard arguments, and therefore, details are omitted.

Lemma 3.5.2. *For any $v \in H^3(0, T; L^2(\Omega))$, we have*

$$\|\partial_\tau v^n - v_t^{n+\frac{1}{2}}\|^2 \le C\tau^3 \int_{t_n}^{t_{n+1}} \|v_{ttt}\|^2 dt.$$

TH-2392_146123010

In order to compute the error between U^n and u^n, it suffices to establish the error $\xi^n := u_h^n - U^n$, for $1 \le n \le N$. Once we have estimates for ξ^n, we can easily get the error estimates for $e^n := U^n - u^n$ by using the triangle inequality and Theorem 3.4.1

Lemma 3.5.3. *Let u and U^n be the solutions of the interface problem (3.1.1)-(3.1.3) and the finite element approximation (3.5.2) at time $t = t_n$, respectively. Then, we have*

$$\max_{0\le n\le N} \|\xi^n\|^2 \le C\tau^4\Big(\int_0^T \|u_{htttt}\|^2 dt + \int_0^T \|u_{httt}\|^2 dt\Big).$$

Proof. Substitute $t = t_n$ and $t = t_{n+1}$ in (3.4.1) and then add to have

$$(\partial_\tau u_{ht}^n, \psi) + \mathcal{B}_{\sigma h}(u_{ht}^{n+\frac{1}{2}}, \psi) + \mathcal{A}_{\beta h}(u_h^{n+\frac{1}{2}}, \psi) = (f^{n+\frac{1}{2}}, \psi) + (\zeta^n, \psi) \ \ \forall \psi \in V_h, \tag{3.5.5}$$

where $\zeta^n := \partial_\tau u_{ht}^n - u_{htt}^{n+\frac{1}{2}}$.

Now, it follows immediately from (3.5.2) and (3.5.5) that

$$(\partial_\tau \eta^n, \psi) + \mathcal{B}_{\sigma h}(\eta^{n+\frac{1}{2}}, \psi) + \mathcal{A}_{\beta h}(\xi^{n+\frac{1}{2}}, \psi) = (\zeta^n, \psi) \ \ \forall \psi \in V_h, \tag{3.5.6}$$

with $\eta^n := u_{ht}^n - v^n$.

It is easy to observe that

$$\partial_\tau \xi^n = \eta^{n+\frac{1}{2}} + \partial_\tau u_h^n - u_{ht}^{n+\frac{1}{2}} = \eta^{n+\frac{1}{2}} + \sigma^n, \ \sigma^n := \partial_\tau u_h^n - u_{ht}^{n+\frac{1}{2}}. \tag{3.5.7}$$

Now, we define a sequence $\{\alpha^n\}_{n=0}^N$ such that $\alpha^0 = 0$ and

$$\alpha^n = \tau \sum_{k=0}^{n-1} \xi^{k+\frac{1}{2}}, \ n = 1, \ldots, N-1.$$

Then, we note that

$$\alpha^{\frac{1}{2}} = \frac{\tau}{4}\xi^1 \ \text{ and } \ \alpha^{n+\frac{1}{2}} = \frac{1}{2}(\alpha^{n+1} + \alpha^n) = \frac{\tau}{2}\left[\sum_{k=0}^{n} \xi^{k+\frac{1}{2}} + \sum_{k=0}^{n-1} \xi^{k+\frac{1}{2}}\right]. \tag{3.5.8}$$

Here, we have used the fact that $\xi^0 = u_h^0 - U^0 = \mathcal{Q}_h u_0 - \mathcal{Q}_h u_0 = 0$. Further, since $\eta^0 = u_{ht}^0 - v^0 = \mathcal{Q}_h v_0 - v_0 = 0$, it follows from (3.5.7) that

$$\eta^1 = \frac{2}{\tau}\xi^1 - 2\sigma^0.$$

Using the above identity in (3.5.6), for $n = 0$, leads to

$$\begin{aligned} &\frac{2}{\tau^2}(\xi^1, \psi) + \frac{1}{\tau}\mathcal{B}_{\sigma h}(\xi^1, \psi) + \frac{1}{\tau}\mathcal{A}_{\beta h}(\alpha^1, \psi) \\ &= (\zeta^0, \psi) + \frac{2}{\tau}(\sigma^0, \psi) + \mathcal{B}_{\sigma h}(\sigma^0, \psi) \ \ \forall \psi \in V_h. \end{aligned} \tag{3.5.9}$$

TH-2392_146123010

Substituting $\psi = \xi^1 = \frac{2}{\tau}\alpha^1$ in (3.5.9) and using the coercivity of $\mathcal{A}_{\beta h}$, and the fact that $\mathcal{B}_{\sigma h}(\xi^1, \xi^1) \geq 0$, we obtain

$$(\xi^1, \xi^1) + \|\nabla\alpha^1\|^2 \leq \frac{\tau^2}{2}(\zeta^0, \xi^1) + \tau(\sigma^0, \xi^1) + \frac{\tau^2}{2}\mathcal{B}_{\sigma h}(\sigma^0, \xi^1).$$

Next, use Cauchy-Schwartz and Young's inequality to have

$$\begin{aligned}\|\xi^1\|^2 + \|\nabla\alpha^1\|^2 &\leq C\Big(\frac{\tau^2}{2}\|\zeta^0\|\|\xi^1\| + \tau\|\sigma^0\|\|\xi^1\| + \frac{\tau^2}{2}\|\sigma^0\|\|\xi^1\|\Big)\\ &\leq C\Big(\frac{\tau^4}{4}\|\zeta^0\|^2 + \tau^2\|\sigma^0\|^2 + \mu\|\xi^1\|^2\Big).\end{aligned}$$

Finally, appropriate $\mu > 0$ leads to

$$\|\xi^1\|^2 + \|\nabla\alpha^1\|^2 \leq C\Big(\frac{\tau^4}{4}\|\zeta^0\|^2 + \tau^2\|\sigma^0\|^2\Big). \tag{3.5.10}$$

Now, for $1 \leq n \leq N-1$, we observe that

$$\xi^n = \tau\sum_{k=0}^{n-1}\partial_\tau\xi^k, \quad \eta^n = \tau\sum_{k=0}^{n-1}\partial_\tau\eta^k.$$

Hence, it follows from (3.5.7) that

$$\begin{aligned}\partial_\tau\xi^n &= \frac{\tau}{2}\Big[\sum_{k=0}^{n}\partial_\tau\eta^k + \sum_{k=0}^{n-1}\partial_\tau\eta^k\Big] + \sigma^n,\\ \xi^{n+\frac{1}{2}} &= \frac{\tau}{2}\Big[\sum_{k=0}^{n}\eta^{k+\frac{1}{2}} + \sum_{k=0}^{n-1}\eta^{k+\frac{1}{2}}\Big] + \frac{\tau}{2}\Big[\sum_{k=0}^{n}\sigma^k + \sum_{k=0}^{n-1}\sigma^k\Big].\end{aligned}$$

Hence, for any $\psi \in V_h$, from above identities together with (3.5.8), we have

$$\begin{aligned}&(\partial_\tau\xi^n, \psi) + \mathcal{B}_{\sigma h}(\xi^{n+\frac{1}{2}}, \psi) + \mathcal{A}_{\beta h}(\alpha^{n+\frac{1}{2}}, \psi)\\ &= \frac{\tau}{2}\Big(\Big[\sum_{k=0}^{n}\partial_\tau\eta^k + \sum_{k=0}^{n-1}\partial_\tau\eta^k\Big], \psi\Big) + \frac{\tau}{2}\mathcal{B}_{\sigma h}\Big(\Big[\sum_{k=0}^{n}\eta^{k+\frac{1}{2}} + \sum_{k=0}^{n-1}\eta^{k+\frac{1}{2}}\Big], \psi\Big)\\ &\quad + (\sigma^n, \psi) + \frac{\tau}{2}\mathcal{B}_{\sigma h}\Big(\Big[\sum_{k=0}^{n}\sigma^k + \sum_{k=0}^{n-1}\sigma^k\Big], \psi\Big)\\ &\quad + \frac{\tau}{2}\mathcal{A}_{\beta h}\Big(\Big[\sum_{k=0}^{n}\xi^{k+\frac{1}{2}} + \sum_{k=0}^{n-1}\xi^{k+\frac{1}{2}}\Big], \psi\Big)\\ &= \frac{\tau}{2}\Big(\partial_\tau\eta^n + 2\sum_{k=0}^{n-1}\partial_\tau\eta^k, \psi\Big) + (\sigma^n, \psi) + \frac{\tau}{2}\mathcal{B}_{\sigma h}\Big(\eta^{n+\frac{1}{2}} + 2\sum_{k=0}^{n-1}\eta^{k+\frac{1}{2}}, \psi\Big)\\ &\quad + \frac{\tau}{2}\mathcal{B}_{\sigma h}\Big(\sigma^n + 2\sum_{k=0}^{n-1}\sigma^k, \psi\Big) + \frac{\tau}{2}\mathcal{A}_{\beta h}\Big(\xi^{n+\frac{1}{2}} + 2\sum_{k=0}^{n-1}\xi^{k+\frac{1}{2}}, \psi\Big).\end{aligned}$$

TH-2392_146123010

Using (3.5.6), for $1 \leq n \leq N-1$, we derive

$$(\partial_\tau \xi^n, \psi) + \mathcal{B}_{\sigma h}(\xi^{n+\frac{1}{2}}, \psi) + \mathcal{A}_{\beta h}(\alpha^{n+\frac{1}{2}}, \psi) = (T_1^n, \psi) + \mathcal{B}_{\sigma h}(T_2^n, \psi)\ \forall \psi \in V_h, \quad (3.5.11)$$

where

$$T_1^n := \frac{\tau}{2}\zeta^n + \tau \sum_{k=0}^{n-1} \zeta^k + \sigma^n \ \ \& \ \ T_2^n := \frac{\tau}{2}\sigma^n + \tau \sum_{k=0}^{n-1} \sigma^k.$$

Substitute $\psi = \xi^{n+\frac{1}{2}} = \partial_\tau \alpha^n$ in (3.5.11) to obtain

$$\begin{aligned} &\|\xi^{n+1}\|^2 - \|\xi^n\|^2 + 2\tau \mathcal{B}_{\sigma h}(\xi^{n+\frac{1}{2}}, \xi^{n+\frac{1}{2}}) + \mathcal{A}_{\beta h}(\alpha^{n+1}, \alpha^{n+1}) \\ &= 2\tau (T_1^n, \xi^{n+\frac{1}{2}}) + 2\tau \mathcal{B}_{\sigma h}(T_2^n, \xi^{n+\frac{1}{2}}) + \mathcal{A}_{\beta h}(\alpha^n, \alpha^n). \end{aligned}$$

Since $\mathcal{B}_{\sigma h}(\xi^{n+\frac{1}{2}}, \xi^{n+\frac{1}{2}}) \geq 0$, so we obtain

$$\begin{aligned} \|\xi^{n+1}\|^2 - \|\xi^n\|^2 + \mathcal{A}_{\beta h}(\alpha^{n+1}, \alpha^{n+1}) \ &\leq \ \mathcal{A}_{\beta h}(\alpha^n, \alpha^n) + 2\tau (T_1^n, \xi^{n+\frac{1}{2}}) \\ &\quad + 2\tau \mathcal{B}_{\sigma h}(T_2^n, \xi^{n+\frac{1}{2}}). \end{aligned} \quad (3.5.12)$$

Now, simple use of Cauchy-Schwartz inequality and coercivity of $\mathcal{A}_{\beta h}$, equation (3.5.12) leads to

$$\begin{aligned} &\|\xi^{n+1}\|^2 - \|\xi^n\|^2 + \|\nabla \alpha^{n+1}\|^2 - \|\nabla \alpha^n\|^2 \\ &\leq \tau \|T_1^n\| \|\xi^{n+\frac{1}{2}}\| + \tau \|T_2^n\| \|\xi^{n+\frac{1}{2}}\|. \end{aligned} \quad (3.5.13)$$

Using Young's inequality in the right hand side of (3.5.13) and then summing from $n = 1$ to $n = l-1$ with $2 \leq l \leq N$, we obtain

$$\begin{aligned} \|\xi^l\|^2 + \|\nabla \alpha^l\|^2 \ &\leq \ \|\xi^1\|^2 + \|\nabla \alpha^1\|^2 + \tau \sum_{n=1}^{l-1} \|T_1^n\|^2 + \tau \sum_{n=1}^{l-1} \|T_2^n\|^2 \\ &\quad + \tau\mu \sum_{n=1}^{l-1} \|\xi^{n+\frac{1}{2}}\|^2 \\ &\leq \ \|\xi^1\|^2 + \|\nabla \alpha^1\|^2 + \tau \sum_{n=1}^{l-1} \|T_1^n\|^2 + \tau \sum_{n=1}^{l-1} \|T_2^n\|^2 \\ &\quad + \mu \max_{2 \leq n \leq N} \|\xi^n\|^2. \end{aligned}$$

Choosing $\mu > 0$ appropriately and observing that $\|\nabla \alpha^l\| \geq 0$, we obtain

$$\max_{2 \leq n \leq N} \|\xi^n\|^2 \leq C \left(\|\xi^1\|^2 + \|\nabla \alpha^1\|^2 + \tau \sum_{n=1}^{l-1} \left(\|T_1^n\|^2 + \|T_2^n\|^2 \right) \right). \quad (3.5.14)$$

TH-2392_146123010

Combining (3.5.10) and (3.5.14), we have

$$\max_{1\le n\le N}\|\xi^n\|^2 \le C\left(\tau^4\|\zeta^0\|^2+\tau^2\|\sigma^0\|^2+\tau\sum_{n=1}^{l-1}\left(\|T_1^n\|^2+\|T_2^n\|^2\right)\right). \tag{3.5.15}$$

Now, we shall estimate both terms T_1^n and T_2^n. For the estimation of T_1^n, use triangle inequality and Cauchy-Schwartz inequality to have

$$\begin{aligned}\|T_1^n\|^2 &\le C\Big(\frac{\tau^2}{4}\|\zeta^n\|^2+\tau^2\|\sum_{k=0}^{n-1}\zeta^k\|^2+\|\sigma^n\|^2\Big)\\ &\le C\Big(\frac{\tau^2}{4}\|\zeta^n\|^2+\tau^2N\sum_{k=0}^{n-1}\|\zeta^k\|^2+\|\sigma^n\|^2\Big)\\ &\le C\Big(\frac{\tau^2}{4}\|\zeta^n\|^2+\tau T\sum_{k=0}^{n-1}\|\zeta^k\|^2+\|\sigma^n\|^2\Big).\end{aligned} \tag{3.5.16}$$

Then, using Lemma 3.5.2, we obtain

$$\begin{aligned}\|T_1^n\|^2 &\le C\Big(\tau^5\int_{t_n}^{t_{n+1}}\|u_{htttt}\|^2dt+\tau^4\int_0^T\|u_{htttt}\|^2dt\\ &\quad+\tau^3\int_{t_n}^{t_{n+1}}\|u_{httt}\|^2dt\Big).\end{aligned} \tag{3.5.17}$$

The following estimate for T_2^n is achieved using the same technique as used for deriving T_1^n

$$\|T_2^n\|^2 \le C\Big(\tau^5\int_{t_n}^{t_{n+1}}\|u_{httt}\|^2dt+\tau^4\int_0^T\|u_{httt}\|^2dt\Big). \tag{3.5.18}$$

Finally, using (3.5.17)-(3.5.18) in (3.5.15), we obtain

$$\max_{1\le n\le N}\|\xi^n\|^2 \le C\tau^4\Big(\int_0^T\|u_{htttt}\|^2dt+\int_0^T\|u_{httt}\|^2dt\Big). \quad \square$$

Now, we are in a position to state the main result of this section.

Theorem 3.5.1. *Let u and U^n be the solutions of the interface problem (3.1.1)-(3.1.3) and the finite element approximation (3.5.2) at time $t=t_n$, respectively. Assume that $u_0\in H^4(\Omega)\cap H_0^1(\Omega)$, $v_0\in H^3(\Omega)\cap H_0^1(\Omega)$ and $f\in H^3(J;L^2(\Omega))\cap H^1(J;H^1(\Omega))$, then we have*

$$\max_{0\le n\le N}\|u^n-U^n\| \le \tilde{C}(u_0,v_0,f)\left(\left(h+\sqrt{\lambda}+\frac{\lambda}{h}\right)^2+\tau^2\right)$$

where $\tilde{C}(u_0,v_0,f) := C\left\{\|u_0\|_4^2+\|v_0\|_3^2+\|f\|_{H^1(H^1)}^2+\|f\|_{H^3(L^2)}^2\right\}^{\frac{1}{2}}$.

TH-2392_146123010

Proof. Applying triangle inequality to

$$u^n - U^n = u^n - u_h^n + u_h^n - U^n,$$

followed by Theorem 3.4.1 and Lemma 3.5.3 leads to

$$\begin{aligned}\|u^n - U^n\| \;\leq\; & C\Bigg\{C(u_0, v_0, f)\left(h + \sqrt{\lambda} + \frac{\lambda}{h}\right)^2 \\ & +\tau^2\left(\int_0^T \|u_{htttt}\|^2 dt + \int_0^T \|u_{httt}\|^2 dt\right)^{\frac{1}{2}}\Bigg\}.\end{aligned}$$

Finally, Lemma 3.4.2 leads to desire result. □

Remark 3.5.1. (a) *The proposed fully discrete finite element scheme can be easily extended for the numerical approximation of the solutions to the following IBVP*

$$\begin{cases} \gamma u_{tt} + \sigma u_t - \nabla \cdot (\beta \nabla u) = f & \text{in } \Omega \times (0, T], \\ u(x, 0) = u_0, \;\; u_t(x, 0) = v_0 & \text{in } \Omega, \\ u(x, t) = 0 & \text{on } \partial\Omega \times (0, T], \end{cases} \tag{3.5.19}$$

coupled with the following jump conditions

$$[u] = 0, \quad \left[\beta \frac{\partial u}{\partial \mathbf{n}}\right] = g \quad \text{along } \Gamma \times (0, T]. \tag{3.5.20}$$

For numerical validation, we refer to numerical Examples 3.6.1-3.6.3.
(b) **Crank-Nicolson scheme for parabolic interface problems.** *For the above IBVP, fully discrete scheme (3.5.2), eliminating v^n, may be read as: Given approximations U^0, $v^0 \in V_h$ of u_0 and v_0, compute U^{n+1} from*

$$\begin{aligned} & \gamma\left(\frac{U^{n+1} - U^n}{\tau}, \psi\right) + \frac{\tau}{2}\mathcal{B}_{\sigma h}\left(\frac{U^{n+1} - U^n}{\tau}, \psi\right) + \frac{\tau}{2}\mathcal{A}_{\beta h}\left(\frac{U^{n+1} + U^n}{\tau}, \psi\right) \\ & = \frac{\tau}{2}\left(\frac{f^{n+1} + f^n}{2}, \psi\right) + \frac{\tau}{2}\left\langle\frac{g^{n+1} + g^n}{2}, \psi\right\rangle_\Gamma + \gamma(v^n, \psi) \;\; \forall \psi \in V_h, \end{aligned} \tag{3.5.21}$$

which is the Crank-Nicolson scheme for parabolic interface problems when $\gamma = 0$ (cf. Example 3.6.1). Here, $\langle\cdot\rangle_{\Gamma_h}$ denotes the L^2 inner product on Γ_h.
(c) **Newmark method for wave equation with interface.** *For wave-type equation (when $\sigma = 0$), fully discrete scheme (3.5.2) can be interpreted as Newmark scheme (cf. [51, 104]). First we calculate U^1 from (3.5.21) and then compute $U^{n+1} \in V_h$ for*

TH-2392_146123010

$n = 1, 2, \ldots, N-1$ *from equation (cf. Example 3.6.2)*

$$\gamma\left(\frac{U^{n+1}-2U^n+U^{n-1}}{\tau},\psi\right)+\tau\mathcal{A}_{\beta h}\left(\frac{U^{n+1}+2U^n+U^{n-1}}{4},\psi\right)$$
$$=\tau\left(\frac{f^{n+1}+2f^n+f^{n-1}}{4},\psi\right)+\tau\left\langle\frac{g^{n+1}+2g^n+g^{n-1}}{4},\psi\right\rangle_\Gamma \quad \forall\psi\in V_h. \qquad (3.5.22)$$

3.6 Numerical Results

In this section, we present some numerical experiments to validate the theoretical findings presented in the previous section. Our main emphasis here is to understand the behavior of the true errors obtained in Theorem 3.5.1. To illustrate the flexibility of the method, different forms of interfaces along with a large scale of variation in the physical coefficients are considered. For our numerical experiment, globally continuous piecewise linear finite elements ($\mathbb{P}_1$) based on fitted triangulations of Ω_i, $i = 1, 2$ are used. The nodes of the triangulations of Ω_1 and Ω_2 coincide on the interface Γ. All the numerical computations are done in the time interval $J = (0, 1]$.

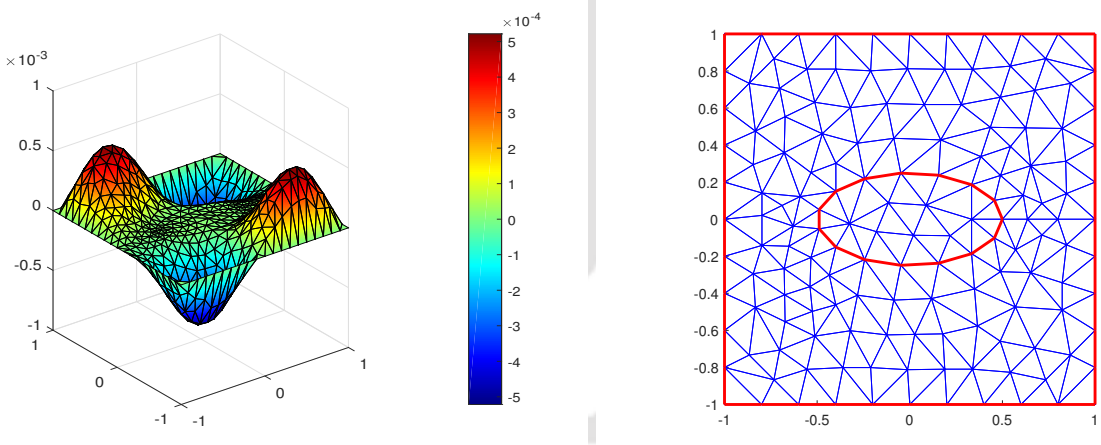

Figure 3.1: Exact solution (left) and triangulation (right) of Ω for $h = 0.282945$ with elliptic interface (Test Example 3.6.1).

Example 3.6.1. *In our first numerical example, we consider the square domain* $\Omega = (-1, 1)\times(-1, 1)$ *and the interface is taken to be the ellipse* $\{(x, y) : 4x^2+16y^2 = r^2 = 1\}$. *We select the data in (3.5.19)-(3.5.20) such that the exact solution* u *is given by*

$$u(x,y,t)=\begin{cases}10^{-1}(1-r^2)t^2\exp(-t) & \text{if } r^2\le 1,\\ 10^{-2}(1-r^2)\sin(0.25\pi t)\sin(\pi x)\sin(\pi y) & \text{if } r^2>1.\end{cases}$$

TH-2392_146123010

Table 3.1: Parameters used in computation (see, Dai *et al.* [33])

Parameters		Domain Ω_1	Domain Ω_2
$k(W/cm^\circ C)$	Thermal conductivity	0.0052	0.0021
$\rho(g/cm^3)$	Skin density	1.2000	1.0000
$c(J/g^\circ C)$	Specific heat	3.4000	3.0600
$w_b(g/cm^3 s)$	Blood perfusion rate	0.0005	0.0005
$c_b(J/g^\circ C)$	Specific heat of blood	4.2000	4.2000
$\tau_q(s)$	Thermal relaxation time	20.000	20.000

In Figure 3.1, we show the exact solution and triangulation of the domain Ω with mesh size $h = 0.282945$. In our numerical convergence test, we choose two different sets of physical coefficients borrowed from Dai *et al.* [33] that corresponds to two different forms of bio heat transfer model. For the non-Fourier bio heat transfer model, we set first the physical coefficients as

$$(\gamma, \sigma, \beta) = (\rho c \tau_q, \rho c + \tau_q w_b c_b, k) = \begin{cases} (81.6, 4.122, 0.0052) & \text{in } 4x^2 + 16y^2 \leq 1, \\ (61.2, 3.102, 0.0021) & \text{in } 4x^2 + 16y^2 > 1. \end{cases}$$

Following [33], physical parameters employed in the computation are as in Table 3.1. Non-Fourier heat transfer is characterized by thermal relaxation time τ_q and it may take value (in the range of $10^{-3}s - 10^3 s$) in heterogeneous materials (*cf.* [96]). Vedavarz *et al.* [133] found that τ_q for some biological tissues lies in the range of $1s - 100s$ at room temperature. In our computation, we use $\tau_q = 20s$ and relaxation time in the range $\tau_q = 20s - 30s$ is observed in [72] for meat products. In the absence of thermal relaxation time τ_q, equation (3.5.19) reduces to the Pennes bio heat model, which is a parabolic equation. The second set of physical coefficients that corresponds to the classical Pennes bio heat transfer model is given by

$$(\gamma, \sigma, \beta) = \begin{cases} (0, 4.08, 0.0052) & \text{in } 4x^2 + 16y^2 \leq 1, \\ (0, 3.06, 0.0021) & \text{in } 4x^2 + 16y^2 > 1. \end{cases}$$

Tables 3.2-3.3 represent the numerical solution errors and convergence rates in both L^2 and H^1 norms for $\gamma = 0$ (Pennes bio heat transfer) and $\gamma \neq 0$ (non-Fourier bio heat transfer), respectively. In both cases, we choose the uniform time step size $\tau = 10^{-4}$. The

TH-2392_146123010

Table 3.2: Example 3.6.1. L^2 and H^1 error for $\gamma = 0$ at $t = 10^{-2}$ with $\tau = 10^{-4}$

h	$\|u - u_h\|_{L^2(\Omega)}$	EOC	$\|u - u_h\|_{H^1(\Omega)}$	EOC
0.1520693	1.21885e-004	-	4.33382e-003	-
0.0890138	3.27518e-005	2.4538	2.22552e-003	1.2445
0.0474901	8.08637e-006	2.2264	1.10704e-003	1.1115
0.0247278	2.04375e-006	2.1076	5.11307e-004	1.1837

Table 3.3: Example 3.6.1. L^2 and H^1 error for $\gamma \neq 0$ at $t = 10^{-2}$ with $\tau = 10^{-4}$

h	$\|u - u_h\|_{L^2(\Omega)}$	EOC	$\|u - u_h\|_{H^1(\Omega)}$	EOC
0.1520693	6.57569e-005	-	4.44165e-003	-
0.0890138	1.62008e-005	2.6159	2.23853e-03	1.2795
0.0474901	3.85869e-006	2.2836	1.1023e-003	1.1276
0.0247278	1.01514e-006	1.9210	5.27391e-004	1.1297

errors at time $t = 10^{-2}$ are listed in the Tables 3.2-3.3. Figure 3.2 clearly demonstrates the second order of convergence in L^2 norm and first order of convergence in H^1 norm. Note that the second set of physical coefficients are chosen to emphasize the fact that our numerical scheme is consistent for the classical Pennes bio heat transfer model and is clearly depicted in Table 3.2.

Example 3.6.2. *In this example, we consider a square domain* $\Omega = (-1, 1) \times (-1, 1)$*, where interface* Γ *is a circle centered at* $(0, 0)$ *with radius* 0.5*. The exact solution is selected as*

$$u(x, y, t) = \begin{cases} 10^{-2}(r_0^2 - r^2)\sin(t) & \text{if } r \leq r_0, \\ 10^{-4}(r_0^2 - r^2)\exp(-t^2)(x^2 - 1)(y^2 - 1)\sin(x)\sin(y) & \text{if } r > r_0. \end{cases}$$

Where $r^2 = x^2 + y^2$ *and* $r_0 = 0.5$*. The source function* f*, interface function* g *and the initial data* u_0*,* v_0 *are determined from the choice of* u *with the following physical coefficients*

$$(\gamma, \sigma, \beta) = (K^{-1}, 0, \rho^{-1}) = \begin{cases} (1, 0, 1500) & \text{for } r \leq r_0, \\ (10, 0, 3000) & \text{for } r > r_0. \end{cases}$$

TH-2392_146123010

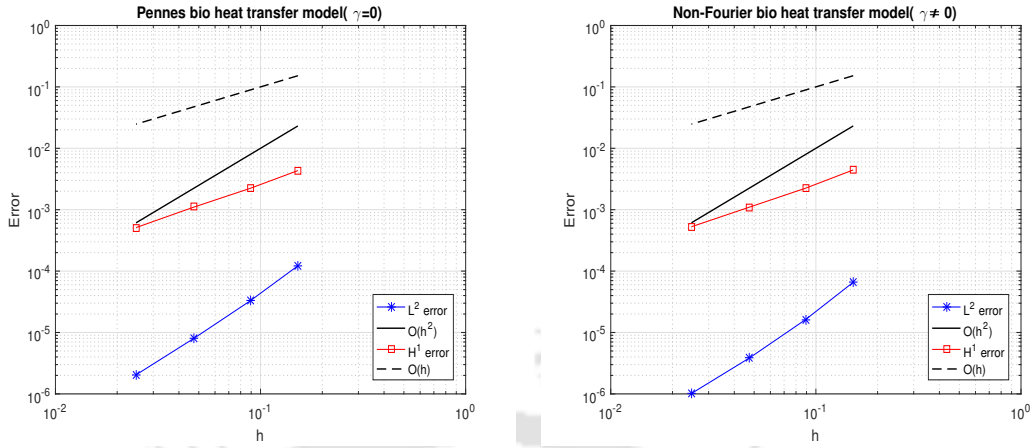

Figure 3.2: Log-log plot of the L^2 norm and H^1 norm versus the mesh size at time $t = 10^{-2}$ in Example 3.6.1.

Here, K represents the bulk modulus and ρ the density. Above choice of coefficients represents a wave equation with discontinuous coefficients (see, [16, 36, 134] and references therein). A large variation in the coefficients is a common occurrence in study of acoustic wave propagation through heterogeneous media in geophysical prospecting [16, 75, 127]. In Figure 3.3 we show the exact solution and triangulation of the domain Ω with mesh size $h = 0.305091$. Errors in L^2 and H^1 norms, and the convergence rate at time $t = 0.01$, for different values of h are listed in Table 3.4. The time step is deliberately taken as small as $\tau = 10^{-5}$ so as to satisfy the CFL condition. It is clear from the Figure 3.4(left) that we have achieved optimal order of convergence in both L^2 and H^1 norms which consolidates our theoretical findings.

Table 3.4: Test Example 3.6.2. L^2 and H^1 error at $t = 10^{-2}$ with $\tau = 10^{-5}$

h	$\|u - u_h\|_{L^2(\Omega)}$	EOC	$\|u - u_h\|_{H^1(\Omega)}$	EOC
0.3050910	1.70555e-006	-	2.79557e-005	-
0.1673780	4.19497e-007	2.3363	1.31639e-005	1.2545
0.0828717	9.12067e-008	2.1707	5.10594e-006	1.3473
0.0420952	1.79800e-008	2.3973	2.14059e-006	1.2834

TH-2392_146123010

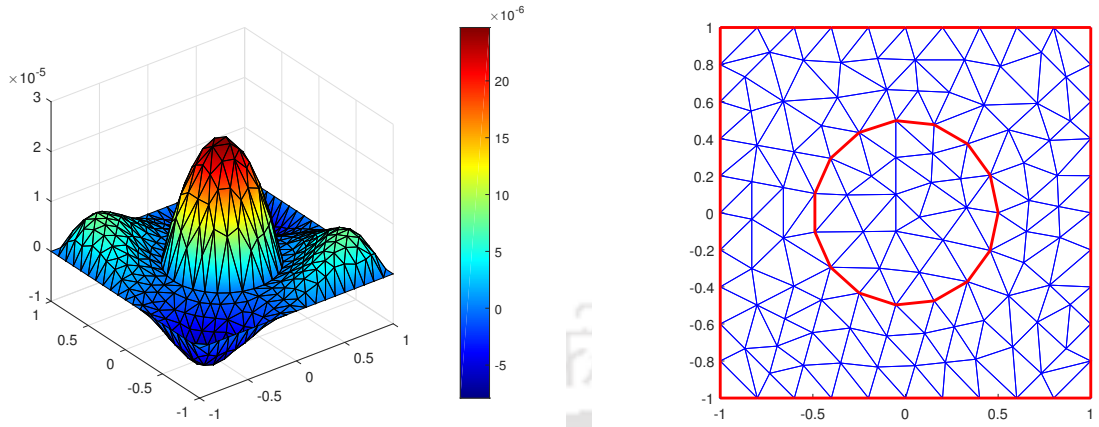

Figure 3.3: Exact solution (left) and triangulation (right) of Ω for $h = 0.305091$ with circular interface (Test Example 3.6.2).

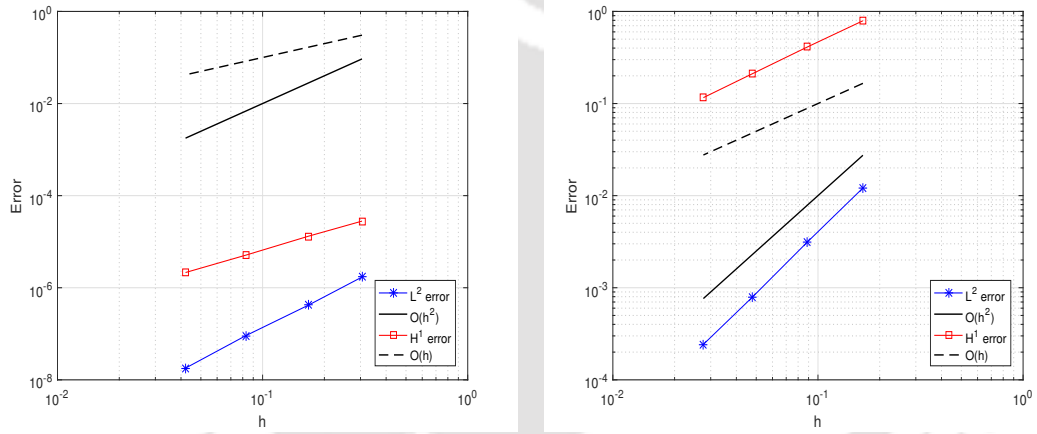

Figure 3.4: Log-log plot of the L^2 norm and H^1 norm versus the mesh size at time $t = 10^{-2}$ and $t = 1$ in Example 3.6.2-3.6.3, respectively.

Example 3.6.3. *In our last example, we consider the interface to be a curve given by* $y = x^2$ *in the computational domain* $\Omega = (-1, 1) \times (-1, 1)$. *We select the data appearing in (3.5.19)-(3.5.20) setting the exact solution as*

$$u(x, y, t) = \begin{cases} (y - x^2)(x^2 - 1)(y^2 - 1)\sin(t) & \text{if } y \leq x^2, \\ 10(y - x^2)\exp(-t)\sin(\pi y) & \text{if } y > x^2. \end{cases}$$

with the following sets of physical coefficients [108] representing a non-Fourier bio heat

TH-2392_146123010

model

$$(\gamma, \sigma, \beta) = \begin{cases} (1, 0.05000, 2.43 \times 10^{-9}) & \text{if } y \leq x^2, \\ (1, 0.05125, 4.53 \times 10^{-10}) & \text{if } y > x^2. \end{cases}$$

In Figure 3.5, we show the exact solution and the triangulation of the domain Ω with mesh size $h = 0.282596$. The numerical solution errors and convergence rates in both L^2 and H^1 norms at final time are listed in Table 3.5. It is clear from Figure 3.4 (right) that we have achieved optimal order of convergence in both L^2 and H^1 norms, which confirm the theoretical prediction as proved in Theorem 3.5.1.

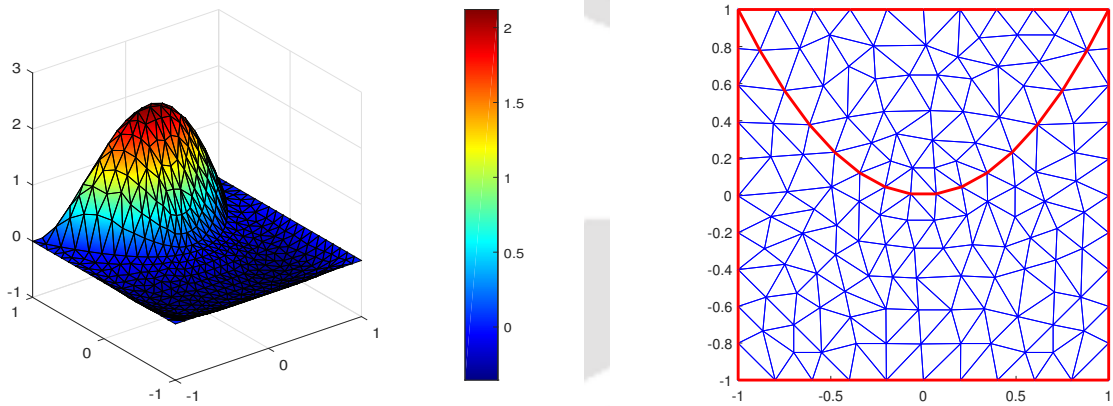

Figure 3.5: Exact solution (left) and triangulation of Ω for $h = 0.282596$ with curve interface (Test Example 3.6.3).

Table 3.5: Example 3.6.3. L^2 and H^1 error at $T = 1$ with $\tau = 10^{-2}$

h	$\|u - u_h\|_{L^2(\Omega)}$	EOC	$\|u - u_h\|_{H^1(\Omega)}$	EOC
0.1656240	1.21061e-002	-	7.91838e-001	-
0.0888431	3.14013e-003	2.1666	4.11632e-001	1.0504
0.0478408	7.88837e-004	2.2327	2.10440e-001	1.0839
0.0276306	2.42590e-004	2.1470	1.15908e-001	1.0864

TH-2392_146123010

TH-2392_146123010

4

Spatially Semidiscrete Error Analysis for DPL Bio Heat Transfer Problem with Interface

This chapter is concerned with *a priori* error analysis for the spatially semidiscrete scheme for the dual-phase-lag (DPL) bio heat model problem (1.1.7)-(1.1.9). We introduce the notions of weak and strong solutions to the model interface problem. Further, we prove the existence of strong solution under suitable regularity assumptions. A new non-standard elliptic type projection operator is introduced involving λ-strip. Its worth to note that this newly defined projection operator is key in the derivation of optimal order of convergence in $L^\infty(L^2)$ for the semidiscrete solution.

4.1 Introduction

Let Ω be a bounded domain in $\mathbb{R}^d (d = 2,\ 3)$ with Lipschitz boundary $\partial\Omega$ and $\Omega_1 \subset \Omega$ is an open domain with C^2 smooth boundary $\Gamma = \partial\Omega_1$ and $\Omega_2 = \Omega \backslash \Omega_1$. In Ω, we now recall the dual-phase-lag (DPL) bio heat model problem of the form

$$u'' + \sigma u' + \delta u - \nabla \cdot (\epsilon \nabla u') - \nabla \cdot (\beta \nabla u) = f \quad \text{in } \Omega \times (0, T] \tag{4.1.1}$$

with initial and boundary conditions

$$u(x, 0) = u_0 \ \ \& \ \ u'(x, 0) = v_0 \ \text{ in } \Omega; \ \ u(x, t) = 0 \quad \text{on } \partial\Omega \times (0, T] \tag{4.1.2}$$

and jump conditions on the interface

$$[u] = 0, \quad \left[\epsilon(x)\frac{\partial u'}{\partial \mathbf{n}} + \beta(x)\frac{\partial u}{\partial \mathbf{n}}\right] = 0 \quad \text{along } \Gamma \times [0, T]. \tag{4.1.3}$$

Here, $[v]$ denotes the jump of a quantity v across the interface Γ, i.e. $[v](x) = v_1|_\Gamma - v_2|_\Gamma$ with $v_i(x) = v(x)|_{\Omega_i}$, $i = 1, 2$ and $\left[\epsilon\frac{\partial u'}{\partial \mathbf{n}} + \beta\frac{\partial u}{\partial \mathbf{n}}\right] = \epsilon_1\frac{\partial u_1'}{\partial \mathbf{n}_1} + \epsilon_2\frac{\partial u_2'}{\partial \mathbf{n}_2} + \beta_1\frac{\partial u_1}{\partial \mathbf{n}_1} + \beta_2\frac{\partial u_2}{\partial \mathbf{n}_2}$ with

TH-2392_146123010

$\frac{\partial}{\partial \mathbf{n}_i}$ denotes the outer normal derivative with respect to $\Omega_i,\ i = 1,\ 2$. Other symbols are as defined in Chapter 1. We assume the coefficient functions are positive and piecewise constants on each subdomain Ω_i and we write

$$(\sigma, \delta, \epsilon, \beta) = \begin{cases} (\sigma_1, \delta_1, \epsilon_1, \beta_1) & \text{in } \Omega_1, \\ (\sigma_2, \delta_2, \epsilon_2, \beta_2) & \text{in } \Omega_2. \end{cases}$$

Further, initial data (u_0, v_0) and external force f are real valued functions and assumed to be sufficiently smooth.

Due to the practical relevance of interface problems in many engineering and industrial applications, numerical methods for interface problems have been investigated widely (for instance, see Section 1.3). There is plenty of literature available on the numerical study of the DPL bio heat model with discontinuous coefficients. One may refer to [94, 128, 130, 138] and reference therein. However, to the best of our knowledge, convergence analysis via finite element method for the dual-phase-lag bio heat model problem is absent in literature. A novel effort is made to provide both mathematical and numerical framework for the study of the dual-phase-lag (DPL) bio heat model problem (4.1.1)-(4.1.3). Equation (4.1.1) is also known as general linear second order hyperbolic equation. There are plenty of literature available for the convergence analysis, without the interface, for the general linear second order hyperbolic equation via finite element algorithm (*cf.* [18, 74, 81, 109] just to name a few). Recently, Nikolić *et al.* [107] has studied *a priori* error analysis for the semidiscrete solution of Westervelt's quasi-linear acoustic wave equation using piecewise linear finite elements. Optimal point-wise in time error estimate for the semidiscrete solution has been derived for sufficiently smooth solution. In [107], derivation of the error analysis heavily depends on the general linear wave model with time dependent coefficients. Fully discrete error analysis is still open for such problems. An attempt has been made to carry over *a priori* error analysis for the general linear second order hyperbolic interface problem (4.1.1)-(4.1.3). Optimal convergence order in both $L^\infty(H^1)$ and $L^\infty(L^2)$ norms have been obtained for the spatially discrete solution.

The rest of this chapter is organized as follows: While in Section 4.2 we introduce the notion of weak solution and strong solution for the interface problem, and then discuss the existence and regularity of the strong solution. In Section 4.3, we recall some basic approximation properties associated with the finite element spaces and introduce a new non-standard elliptic type projection operator involving λ-strip, which is crucial for the argument of convergence. Optimal *a priori* error estimate for the semidiscrete solution are derived in Section 4.4.

TH-2392_146123010

4.2 Well-posedness of the Model Interface Problem

This section is devoted to existence, uniqueness and regularity for the solutions to the model interface problem (4.1.1)-(4.1.3). The solution to the interface problem has a higher regularity in each individual region than in the entire domain. This regularity result is critical for our further numerical analysis.

Before proceeding further, let us recall spaces $W = L^2(\Omega)$, $V = H_0^1(\Omega)$ and $V' = H^{-1}(\Omega)$ along with the global bilinear maps $\mathcal{A}(\cdot,\cdot)$ and $\mathcal{B}(\cdot,\cdot)$, as discussed in Chapter 1. We now define the weak form of our model problem (4.1.1)-(4.1.3). We adapt following notion of weak solution.

Definition 4.2.1. *A function $u \in H^1(V) \cap H^2(W)$ is called a weak solution of (4.1.1)-(4.1.2) if $u(0) = u_0$ and $u'(0) = v_0$, and it satisfies following weak formulation*

$$(u'', v) + \mathcal{B}_\sigma(u', v) + \mathcal{B}_\delta(u, v) + \mathcal{A}_\epsilon(u', v) + \mathcal{A}_\beta(u, v) = \langle f(t,\cdot), v\rangle_{V'\times V} \tag{4.2.1}$$

for all $v \in H_0^1(\Omega)$ and a.e. $t \in (0, T]$. Here, $\langle\cdot,\cdot\rangle_{V'\times V}$ denotes the standard duality product.

Existence and uniqueness of a solution to the variational problem (4.2.1) is proved in [71, 120, 131, 132], for instance, we refer to ([132], Theorem 1). For suitable initial data (u_0, v_0) and forcing function f, we assume weak solution $u \in C^1([0, T]; V) \cap C^2([0, T]; W)$.

Remark 4.2.1. *Apart from bio heat modeling, a substantial number of articles deal with model problem (4.2.1) and it can be applied to any system where elastic bodies interact, provided that the model problem is linear. Numerous examples can be found in [80, 89, 131], for example, viscous wave equation, networks of linked beams, hybrid chimney etc.*

Definition 4.2.2. *A function $u \in H^1(\mathcal{Y}) \cap H^2(W)$ is called a strong solution of (4.1.1)-(4.1.3) if $u(0) = u_0$ and $u'(0) = v_0$ with jump conditions (4.1.3), and the relation*

$$\begin{aligned} &u''(x,t) + \sigma(x)u'(x,t) + \delta(x)u(x,t) - \nabla\cdot(\epsilon(x)\nabla u'(x,t) + \beta(x)\nabla u(x,t)) \\ &= f(x,t) \end{aligned} \tag{4.2.2}$$

holds for a.e. $t \in (0, T]$ and a.e. $x \in \Omega_i$ $(i = 1,\ 2)$.

Before proving the existence of a strong solution to the interface problem, we first establish the following result.

Lemma 4.2.1. *Let u be the weak solution of (4.1.1)-(4.1.3). Assume that $u \in H^1(\mathcal{Y}) \cap H^2(W)$, then u is a strong solution for (4.1.1)-(4.1.3).*

TH-2392_146123010

Proof. For $u \in H^1(\mathcal{Y}) \cap H^2(W)$ and *a.e.* $t \in (0, T]$, upon integration by parts, we obtain

$$\begin{aligned}
&\int_{\Omega_i} -\nabla \cdot (\epsilon_i \nabla u' + \beta_i \nabla u) v dx \\
&= \int_{\Omega_i} \epsilon_i \nabla u' \cdot \nabla v dx + \int_{\Omega_i} \beta_i \nabla u \cdot \nabla v dx \\
&= (f - u'' - \sigma_i u' - \delta_i u, v)_{\Omega_i} \quad \forall v \in H_0^1(\Omega_i) \qquad (4.2.3)
\end{aligned}$$

which implies that

$$-\nabla \cdot (\epsilon_i \nabla u'(x,t) + \beta_i \nabla u(x,t)) = f(x,t) - u''(x,t) - \sigma_i u'(x,t) - \delta_i u(x,t)$$

holds for *a.e.* $t \in (0, T]$ and *a.e.* $x \in \Omega_i$ $(i = 1,\ 2)$. It remains to show that the weak solution also satisfies the jump conditions (4.1.3). Applying integration by parts, for *a.e.* $t \in (0, T]$, we have

$$\begin{aligned}
0 &= \sum_{i=1}^{2} \int_{\Omega_i} (u'' + \sigma_i u' + \delta_i u - f) v dx + \sum_{i=1}^{2} \int_{\Omega_i} -\nabla \cdot (\epsilon_i \nabla u' + \beta_i \nabla u) v dx \\
&= \sum_{i=1}^{2} \int_{\Omega_i} (u'' + \sigma_i u' + \delta_i u - f) v dx + \sum_{i=1}^{2} \int_{\Omega_i} (\epsilon_i \nabla u' \cdot \nabla v + \beta_i \nabla u \cdot \nabla v) dx \\
&\quad - \int_{\Gamma} \left[\epsilon \frac{\partial u'}{\partial \mathbf{n}} + \beta \frac{\partial u}{\partial \mathbf{n}} \right] v ds \\
&= \sum_{i=1}^{2} (u'' + \sigma_i u' + \delta_i u - f, v)_{\Omega_i} + \sum_{i=1}^{2} (A_\epsilon^i(u', v) + A_\beta^i(u, v)) \\
&\quad - \int_{\Gamma} \left[\epsilon \frac{\partial u'}{\partial \mathbf{n}} + \beta \frac{\partial u}{\partial \mathbf{n}} \right] v ds \quad \forall v \in V. \qquad (4.2.4)
\end{aligned}$$

Above relation and the definition of weak solution it follows that

$$\int_{\Gamma} \left[\epsilon \frac{\partial u'}{\partial \mathbf{n}} + \beta \frac{\partial u}{\partial \mathbf{n}} \right] v ds = 0 \quad \forall v \in V.$$

The arbitrariness of v shows that u satisfies the second jump condition in (4.1.3). The first condition in (4.1.3) is a direct consequence of the fact that $u \in H^1(V)$. This completes the proof. □

In general, the solution u of the problem (4.1.1)-(4.1.3) does not belong to $H^1(H^2(\Omega))$ due to the presence of discontinuous coefficients. We can get better local regularity using local smoothness of the coefficients. From Lemma 4.2.1, it is clear that the existence of a strong solution depends on higher regularity of the weak solution, which is the main object of the Theorem 4.2.1. Further, *a priori* estimates for the solution to the problem (4.1.1)-(4.1.3) are also presented in Lemma 4.2.2 under appropriate regularity conditions on the initial functions u_0, v_0 and f.

TH-2392_146123010

Theorem 4.2.1. *Let $u_0 \in \mathcal{Y}$, $v_0 \in X$ and $f \in H^1(J;W)$, then the interface problem (4.1.1)-(4.1.3) admits a unique strong solution.*

Proof. Let $u \in C^1(J;V) \cap C^2(J;W)$ be a weak solution to the interface problem (4.1.1)-(4.1.3) satisfying (4.2.1). We consider following auxiliary problem: Find $w \in H^1(J;\mathcal{Y})$ such that

$$\mathcal{A}_\epsilon(w',v) + \mathcal{A}_\beta(w,v) = (f - u'' - \sigma u' - \delta u, v) \quad \forall v \in V, \tag{4.2.5}$$

with $[w] = 0$ and $\left[\beta \frac{\partial w}{\partial \mathbf{n}} + \epsilon \frac{\partial w'}{\partial \mathbf{n}}\right] = 0$ across the interface Γ, and $w(x,0) = u_0$. For the existence and uniqueness of a solution to the problem (4.2.5), we refer to [8]. Further, $w \in H^1(\mathcal{Y})$ satisfies following *a priori* estimate

$$\|w\|_{H^1(\mathcal{Y})} \leq C(\|f - u'' - \sigma u' - \delta u\|_{L^2(J;W)} + \|u_0\|_{\mathcal{Y}}). \tag{4.2.6}$$

Subtracting (4.2.5) from (4.2.1), we have

$$\mathcal{A}_\epsilon(w' - u', v) + \mathcal{A}_\beta(w - u, v) = 0 \quad \forall\ v \in V$$

which implies that $w(x,t) = u(x,t)$ for *a.e.* $t \in (0,T]$ and *a.e.* $x \in \Omega$. Therefore $u \in H^1(J;\mathcal{Y})$ and due to Lemma 4.2.1 it is a strong solution to the interface problem (4.1.1)-(4.1.3). This completes the proof. □

Remark 4.2.2. *We are well aware of the fact that the rate of convergence of finite element approximations depends on the 'smoothness' of a solution. In Theorem 4.2.1, we have shown that interface problem (4.1.1)-(4.1.3) admits a unique strong solution $u \in H^1(\mathcal{Y}) \cap H^2(W)$ for appropriate initial data and source function. In fact, strong solution $u \in H^1(J;\mathcal{Y}) \cap C^1(J;V) \cap C^2(J;W)$. In articles on the finite element method for general linear second-order hyperbolic equations without the interface, related to convergence, it is assumed higher order time derivatives of the solutions (cf. [18, 74, 81, 107, 109]). Therefore, we will be required additional regularity of u which guarantee the convergence results.*

Lemma 4.2.2. *Let $u_0,\ v_0 \in H^3(\Omega) \cap H_0^1(\Omega)$ and $f \in H^1(J;H^1(\Omega))$. Then the strong solution u to the interface problem (4.1.1)-(4.1.3) satisfies following a priori estimate*

$$\|u\|_{H^2(\mathcal{Y})} \leq C(\|u_0\|_3 + \|v_0\|_3 + \|f\|_{H^1(J;H^1(\Omega))}).$$

Proof. Suppose $z \in H^1(J;\mathcal{Y}) \cap C^1(J;V) \cap C^2(J;W)$ satisfies following variational formulation

$$(z'',v) + \mathcal{B}_\sigma(z',v) + \mathcal{B}_\delta(z,v) + \mathcal{A}_\epsilon(z',v) + \mathcal{A}_\beta(z,v) = (f',v) \ \ \forall v \in H_0^1(\Omega) \tag{4.2.7}$$

TH-2392_146123010

with $z(0) = v_0$ and $z'(0) = z_0$. Here, $z_0 \in X$ is defined as

$$z_0 = -\sigma_l v_0 - \delta_l u_0 + \nabla \cdot (\epsilon_l \nabla v_0 + \beta_l \nabla u_0) + f(0) \ \text{ in } \Omega_l, \ l = 1, 2.$$

Using the fact that $u \in C^2(J; W)$, it is easy to verify that $(z_0 - u''(0), v) = 0$ for all $v \in V$.

Now, we define $w(t) = u_0 + \int_0^t z ds, \ t \in [0, T]$ so that $w(0) = u_0, \ w'(0) = z(0) = v_0$ and $w''(0) = z_0$. Further, for all $v \in V$, we observe that w satisfies following equation

$$(w''', v) + \mathcal{B}_\sigma(w'', v) + \mathcal{B}_\delta(w', v) + \mathcal{A}_\epsilon(w'', v) + \mathcal{A}_\beta(w', v) = (f', v) \ \ \forall v \in V \tag{4.2.8}$$

which can be written as

$$\frac{d}{dt}\Big\{(w'', v) + \mathcal{B}_\sigma(w', v) + \mathcal{B}_\delta(w, v) + \mathcal{A}_\epsilon(w', v) + \mathcal{A}_\beta(w, v) - (f, v)\Big\} = 0. \tag{4.2.9}$$

Now, differentiate (4.2.1) with respect to t to obtain

$$\frac{d}{dt}\Big\{(u'', v) + \mathcal{B}_\sigma(u', v) + \mathcal{B}_\delta(u, v) + \mathcal{A}_\epsilon(u', v) + \mathcal{A}_\beta(u, v) - (f, v)\Big\} = 0, \tag{4.2.10}$$

for all $v \in V$. For similar type of arguments in the context of wave equations, we refer to ([93], pages 95-98). Then subtracting (4.2.9) from (4.2.10) yields

$$\frac{d}{dt}\Big\{(p'', v) + \mathcal{B}_\sigma(p', v) + \mathcal{B}_\delta(p, v) + \mathcal{A}_\epsilon(p', v) + \mathcal{A}_\beta(p, v)\Big\} = 0 \ \ \forall v \in V,$$

where $p(t) = u(t) - w(t)$. Integrating the above equation from 0 to t, we derive

$$(p'', v) + \mathcal{B}_\sigma(p', v) + \mathcal{B}_\delta(p, v) + \mathcal{A}_\epsilon(p', v) + \mathcal{A}_\beta(p, v) = 0 \ \forall v \in V. \tag{4.2.11}$$

Note that $p(0) = 0$ and $p'(0) = 0$, which implies that $u = w$. Then use the fact $u' = w' = z \in H^1(\mathcal{Y})$ to conclude that $u \in H^2(\mathcal{Y})$. Further, for $v = u''$, equation (4.2.1) yields

$$\int_0^t \|u''\|^2 ds \le C\Big(\sum_{l=1}^{2}\big\{\|u_0\|^2_{1,\Omega_l} + \|v_0\|^2_{1,\Omega_l}\big\} + \|f\|^2_{L^2(J;W)}\Big),$$

which together with (4.2.6) leads to following *a priori* estimate

$$\|u\|_{H^1(\mathcal{Y})} \le C(\|u_0\|_{\mathcal{Y}} + \|v_0\|_X + \|f\|_{L^2(J;W)}). \tag{4.2.12}$$

Using estimate (4.2.12) for z satisfying (4.2.7), we obtain

$$\begin{aligned} \|z\|_{H^1(\mathcal{Y})} &\le C(\|v_0\|_{\mathcal{Y}} + \|z'(0)\|_X + \|f'\|_{L^2(J;W)}) \\ &\le C(\|u_0\|_3 + \|v_0\|_3 + \|f\|_{H^1(J;H^1(\Omega))}). \end{aligned}$$

This together with the fact that $u' = z$ leads to desired estimate. This completes the rest of the proof. □

TH-2392_146123010

Remark 4.2.3. *In the previous result, for* $u_0,\ v_0 \in H^3(\Omega)\cap H_0^1(\Omega)$ *and* $f \in H^1(J;H^1(\Omega))$*, we have shown that the strong solution* u *to the interface problem (4.1.1)-(4.1.3) belongs to* $H^2(J;\mathcal{Y}) \cap C^2(J;V) \cap C^3(J;W)$*. An argument similar to that of the preceding, and after having change the smoothness condition to* $u_0,\ v_0 \in H^4(\Omega) \cap H_0^1(\Omega)$ *and* $f \in H^2(J;H^1(\Omega))$ *leads to an improvement in the regularity of the strong solution* u*. More precisely, for sufficiently smooth initial data and source function* f*, we assume* $u \in H^3(J;\mathcal{Y})$*. Results of this section are also hold true in a bounded and convex domain* $\Omega \subset \mathbb{R}^3$ *with* C^2 *smooth interface* Γ*.*

4.3 Auxiliary Results

This section recalls some auxiliary projections and their approximation properties from previous chapters.

For a finite element approximation, based on a fitted triangulation $\mathcal{T}_h$, we approximate bilinear maps associated with equation (4.1.1). For instance, bilinear maps $\mathcal{A}(\cdot,\cdot)$ and $\mathcal{B}(\cdot,\cdot)$ are approximated by $\mathcal{A}_h(\cdot,\cdot)$ and $\mathcal{B}_h(\cdot,\cdot)$. For better illustration, we refer to Chapter 1. On the other hand error analysis requires some appropriate intermediate projection operators. We define elliptic projection operator $\mathcal{Q}_{\epsilon h}$ connecting operators $\mathcal{A}_\epsilon$ and $\mathcal{A}_{\epsilon h}$ by

$$\mathcal{A}_{\epsilon h}(\mathcal{Q}_{\epsilon h}v, v_h) = \mathcal{A}_\epsilon(v, v_h) = \mathcal{A}_\epsilon^1(v, v_h) + \mathcal{A}_\epsilon^2(v, v_h)\ \forall v_h \in V_h,\ v \in \mathcal{Y}. \tag{4.3.1}$$

Similarly, elliptic projection operator $\mathcal{Q}_{\beta h}$ connects operators $\mathcal{A}_\beta$ and $\mathcal{A}_{\beta h}$ by

$$\mathcal{A}_{\beta h}(\mathcal{Q}_{\beta h}v, v_h) = \mathcal{A}_\beta(v, v_h) = \mathcal{A}_\beta^1(v, v_h) + \mathcal{A}_\beta^2(v, v_h)\ \forall v_h \in V_h,\ v \in \mathcal{Y}. \tag{4.3.2}$$

Here, $\mathcal{A}_\epsilon^l$ and $\mathcal{A}_\beta^l$ $(l = 1,\ 2)$ are local bilinear maps as defined in Chapter 1. To simplify the notation, we will write $\mathcal{Q}_h$ in place of $\mathcal{Q}_{\epsilon h}$ or $\mathcal{Q}_{\beta h}$ when no risk of confusion arises. Regarding the approximation properties of $\mathcal{Q}_h$ operator defined by (4.3.1) or (4.3.2), we refer to Lemma 3.3.4 in Chapter 3.

Another important operator is the L^2 projection $\mathcal{L}_h : L^2(\Omega) \to V_h$ defined by

$$(\mathcal{L}_h v, \phi) = (v, \phi)\ \forall \phi \in V_h,\ v \in L^2(\Omega) \tag{4.3.3}$$

and the error estimates as discussed in Lemma 3.3.5 holds.

Remark 4.3.1. *Elliptic projection operator* $\mathcal{Q}_{\epsilon h}$ *defined by (4.3.1) is also valid in the space* $\hat{X} := \{\xi \in X : [\xi] = 0$ *along* Γ *&* $\xi = 0$ *on* $\partial\Omega\}$ *and satisfies following stability*

$$\|\mathcal{Q}_{\epsilon h}v\|_1 \le C\|v\|_X\ \ \forall v \in \hat{X}. \tag{4.3.4}$$

TH-2392_146123010

Further, following approximation results hold

$$\|v - \mathcal{Q}_{\epsilon h} v\| + h \sum_{l=1}^{2} \|v - \mathcal{Q}_{\epsilon h} v\|_{1,\Omega_l} \leq Ch^2 \{\|v\|_{2,\Omega_1} + \|v\|_{2,\Omega_2}\},$$

for all $v \in \hat{X} \cap H^2(\Omega_1) \cap H^2(\Omega_2)$. *Similar remarks hold for the elliptic projection* $\mathcal{Q}_{\beta h}$ *and* L^2 *projection* $\mathcal{L}_h$. *For details, we refer to [39].*

For given $v \in \hat{X}$, there exists $w \in \mathcal{Y}$ (*cf.* [31]) satisfying

$$\sum_{l=1}^{2} \mathcal{A}_{\epsilon}^{l}(w, \phi) = (v - \mathcal{Q}_{\epsilon h} v, \phi) \ \ \forall \phi \in \hat{X}. \tag{4.3.5}$$

Equation (4.3.5) together with (4.3.1), Lemma 1.2.2 and Lemma 3.3.4 leads to

$$\begin{aligned}
\|v - \mathcal{Q}_{\epsilon h} v\|^2 &= \sum_{l=1}^{2} \mathcal{A}_{\epsilon}^{l}(w - \mathcal{Q}_{\epsilon h} w, v - \mathcal{Q}_{\epsilon h} v) + \sum_{l=1}^{2} \mathcal{A}_{\epsilon}^{l}(\mathcal{Q}_{\epsilon h} w, v - \mathcal{Q}_{\epsilon h} v) \\
&\leq C\|w - \mathcal{Q}_{\epsilon h} w\|_1 \sum_{l=1}^{2} \|v - \mathcal{Q}_{\epsilon h} v\|_{1,\Omega_l} - \mathcal{A}_{\epsilon h}^{\Delta}(\mathcal{Q}_{\epsilon h} v, \mathcal{Q}_{\epsilon h} w) \\
&\leq Ch\|w\|_{\mathcal{Y}} \sum_{l=1}^{2} \|v - \mathcal{Q}_{\epsilon h} v\|_{1,\Omega_l} + Ch\|\mathcal{Q}_{\epsilon h} v\|_1 \|\mathcal{Q}_{\epsilon h} w\|_1 \\
&\leq Ch\|v - \mathcal{Q}_{\epsilon h} v\| \|v\|_X.
\end{aligned} \tag{4.3.6}$$

In the last inequality, we have used the fact that $\|w\|_{\mathcal{Y}} \leq C\|v - \mathcal{Q}_{\epsilon h} v\|$ and stability estimate (4.3.4). As a consequence of estimate (4.3.6), we obtain

$$\|v - \mathcal{L}_h v\| \leq \|v - \mathcal{Q}_{\epsilon h} v\| \leq Ch\|v\|_X \ \forall v \in \hat{X}. \tag{4.3.7}$$

Here, we have used the fact that $\mathcal{L}_h v$ is the best approximation of $v \in L^2(\Omega)$ with respect to L^2 norm.

Now, inverse inequality and estimates (4.3.6)-(4.3.7) lead to following stability for L^2 projection

$$\begin{aligned}
\|\mathcal{L}_h v\|_1 &\leq \|\mathcal{L}_h v - \mathcal{Q}_{\epsilon h} v\|_1 + \|\mathcal{Q}_{\epsilon h} v\|_1 \\
&\leq Ch^{-1}\|\mathcal{L}_h v - \mathcal{Q}_h v\| + C\|v\|_X \\
&\leq C\|v\|_X \ \forall v \in \hat{X}.
\end{aligned} \tag{4.3.8}$$

Remark 4.3.2. *In Lemma 4.2.2, we have proved that the solution to the interface problem is sufficiently smooth in each individual subdomain* Ω_1 *and* Ω_2 *for smooth given data. Assuming* $u \in C^2(J; X)$ *with* $[u] = 0$ *along* Γ *and* $u = 0$ *on* $\partial\Omega$, *we obtain*

$$[u''(t)] = 0 \text{ on } \Gamma \ \& \ u''(t) = 0 \text{ on } \partial\Omega \ \ \text{for } t \in [0, T].$$

TH-2392_146123010

This together with (4.3.8) yields

$$\|\mathcal{L}_h u''(0)\|_1 \leq C\|u''(0)\|_X \leq C(\|u_0\|_3 + \|v_0\|_3 + \|f\|_{H^1(H^1)}). \tag{4.3.9}$$

Now, we are in a position to define our new non-standard elliptic type projection operator which is crucial for our error analysis. For $v \in H^1(J;\mathcal{Y})$, find $\xi_v \in H^1(J;V_h)$ such that for *a.e.* $t \in [0,T]$

$$\mathcal{A}_{\epsilon h}(\xi_v'(t), v_h) + \mathcal{A}_{\beta h}(\xi_v(t), v_h) = \mathcal{A}_{\epsilon}(v'(t), v_h) + \mathcal{A}_{\beta}(v(t), v_h)\ \forall v_h \in V_h, \tag{4.3.10}$$

with $\xi_v(0) = \mathcal{Q}_{\beta h} v(0) \in V_h$.

One can follow the proof of Theorem 2.3.1 and Theorem 2.3.2 in Chapter 2 to derive the following optimal point-wise-in time error estimates for the newly introduced elliptic type projection operator.

Lemma 4.3.1. *For any $v \in H^1(J;\mathcal{Y})$ and a.e. $t \in J$, there is a positive constant C independent of the mesh parameter h such that*

$$\|v(t) - \xi_v(t)\| + h\|v(t) - \xi_v(t)\|_1 \leq C(h^2 + \lambda)\Big(\|v\|_{H^1(\mathcal{Y})} + \|v(0)\|_{\mathcal{Y}}\Big).$$

4.4 Spatially Semidiscrete Error Analysis

This section deals with the pointwise-in-time error analysis for the spatially discrete scheme. First we derive stability results for the semidiscrete solution. Optimal order of convergence for $L^\infty(L^2)$ and $L^\infty(H^1)$ norms are established when the global regularity of the solution is low on the entire domain. The stability error analysis is very crucial to established optimal error estimates for fully discrete solution .

The continuous time Galerkin finite element approximation to (4.2.1) is stated as follows: Find $u_h : [0,T] \to V_h$ such that

$$\begin{aligned}&(u_h'', v_h) + \mathcal{B}_{\sigma h}(u_h', v_h) + \mathcal{B}_{\delta h}(u_h, v_h) + \mathcal{A}_{\epsilon h}(u_h', v_h) + \mathcal{A}_{\beta h}(u_h, v_h)\\ &= (f, v_h)\ \forall v_h \in V_h,\ t \in (0,T],\end{aligned} \tag{4.4.1}$$

with $u_h(0) = \mathcal{Q}_h u_0$ and $u_h'(0) = \mathcal{Q}_h v_0$.

Following result deals with the existence and regularity of u_h. The basic technique is borrowed from [107].

Theorem 4.4.1. *For each $h \in (0, h_0]$, there exists a unique function $u_h \in C^2(J;V_h)$ satisfying (4.4.1).*

TH-2392_146123010

Proof: Let $V_h \subset H_0^1(\Omega)$ be the finite element space defined on $\mathcal{T}_h$ with basis functions $\{\phi_i\}_{i=1}^{N_h}$. We consider Galerkin approximations in space

$$u_h(x,t) = \sum_{i=1}^{N_h} c_i(t)\phi_i(x)$$

where $c_i : (0,T] \to \mathbb{R}$ are coefficient functions for $i \in [1, N_h]$.

We denote by $\mathbf{c}_{h,0} = [c_{1,0}, \ldots, c_{N_h,0}]^T$ and $\mathbf{c}_{h,1} = [c_{1,1}, \ldots, c_{N_h,1}]^T$ the components of the given initial approximations $u_h(0)$ and $u_h'(0)$, respectively. Then our semidiscrete problem is to find $\mathbf{c}_h(t) = [c_1(t), \ldots, c_{N_h}(t)]^T$, for $t \in (0,T]$, such that

$$\begin{cases} M_h\mathbf{c}_h''(t) + K_h\mathbf{c}_h'(t) + L_h\mathbf{c}_h(t) + C_h\mathbf{c}_h'(t) + D_h\mathbf{c}_h(t) = F_h(t), \\ \mathbf{c}_h(0) = \mathbf{c}_{h,0} \ \text{ and } \ \mathbf{c}_h'(0) = \mathbf{c}_{h,1}. \end{cases} \tag{4.4.2}$$

Coefficient matrices are given by

$$\begin{aligned} M_h &= [M_{i,j}], \quad M_{i,j} = (\phi_i, \phi_j), \\ K_h &= [K_{i,j}], \quad K_{i,j} = \mathcal{B}_\sigma(\phi_i, \phi_j), \\ L_h &= [L_{i,j}], \quad L_{i,j} = \mathcal{B}_\delta(\phi_i, \phi_j), \\ C_h &= [C_{i,j}], \quad C_{i,j} = \mathcal{A}_\epsilon(\phi_i, \phi_j), \\ D_h &= [D_{i,j}], \quad D_{i,j} = \mathcal{A}_\beta(\phi_i, \phi_j) \end{aligned}$$

and the source term is given by $F_h = [F_1, \ldots, F_{N_h}]^T$, $F_j = (f, \phi_j)$, with $1 \le i, j \le N_h$. Note that the matrices and the right-hand-side vectors are all well-defined since

$$\begin{aligned} &|(\phi_i, \phi_j)| \le \|\phi_i\|\|\phi_j\|, \\ &|\mathcal{B}(\phi_i, \phi_j)| \le C_1\|\phi_i\|\|\phi_j\|, \\ &|\mathcal{A}(\phi_i, \phi_j)| \le C_2\|\phi_i\|_1\|\phi_j\|_1, \\ &|(f, \phi_j)| \le \|f\|\|\phi_j\| \le \|f\|_{L^\infty(L^2)}\|\phi_j\|, \end{aligned}$$

for all $t \in J$. Furthermore, for any $z \in \mathbb{R}^{N_h} \setminus 0$, we have

$$z^T M_h z = \int_\Omega \Big|\sum_{i=1}^{N_h} z_i w_i\Big|^2 dx \ge \Big|\sum_{i=1}^{N_h} z_i w_i\Big|_{L^2}^2 > 0$$

for all $t \in J$. Hence, the matrix M_h is invertible for all $t \in J$ and the matrix equation in (4.4.2) can be rewritten as

$$\mathbf{c}_h'' + M_h^{-1}K_h\mathbf{c}_h' + M_h^{-1}L_h\mathbf{c}_h + M_h^{-1}C_h\mathbf{c}_h' + M_h^{-1}D_h\mathbf{c}_h = M_h^{-1}F_h. \tag{4.4.3}$$

Now the existence of a solution $u_h \in C^2(J; V_h)$ follows from the standard ODE theory. This completes the rest of the proof. $\square$

TH-2392_146123010

Remark 4.4.1. *Assuming $f \in C^1(J;W)$ and setting*

$$\mathbf{c}_h''(0) = M_h^{-1}F_h(0) - M_h^{-1}K_h\mathbf{c}_{h,1} - M_h^{-1}L_h\mathbf{c}_{h,0} - M_h^{-1}C_h\mathbf{c}_{h,1} - M_h^{-1}D_h\mathbf{c}_{h,0},$$

we further observe that $u_h \in C^3(J;V_h)$. Next Lemma assumes $f \in H^3(J;H^2(\Omega))$ and which guarantee the existence of $u_h \in C^4(J;V_h)$ satisfying (4.4.1).

Regarding the stability of u_h at the initial stage, we have the following result.

Lemma 4.4.1. *Let u_h satisfy (4.4.1). Then, for $i = 2, 3, 4$, we have*

$$\|D_t^i u_h(0)\| \le C\big(\|u_0\|_{2i-2} + \|v_0\|_{2i-2} + \|f\|_{H^{i-1}(H^2)}\big),$$
$$\|D_t^{i-1} u_h(0)\|_1 \le C\big(\|u_0\|_{2i-3} + \|v_0\|_{2i-3} + \|f\|_{H^{i-2}(H^1)}\big),$$

where $D_t^i = \frac{\partial^i}{\partial t^i}$.

Proof: Taking $t \to 0^+$ in (4.4.1) and then using definition of $\mathcal{Q}_h$ operator, we obtain

$$\begin{aligned}
(u_h''(0), v_h) &= -\mathcal{B}_{\sigma h}(u_h'(0), v_h) - \mathcal{B}_{\delta h}(u_h(0), v_h) \\
&\quad -\mathcal{A}_{\epsilon h}(u_h'(0), v_h) - \mathcal{A}_{\beta h}(u_h(0), v_h) + (f(0), v_h) \\
&= -\mathcal{B}_{\sigma h}(\mathcal{Q}_{\epsilon h}v_0, v_h) - \mathcal{B}_{\beta h}(\mathcal{Q}_{\beta h}u_0, v_h) \\
&\quad -\mathcal{A}_{\epsilon h}(\mathcal{Q}_{\epsilon h}v_0, v_h) - \mathcal{A}_{\beta h}(\mathcal{Q}_{\beta h}u_0, v_h) + (f(0), v_h) \\
&= -\mathcal{B}_{\sigma h}(\mathcal{Q}_{\epsilon h}v_0, v_h) - \mathcal{B}_{\beta h}(\mathcal{Q}_{\beta h}u_0, v_h) \\
&\quad -\mathcal{A}_{\epsilon}(v_0, v_h) - \mathcal{A}_{\beta}(u_0, v_h) + (f(0), v_h). \qquad (4.4.4)
\end{aligned}$$

Here, we have used the fact that $u_h \in C^2(J;V_h)$. For the third and fourth term in (4.4.4), we use Green's formula and boundary condition to derive

$$\mathcal{A}_\epsilon(v_0, v_h) = -(\nabla\cdot(\epsilon\nabla v_0), v_h) \le C\|v_0\|_2\|v_h\|,$$
$$\mathcal{A}_\beta(u_0, v_h) = -(\nabla\cdot(\beta\nabla u_0), v_h) \le C\|u_0\|_2\|v_h\|.$$

Hence, (4.4.4) yields

$$\|u_h''(0)\| \le C\big(\|u_0\|_2 + \|v_0\|_2 + \|f\|_{H^1(L^2)}\big). \qquad (4.4.5)$$

In the previous estimate, we have used the fact that

$$\sup_{0\le t\le T}\|f(t)\| \le C\|f\|_{H^1(J;W)}.$$

In fact, for any Banach space $\mathcal{B}$, we know that (*cf.* [116], Proposition 7.1)

$$\sup_{0\le t\le T}\|v(t)\|_{\mathcal{B}} \le C\|v\|_{H^1(J;\mathcal{B})}\ \forall v \in H^1(J;\mathcal{B}). \qquad (4.4.6)$$

TH-2392_146123010

where the positive constant C depends on final time T. Also, from the definition of $\mathcal{Q}_h$ operator, we can easily derive

$$\|u_h'(0)\|_1 = \|\mathcal{Q}_{\epsilon h} v_0\|_1 \leq C\|v_0\|_1. \tag{4.4.7}$$

For $i = 3$, taking $t \to 0^+$ in (4.2.1) and using (4.4.4), we have

$$\begin{aligned}(u_h''(0) - u''(0), v_h) &= \mathcal{B}_\sigma(v_0, v_h) - \mathcal{B}_{\sigma h}(\mathcal{Q}_{\epsilon h} v_0, v_h) + \mathcal{B}_\delta(u_0, v_h) \\ &\quad -\mathcal{B}_{\delta h}(\mathcal{Q}_{\beta h} u_0, v_h) \\ &= \mathcal{B}_\sigma^\Delta(v_0, v_h) + \mathcal{B}_{\sigma h}(v_0 - \mathcal{Q}_{\epsilon h} v_0, v_h) + \mathcal{B}_\delta^\Delta(u_0, v_h) \\ &\quad +\mathcal{B}_{\delta h}(u_0 - \mathcal{Q}_{\beta h} u_0, v_h) \\ &\leq C(h^2 + \lambda)(\|u_0\|_2 + \|v_0\|_2)\|v_h\|. \end{aligned} \tag{4.4.8}$$

In the last inequality, we have used Lemma 3.3.1 and Lemma 3.3.4, and the fact that $u \in C^2(J; W)$. Then use definition of L^2 projection and (4.4.8) to obtain

$$\begin{aligned}(u_h''(0) - \mathcal{L}_h u''(0), v_h) &= (u_h''(0) - u''(0), v_h) \\ &\leq C(h^2 + \lambda)(\|u_0\|_2 + \|v_0\|_2)\|v_h\|, \end{aligned} \tag{4.4.9}$$

which imply

$$\|u_h''(0) - \mathcal{L}_h u''(0)\| \leq Ch(\|u_0\|_2 + \|v_0\|_2). \tag{4.4.10}$$

Estimate (4.4.10) together with inverse inequality and (4.3.9) yields

$$\begin{aligned}\|u_h''(0)\|_1 &\leq Ch^{-1}\|u_h''(0) - \mathcal{L}_h u''(0)\| + \|\mathcal{L}_h u''(0)\|_1 \\ &\leq C(\|u_0\|_3 + \|v_0\|_3 + \|f\|_{H^1(H^1)}). \end{aligned} \tag{4.4.11}$$

Next, for $u_h \in C^3(J; V_h)$ we differentiate (4.4.1) with respect to t and then take $t \to 0^+$ to have

$$\begin{aligned}(u_h'''(0), v_h) &= -\mathcal{B}_{\sigma h}(u_h''(0), v_h) - \mathcal{B}_{\delta h}(u_h'(0), v_h) \\ &\quad -\mathcal{A}_{\epsilon h}(u_h''(0), v_h) - \mathcal{A}_{\beta h}(u_h'(0), v_h) + (f'(0), v_h) \\ &= -\mathcal{B}_{\sigma h}(u_h''(0), v_h) - \mathcal{B}_{\delta h}(\mathcal{Q}_{\epsilon h} v_0, v_h) \\ &\quad -\mathcal{A}_{\epsilon h}(u_h''(0) - \mathcal{Q}_{\epsilon h} u''(0), v_h) - \mathcal{A}_{\beta h}(\mathcal{Q}_{\epsilon h} v_0 - \mathcal{Q}_{\beta h} u'(0), v_h) \\ &\quad -\sum_{l=1}^{2} \left\{ \mathcal{A}_\epsilon^l(u''(0), v_h) + \mathcal{A}_\beta^l(u'(0), v_h) \right\} + (f'(0), v_h). \end{aligned} \tag{4.4.12}$$

Now, for $u \in C^2(J; \mathcal{Y})$, use the fact that

$$\left[\epsilon(x) \frac{\partial u''(t)}{\partial \mathbf{n}} + \beta(x) \frac{\partial u'(t)}{\partial \mathbf{n}} \right] = 0 \quad \text{along } \Gamma \times [0, T]$$

TH-2392_146123010

in the equation (4.4.12) to obtain

$$\begin{aligned}(u_h'''(0), v_h) &= -\mathcal{B}_{\sigma h}(u_h''(0), v_h) - \mathcal{B}_{\delta h}(\mathcal{Q}_{\epsilon h} v_0, v_h) \\ &\quad -\mathcal{A}_{\epsilon h}(u_h''(0) - \mathcal{Q}_{\epsilon h} u''(0), v_h) - \mathcal{A}_{\beta h}(\mathcal{Q}_{\epsilon h} v_0 - \mathcal{Q}_{\beta h} v_0, v_h) \\ &\quad + \sum_{l=1}^{2} \Big\{ (\nabla \cdot \epsilon_l \nabla u''(0), v_h)_{\Omega_l} + (\nabla \cdot \beta \nabla u'(0), v_h)_{\Omega_l} \Big\} + (f'(0), v_h) \\ &\leq C \Big\{ \|u_h''(0)\| + h^{-1}(\|u_h''(0) - \mathcal{Q}_{\epsilon h} u''(0)\|_1 + \|\mathcal{Q}_{\epsilon h} v_0 - \mathcal{Q}_{\beta h} v_0\|_1) \\ &\quad + \sum_{l=1}^{2} \|u''(0)\|_{2,\Omega_l} + \|v_0\|_2 + \|f\|_{H^2(L^2)} \Big\} \|v_h\|. \end{aligned} \tag{4.4.13}$$

From (4.4.9) and Remark 4.3.1, we have

$$\begin{aligned}&\|u_h''(0) - \mathcal{Q}_{\epsilon h} u''(0)\|_1 \\ &\leq Ch^{-1}\|u_h''(0) - \mathcal{L}_h u''(0)\| + \|\mathcal{L}_h u''(0) - \mathcal{Q}_{\epsilon h} u''(0)\|_1 \\ &\leq C(\|u_0\|_2 + \|v_0\|_2) + Ch \sum_{l=1}^{2} \|u''(0)\|_{2,\Omega_l} \\ &\leq Ch(\|u_0\|_4 + \|v_0\|_4 + \|f\|_{H^1(H^2)}). \end{aligned} \tag{4.4.14}$$

In the last inequality, we have used the fact that $\|u_0\|_K \leq Ch\|u_0\|_{2,K}$ for all $K \in \mathcal{T}_h$. Using (4.4.14) in (4.4.13), we obtain

$$\|u_h'''(0)\| \leq C(\|u_0\|_4 + \|v_0\|_4 + \|f\|_{H^2(H^2)}).$$

The case $i = 4$ can be done in a similar and hence details are omitted. This completes the rest of the proof. □

Differentiating (4.4.1) twice with respect to t and substitute $v_h = u_h'''$ to have

$$\begin{aligned}&\frac{1}{2}\frac{d}{dt}\Big\{\|u_h'''\|^2 + \mathcal{B}_{\delta h}(u_h'', u_h'') + \mathcal{A}_{\beta h}(u_h'', u_h'')\Big\} + \mathcal{B}_{\sigma h}(u_h''', u_h''') + \mathcal{A}_{\epsilon h}(u_h''', u_h''') \\ &= (f'', u_h'''). \end{aligned} \tag{4.4.15}$$

Integration from 0 to t and using standard arguments lead to

$$\begin{aligned}&\|u_h''(t)\|^2 + \|u_h'''(t)\|^2 + \|u_h''(t)\|_1^2 + \int_0^t \|u_h'''\|^2 dt + \int_0^t \|u_h'''\|_1^2 dt \\ &\leq C\Big(\|u_h''(0)\|^2 + \|u_h'''(0)\|^2 + \|u_h''(0)\|_1^2 + \int_0^t \|f''\|^2 dt\Big). \end{aligned}$$

Using Lemma 4.4.1 in the above equation, we get

$$\|u_h'''\|^2 + \|u_h''\|_1^2 + \int_0^t \|u_h'''\|_1^2 dt \leq C\Big(\|u_0\|_4^2 + \|v_0\|_4^2 + \|f\|_{H^2(H^2)}^2\Big). \tag{4.4.16}$$

TH-2392_146123010

Similarly, we obtain

$$\|u_h''''\|^2 + \|u_h'''\|_1^2 + \int_0^t \|u_h''''\|_1^2 dt \leq C\Big(\|u_0\|_6^2 + \|v_0\|_6^2 + \|f\|_{H^3(H^2)}^2\Big). \tag{4.4.17}$$

Now, we prove the convergence result for the semidiscrete scheme in $L^\infty(L^2)$ norm.

Theorem 4.4.2. *Let u and u_h be the solutions of problems (4.1.1)-(4.1.3) and (4.4.1), respectively. Then, for $u_0,\ v_0 \in \mathcal{Y}$ and $f \in L^2(J;W)$, we have*

$$\|u - u_h\|_{L^\infty(J;L^2(\Omega))} \leq C(u)\left(h + \sqrt{\lambda} + \frac{\lambda}{h}\right)^2,$$

where $C(u) := C\left\{\|u_0\|_{\mathcal{Y}}^2 + \|v_0\|_{\mathcal{Y}}^2 + \|u\|_{H^1(\mathcal{Y})}\right\}^{\frac{1}{2}}$.

Proof. Define the error $e(t)$ as $e(t) := u(t) - u_h(t)$ and then subtracting (4.2.1) from (4.4.1) with some natural rearrangements, we obtain

$$\begin{aligned}
&(e'', v_h) + \mathcal{B}_{\sigma h}(e', v_h) + \mathcal{B}_{\delta h}(e, v_h) + \mathcal{A}_{\epsilon h}(e', v_h) + \mathcal{A}_{\beta h}(e, v_h) \\
&= -\mathcal{B}_{\sigma h}^{\Delta}(u', v_h) - \mathcal{B}_{\delta h}^{\Delta}(u, v_h) - \mathcal{A}_{\epsilon h}^{\Delta}(u', v_h) - \mathcal{A}_{\beta h}^{\Delta}(u, v_h)\ \forall v_h \in V_h.
\end{aligned} \tag{4.4.18}$$

Now, we split $e(t)$ into standard ρ and θ as

$$e = \rho + \theta,\ \rho := u - \xi_u,\ \theta := \xi_u - u_h,$$

where ξ_u is the projection operator defined as in (4.3.10).

Then equation (4.4.18) reduces to

$$\begin{aligned}
&(\theta'', v_h) + \mathcal{B}_{\sigma h}(\theta', v_h) + \mathcal{B}_{\delta h}(\theta, v_h) + \mathcal{A}_{\epsilon h}(\theta', v_h) + \mathcal{A}_{\beta h}(\theta, v_h) \\
&= -(\rho'', v_h) - \mathcal{B}_{\sigma h}(\rho', v_h) - \mathcal{B}_{\delta h}(\rho, v_h) - \mathcal{A}_{\epsilon h}(\rho', v_h) - \mathcal{A}_{\beta h}(\rho, v_h) \\
&\quad -\mathcal{B}_{\sigma h}^{\Delta}(u', v_h) - \mathcal{B}_{\delta h}^{\Delta}(u, v_h) - \mathcal{A}_{\epsilon h}^{\Delta}(u', v_h) - \mathcal{A}_{\beta h}^{\Delta}(u, v_h)\ \forall v_h \in V_h.
\end{aligned} \tag{4.4.19}$$

Using the definition of ξ_u, we observe that

$$\begin{aligned}
&\mathcal{A}_{\epsilon h}(\rho', v_h) + \mathcal{A}_{\beta h}(\rho, v_h) \\
&= \mathcal{A}_{\epsilon h}(u', v_h) + \mathcal{A}_{\beta h}(u, v_h) - \big\{\mathcal{A}_{\epsilon h}(\xi_u', v_h) + \mathcal{A}_{\beta h}(\xi_u, v_h)\big\} \\
&= \mathcal{A}_{\epsilon h}(u', v_h) + \mathcal{A}_{\beta h}(u, v_h) - \big\{\mathcal{A}_{\epsilon}(u', v_h) + \mathcal{A}_{\beta}(u, v_h)\big\}.
\end{aligned}$$

Above equation together with (4.4.19) leads to

$$\begin{aligned}
&(\theta'', v_h) + \mathcal{B}_{\delta h}(\theta, v_h) + \mathcal{A}_{\epsilon h}(\theta', v_h) + \mathcal{A}_{\beta h}(\theta, v_h) \\
&= -(\rho'', v_h) - \mathcal{B}_{\sigma h}(e', v_h) - \mathcal{B}_{\delta h}(\rho, v_h) \\
&\quad -\mathcal{B}_{\sigma h}^{\Delta}(u', v_h) - \mathcal{B}_{\delta h}^{\Delta}(u, v_h)\ \forall v_h \in V_h,
\end{aligned} \tag{4.4.20}$$

TH-2392_146123010

which can be rewritten as

$$\begin{aligned}&\frac{d}{dt}(\theta', v_h) - (\theta', v_h') + \mathcal{B}_{\delta h}(\theta, v_h) + \frac{d}{dt}\mathcal{A}_{\epsilon h}(\theta, v_h) - \mathcal{A}_{\epsilon h}(\theta, v_h') + \mathcal{A}_{\beta h}(\theta, v_h)\\ &= -\frac{d}{dt}(\rho', v_h) + (\rho', v_h') - \frac{d}{dt}\mathcal{B}_{\sigma h}(e, v_h) + \mathcal{B}_{\sigma h}(e, v_h') - \mathcal{B}_{\delta h}(\rho, v_h)\\ &\quad -\mathcal{B}^{\Delta}_{\sigma h}(u', v_h) - \mathcal{B}^{\Delta}_{\delta h}(u, v_h)\ \forall v_h \in V_h. \end{aligned} \tag{4.4.21}$$

Following Baker [15], we define $\hat{v} : [0, T] \times \Omega \to \mathbb{R}$ as

$$\hat{v}(., t) = \int_t^{\zeta} \theta(., s)ds\ , \quad 0 \le t \le T,$$

for some fixed $\zeta \in [0, T]$. Then, clearly $\hat{v} \in V_h$ as $\theta = \xi_u - u_h \in V_h$. Also, observe that

$$\hat{v}(., \zeta) = 0 \ \text{ and } \ \frac{d}{dt}\hat{v}(., t) = -\theta(., t)\ , \ \ 0 \le t \le T. \tag{4.4.22}$$

Setting $v_h = \hat{v}$ in (4.4.21) and making some rearrangements, we obtain

$$\begin{aligned}&\frac{d}{dt}(\theta', \hat{v}) + \frac{1}{2}\frac{d}{dt}(\theta, \theta) + \mathcal{B}_{\sigma h}(\theta, \theta) - \frac{1}{2}\frac{d}{dt}\mathcal{B}_{\delta h}(\hat{v}, \hat{v})\\ &+\frac{d}{dt}\mathcal{A}_{\epsilon h}(\theta, \hat{v}) + \mathcal{A}_{\epsilon h}(\theta, \theta) - \frac{1}{2}\frac{d}{dt}\mathcal{A}_{\beta h}(\hat{v}, \hat{v})\\ &= -\frac{d}{dt}(\rho', \hat{v}) - (\rho', \theta) - \frac{d}{dt}\mathcal{B}_{\sigma h}(e, \hat{v}) - \mathcal{B}_{\sigma h}(\rho, \theta) - \mathcal{B}_{\delta h}(\rho, \hat{v})\\ &\quad -\mathcal{B}^{\Delta}_{\sigma h}(u', \hat{v}) - \mathcal{B}^{\Delta}_{\delta h}(u, \hat{v}).\end{aligned}$$

Integrating from 0 to ζ and using $\hat{v}(\zeta) = 0$, we get

$$\begin{aligned}&-(\theta'(0), \hat{v}(0)) + \frac{1}{2}\|\theta(\zeta)\|^2 - \frac{1}{2}\|\theta(0)\|^2 + \int_0^{\zeta} \mathcal{B}_{\sigma h}(\theta, \theta)ds + \frac{1}{2}\mathcal{B}_{\delta h}(\hat{v}(0), \hat{v}(0))\\ &-\mathcal{A}_{\epsilon h}(\theta(0), \hat{v}(0)) + \int_0^{\zeta} \mathcal{A}_{\epsilon h}(\theta, \theta)ds + \frac{1}{2}\mathcal{A}_{\beta h}(\hat{v}(0), \hat{v}(0))\\ &= (\rho'(0), \hat{v}(0)) - \int_0^{\zeta} (\rho', \theta)ds + \mathcal{B}_{\sigma h}(e(0), \hat{v}(0)) - \int_0^{\zeta} \mathcal{B}_{\sigma h}(\rho, \theta)ds\\ &\quad - \int_0^{\zeta} \mathcal{B}_{\delta h}(\rho, \hat{v})ds - \int_0^{\zeta} \mathcal{B}^{\Delta}_{\sigma h}(u', \hat{v})ds - \int_0^{\zeta} \mathcal{B}^{\Delta}_{\delta h}(u, \hat{v})ds.\end{aligned} \tag{4.4.23}$$

Observe that $\theta(0) = \xi_u(0) - u_h(0) = \mathcal{Q}_h u(0) - \mathcal{Q}_h u_0 = 0$, hence (4.4.23) becomes

$$\begin{aligned}&\frac{1}{2}\|\theta(\zeta)\|^2 + \int_0^{\zeta} \|\theta\|^2 ds + \int_0^{\zeta} \|\theta\|_1^2 ds + \frac{1}{2}\|\hat{v}(0)\|_1^2\\ &\le (e'(0), \hat{v}(0)) - \int_0^{\zeta} (\rho', \theta)ds + \mathcal{B}_{\sigma h}(e(0), \hat{v}(0)) - \int_0^{\zeta} \mathcal{B}_{\sigma h}(\rho, \theta)ds\\ &\quad - \int_0^{\zeta} \mathcal{B}_{\delta h}(\rho, \hat{v})ds - \int_0^{\zeta} \mathcal{B}^{\Delta}_{\sigma h}(u', \hat{v})ds - \int_0^{\zeta} \mathcal{B}^{\Delta}_{\delta h}(u, \hat{v})ds.\end{aligned} \tag{4.4.24}$$

TH-2392_146123010

Then Cauchy-Schwartz inequality, Lemma 3.3.1 and continuity of $\mathcal{B}_h$ operator leads to

$$\begin{aligned}
&\frac{1}{2}\|\theta(\zeta)\|^2+\int_0^\zeta\|\theta\|^2ds+\int_0^\zeta\|\theta\|_1^2ds+\frac{1}{2}\|\hat{v}(0)\|_1^2\\
&\leq C\bigg(\|e'(0)\|\|\hat{v}(0)\|+\int_0^\zeta\|\rho'\|\|\theta\|ds+\|e(0)\|\|\hat{v}(0)\|+\int_0^\zeta\|\rho\|\|\theta\|ds\\
&\quad+\int_0^\zeta\|\rho\|\|\hat{v}\|ds+\left(h+\sqrt{\lambda}+\frac{\lambda}{h}\right)^2\int_0^\zeta\|u'\|_{\mathcal{Y}}\|\hat{v}\|ds\\
&\quad+\left(h+\sqrt{\lambda}+\frac{\lambda}{h}\right)^2\int_0^\zeta\|u\|_{\mathcal{Y}}\|\hat{v}\|ds\bigg). \qquad (4.4.25)
\end{aligned}$$

Since θ is continuous in the time variable, we select ζ such that $\|\theta(\zeta)\|=\max_{0\leq t\leq T}\|\theta(t)\|$. Then we observe that $\|\hat{v}(t)\|\leq C(T)\|\theta(\zeta)\|,\ t\in[0,T]$, which in combination with (4.4.25) leads to

$$\begin{aligned}
\|\theta(\zeta)\| \ \leq\ & C\bigg(\|e'(0)\|+\|e(0)\|+\int_0^\zeta(\|\rho'\|+\|\rho\|)ds\\
&+\left(h+\sqrt{\lambda}+\frac{\lambda}{h}\right)^2\int_0^\zeta(\|u'\|_{\mathcal{Y}}+\|u\|_{\mathcal{Y}})ds\bigg).
\end{aligned}$$

This together with Lemma 4.3.1 leads to Theorem 4.4.2.

Remark 4.4.2. *Theorem 4.4.2 is an extension of Theorem 5.6 in [107] to general linear hyperbolic equation with interface. It is worth to note that Theorem 5.6 in [107] is concerned on the convergence of finite element solution to the exact solution of linearized Westervelt equation with variable coefficients without interface.*

TH-2392_146123010

5

Fully Discrete Error Analysis for DPL Bio Heat Transfer Problem with Interface

This chapter is devoted to the extension of spatially semidiscrete *a priori* error analysis to the fully discrete approximation for the dual-phase-lag (DPL) bio heat transfer model problem (1.1.7)-(1.1.9). Following Baker [15], Crank-Nicolson scheme is applied for the temporal discretization after reformulating the governing equation as first-order system. Optimal order of convergence in $L^\infty(L^2)$ norm is derived for the fully discrete solution. Finally, two dimensional test experiments are presented to testify our theoretical results.

5.1 Introduction

We shall begin with first recalling the dual-phase-lag (DPL) bio heat transfer model problem of the form

$$u'' + \sigma u' + \delta u - \nabla \cdot (\epsilon \nabla u') - \nabla \cdot (\beta \nabla u) = f \quad \text{in } \Omega \times (0, T] \tag{5.1.1}$$

with initial and boundary conditions

$$u(x,0) = u_0 \ \ \& \ \ u'(x,0) = v_0 \ \text{ in } \Omega; \ \ u(x,t) = 0 \quad \text{on } \partial\Omega \times (0,T] \tag{5.1.2}$$

and jump conditions on the interface

$$[u] = 0, \quad \left[\epsilon(x)\frac{\partial u'}{\partial \mathbf{n}} + \beta(x)\frac{\partial u}{\partial \mathbf{n}}\right] = 0 \quad \text{along } \Gamma \times [0,T]. \tag{5.1.3}$$

where Ω is a bounded domain in $\mathbb{R}^d (d = 2,\ 3)$ with Lipschitz boundary $\partial\Omega$ and $\Omega_1 \subset \Omega$ is an open domain with C^2 smooth boundary $\Gamma = \partial\Omega_1$ and $\Omega_2 = \Omega \backslash \Omega_1$. Other symbols and notations are as defined in Chapter 1. We assume the coefficient functions are

TH-2392_146123010

positive and piecewise constants on each subdomain Ω_i and we write

$$(\sigma, \delta, \epsilon, \beta) = \begin{cases} (\sigma_1, \delta_1, \epsilon_1, \beta_1) & \text{in } \Omega_1, \\ (\sigma_2, \delta_2, \epsilon_2, \beta_2) & \text{in } \Omega_2. \end{cases}$$

Further, for the purpose of error analysis, initial data (u_0, v_0) and external force f are assumed to be sufficiently smooth real valued functions so that a weak solution $u \in H^1(V) \cap H^2(W)$ satisfying

$$(u'', v) + \mathcal{B}_\sigma(u', v) + \mathcal{B}_\delta(u, v) + \mathcal{A}_\epsilon(u', v) + \mathcal{A}_\beta(u, v) = \langle f(t, \cdot), v\rangle_{V' \times V} \tag{5.1.4}$$

and $(u(0), v(0)) = (u_0, v_0)$ is also a strong solution to the problem (5.1.1)-(5.1.3) and belongs to desired Sobolev spaces. For details, we refer to Chapter 4.

Now, we divide the time interval $I = [0, T]$ into N equally spaced subintervals $I_n = (t_{n-1}, t_n]$, $n = 1, 2, \ldots, N$ with $t_0 = 0$, and $t_N = T$ and $\tau = t_n - t_{n-1}$, the time step. For a sequence $\{p^n\}_{n=0}^N \subset L^2(\Omega)$, we define

$$\partial_\tau p^n = \frac{p^{n+1} - p^n}{\tau} \quad \text{and} \quad p^{n+\frac{1}{2}} = \frac{1}{2}(p^{n+1} + p^n), \;\; n = 0, 1, \ldots, N-1.$$

Also, for a continuous mapping $\phi : [0, T] \to L^2(\Omega)$, we define $\phi^n = \phi(\cdot, t_n)$, $0 \le n \le N$. Then the fully discrete finite element approximation to the problem (5.1.1)-(5.1.3) is defined as follows: Find $U^n \in V_h$ such that

$$\partial_\tau U^n = p^{n+\frac{1}{2}} \;\text{ for }\; n = 0,\; 1, \ldots,\; N-1 \tag{5.1.5}$$

and

$$\begin{aligned} &(\partial_\tau p^n, \psi) + \mathcal{B}_{\sigma h}(p^{n+\frac{1}{2}}, \psi) + \mathcal{B}_{\delta h}(U^{n+\frac{1}{2}}, \psi) + \mathcal{A}_{\epsilon h}(p^{n+\frac{1}{2}}, \psi) + \mathcal{A}_{\beta h}(U^{n+\frac{1}{2}}, \psi) \\ &= (f^{n+\frac{1}{2}}, \psi) \;\; \forall \psi \in V_h, \end{aligned} \tag{5.1.6}$$

with $U^0 = \mathcal{Q}_h u_0$ and $p^0 = \mathcal{Q}_h v_0$. Here, $\mathcal{A}_h$ and $\mathcal{B}_h$ are as defined in Chapter 1. Further, $\mathcal{Q}_h$ is the elliptic projection defined by (2.2.4)(or (2.2.5)).

The following Lemma gives the existence and uniqueness of the fully discrete solution U^n of u^n in terms of the auxiliary variable p^n and in fact gives a computational algorithm to find U^n .

Lemma 5.1.1. *There exists a unique sequence $\{U^n\}_{n=0}^N \subset V_h$ and a corresponding unique sequence $\{p^n\}_{n=0}^N \subset V_h$ satisfying (5.1.5)-(5.1.6).*

Proof. From (5.1.5), we have

$$U^{n+1} = \frac{\tau}{2}(p^{n+1} + p^n) + U^n. \tag{5.1.7}$$

TH-2392_146123010

Using (5.1.7) in (5.1.6), we get

$$\mathcal{A}_\tau(p^{n+1},\psi)=\mathcal{F}^n(\psi)\ \ \forall\psi\in V_h, \tag{5.1.8}$$

where $\mathcal{A}_\tau$ is the bilinear form given by

$$\begin{aligned}\mathcal{A}_\tau(w,v) &= (w,v)+\frac{\tau}{2}\mathcal{B}_{\sigma h}(w,v)+\frac{\tau^2}{4}\mathcal{B}_{\delta h}(w,v)\\ &\quad+\frac{\tau}{2}\mathcal{A}_{\epsilon h}(w,v)+\frac{\tau^2}{4}\mathcal{A}_{\beta h}(w,v)\ \ \forall w,v\in V\end{aligned}$$

and $\mathcal{F}^n$ is the linear functional given by

$$\begin{aligned}\mathcal{F}^n(\psi) &= (p^n,\psi)-\frac{\tau}{2}\mathcal{B}_{\sigma h}(p^n,\psi)-\tau\mathcal{B}_{\delta h}(U^n,\psi)-\frac{\tau^2}{4}\mathcal{B}_{\delta h}(p^n,\psi)\\ &\quad-\frac{\tau}{2}\mathcal{A}_{\epsilon h}(p^n,\psi)-\frac{\tau^2}{4}\mathcal{A}_{\beta h}(p^n,\psi)-\tau\mathcal{A}_{\beta h}(U^n,\psi)+\tau(f^{n+\frac{1}{2}},\psi)\ \forall\psi\in V.\end{aligned}$$

Due to positivity of bilinear maps $\mathcal{B}_h$ and $\mathcal{A}_h$, there exists uniquely defined $p^{n+1}\in V_h$ satisfying equation (5.1.8) and subsequently U^{n+1} exists uniquely for $0\le n\le N-1$.□

Later on, we will need the following results. The proofs involve the use of Taylor's series and standard arguments, and therefore, details are omitted.

Lemma 5.1.2. *For any $v\in H^3(J;L^2(\Omega))$, we have*

$$\|\partial_\tau v^n-v_t^{n+\frac{1}{2}}\|^2\le C\tau^3\int_{t_n}^{t_{n+1}}\|v'''\|^2dt.$$

The layout of this chapter is as follows: While Section 5.1 introduces the fully discrete scheme and established the existence of its solution, we discuss the convergence behavior of fully discrete approximation for the interface problem in Section 5.2. Optimal *a priori* error estimates are derived for the fully discrete solution. Finally, in Section 5.3 we present some numerical results to validate our theoretical findings.

5.2 Fully discrete error analysis

In this section, we study the convergence of fully discrete finite element scheme (5.1.5)-(5.1.6). Optimal *a priori* error estimate in $L^\infty(L^2)$-norm is derived.

In order to compute the error between U^n and u^n, it suffices to establish the error $\omega^n:=u_h^n-U^n$, for $1\le n\le N$. Once we have estimate for ω^n, we can easily get the error estimate for $e^n:=U^n-u^n$ by using the triangle inequality, Theorem 4.4.2 and the Lemma 5.2.1 given below.

Lemma 5.2.1. *Let u and U^n be the solutions of the interface problem (5.1.1)-(5.1.3) and the finite element approximation (5.1.5)-(5.1.6), respectively. Then, we have*

$$\max_{1\le n\le N}\|\omega^n\|^2\le C\tau^4\Big(\int_0^T\|u_{htttt}\|^2dt+\int_0^T\|u_{httt}\|_1^2dt\Big).$$

TH-2392_146123010

Proof. Substitute $t = t_n$ and $t = t_{n+1}$ in (4.4.1) and then add to have

$$\begin{aligned}&(\partial_\tau u_{ht}^n, \psi) + \mathcal{B}_{\sigma h}(u_{ht}^{n+\frac{1}{2}}, \psi) + \mathcal{B}_{\delta h}(u_h^{n+\frac{1}{2}}, \psi) + \mathcal{A}_{\epsilon h}(u_{ht}^{n+\frac{1}{2}}, \psi) + \mathcal{A}_{\beta h}(u_h^{n+\frac{1}{2}}, \psi)\\ &= (f^{n+\frac{1}{2}}, \psi) + (\rho^n, \psi) \ \ \forall \psi \in V_h, \end{aligned} \tag{5.2.1}$$

where $\rho^n := \partial_\tau u_{ht}^n - u_{htt}^{n+\frac{1}{2}}$. Now, subtracting (5.1.6) from (5.2.1), we have

$$\begin{aligned}&(\partial_\tau q^n, \psi) + \mathcal{B}_{\sigma h}(q^{n+\frac{1}{2}}, \psi) + \mathcal{B}_{\delta h}(\omega^{n+\frac{1}{2}}, \psi) + \mathcal{A}_{\epsilon h}(q^{n+\frac{1}{2}}, \psi) + \mathcal{A}_{\beta h}(\omega^{n+\frac{1}{2}}, \psi)\\ &= (\rho^n, \psi) \ \ \forall \psi \in V_h, \end{aligned} \tag{5.2.2}$$

with $q^n := u_{ht}^n - p^n$.

From (5.1.5), it is easy to observe that

$$\partial_\tau \omega^n = q^{n+\frac{1}{2}} + \partial_\tau u_h^n - u_{ht}^{n+\frac{1}{2}} = q^{n+\frac{1}{2}} + \alpha^n, \ \alpha^n := \partial_\tau u_h^n - u_{ht}^{n+\frac{1}{2}}, \tag{5.2.3}$$

so that

$$\omega^n = \tau \sum_{k=0}^{n-1} \partial_\tau \omega^k = \tau \sum_{k=0}^{n-1} q^{k+\frac{1}{2}} + \tau \sum_{k=0}^{n-1} \alpha^k \ \ \& \ \ q^n = \tau \sum_{k=0}^{n-1} \partial_\tau q^k.$$

Here, we have used the fact that $\omega^0 = u_h^0 - U^0 = \mathcal{Q}_h u_0 - \mathcal{Q}_h u_0 = 0$ and $q^0 = u_{ht}^0 - p^0 = \mathcal{Q}_h v_0 - \mathcal{Q}_h v_0 = 0$. Hence, using the above relations it follows that

$$\partial_\tau \omega^n = \frac{\tau}{2}\left(\sum_{k=0}^{n} \partial_\tau q^k + \sum_{k=0}^{n-1} \partial_\tau q^k \right) + \alpha^n, \tag{5.2.4}$$

$$\omega^{n+\frac{1}{2}} = \frac{\tau}{2}\left(\sum_{k=0}^{n} q^{k+\frac{1}{2}} + \sum_{k=0}^{n-1} q^{k+\frac{1}{2}} \right) + \frac{\tau}{2}\left(\sum_{k=0}^{n} \alpha^k + \sum_{k=0}^{n-1} \alpha^k \right). \tag{5.2.5}$$

Now, we define a sequence $\{s^n\}_{n=0}^N$ such that $s^0 = 0$ and

$$s^n = \tau \sum_{k=0}^{n-1} \omega^{k+\frac{1}{2}}, \ n = 1, \ldots, N-1,$$

so that

$$s^{n+\frac{1}{2}} = \frac{\tau}{2}\left(\sum_{k=0}^{n} \omega^{k+\frac{1}{2}} + \sum_{k=0}^{n-1} \omega^{k+\frac{1}{2}} \right). \tag{5.2.6}$$

TH-2392_146123010

Hence, for any $\psi \in V_h$, using the identities (5.2.4)-(5.2.6) we obtain

$$\begin{aligned}
&(\partial_\tau \omega^n, \psi) + \mathcal{B}_{\sigma h}(\omega^{n+\frac{1}{2}}, \psi) + \mathcal{B}_{\delta h}(s^{n+\frac{1}{2}}, \psi) + \mathcal{A}_{\epsilon h}(\omega^{n+\frac{1}{2}}, \psi) + \mathcal{A}_{\beta h}(s^{n+\frac{1}{2}}, \psi) \\
&= \frac{\tau}{2}\sum_{k=0}^{n}\Big\{(\partial_\tau q^k, \psi) + \mathcal{B}_{\sigma h}(q^{k+\frac{1}{2}}, \psi) + \mathcal{B}_{\delta h}(\omega^{k+\frac{1}{2}}, \psi) + \mathcal{A}_{\epsilon h}(q^{k+\frac{1}{2}}, \psi) \\
&\quad + \mathcal{A}_{\beta h}(\omega^{k+\frac{1}{2}}, \psi)\Big\} + \frac{\tau}{2}\sum_{k=0}^{n-1}\Big\{(\partial_\tau q^k, \psi) + \mathcal{B}_{\sigma h}(q^{k+\frac{1}{2}}, \psi) + \mathcal{B}_{\delta h}(\omega^{k+\frac{1}{2}}, \psi) \\
&\quad + \mathcal{A}_{\epsilon h}(q^{k+\frac{1}{2}}, \psi) + \mathcal{A}_{\beta h}(\omega^{k+\frac{1}{2}}, \psi)\Big\} + (\alpha^n, \psi) + \frac{\tau}{2}\mathcal{B}_{\sigma h}\Big(\sum_{k=0}^{n}\alpha^k + \sum_{k=0}^{n-1}\alpha^k, \psi\Big) \\
&\quad + \frac{\tau}{2}\mathcal{A}_{\epsilon h}\Big(\sum_{k=0}^{n}\alpha^k + \sum_{k=0}^{n-1}\alpha^k, \psi\Big).
\end{aligned}$$

Using (5.2.2), for $1 \le n \le N-1$, we derive

$$\begin{aligned}
&(\partial_\tau \omega^n, \psi) + \mathcal{B}_{\sigma h}(\omega^{n+\frac{1}{2}}, \psi) + \mathcal{B}_{\delta h}(s^{n+\frac{1}{2}}, \psi) + \mathcal{A}_{\epsilon h}(\omega^{n+\frac{1}{2}}, \psi) + \mathcal{A}_{\beta h}(s^{n+\frac{1}{2}}, \psi) \\
&= (T_1^n, \psi) + \mathcal{B}_{\sigma h}(T_2^n, \psi) + \mathcal{A}_{\epsilon h}(T_2^n, \psi)\ \forall \psi \in V_h, \qquad (5.2.7)
\end{aligned}$$

where

$$T_1^n := \frac{\tau}{2}\rho^n + \tau\sum_{k=0}^{n-1}\rho^k + \alpha^n \ \ \& \ \ T_2^n := \frac{\tau}{2}\alpha^n + \tau\sum_{k=0}^{n-1}\alpha^k.$$

Substituting $\psi = \omega^{n+\frac{1}{2}} = \partial_\tau s^n$ in (5.2.7) and making some rearrangements, we arrive at

$$\begin{aligned}
&(\omega^{n+1}, \omega^{n+1}) + 2\tau\mathcal{B}_{\sigma h}(\omega^{n+\frac{1}{2}}, \omega^{n+\frac{1}{2}}) + \mathcal{B}_{\delta h}(s^{n+1}, s^{n+1}) + 2\tau\mathcal{A}_{\epsilon h}(\omega^{n+\frac{1}{2}}, \omega^{n+\frac{1}{2}}) \\
&+\mathcal{A}_{\beta h}(s^{n+1}, s^{n+1}) = (\omega^n, \omega^n) + \mathcal{B}_{\delta h}(s^n.s^n) + \mathcal{A}_{\beta h}(s^n, s^n) + 2\tau(T_1^n, \omega^{n+\frac{1}{2}}) \\
&\qquad +2\tau\mathcal{B}_{\sigma h}(T_2^n, \omega^{n+\frac{1}{2}}) + 2\tau\mathcal{A}_{\epsilon h}(T_2^n, \omega^{n+\frac{1}{2}}).
\end{aligned}$$

Next, using Cauchy-Schwartz inequality, coercivity and continuity of the bilinear maps $\mathcal{B}$ and $\mathcal{A}$, we obtain

$$\begin{aligned}
&(\omega^{n+1}, \omega^{n+1}) + 2\tau\|\omega^{n+\frac{1}{2}}\|^2 + \mathcal{B}_{\delta h}(s^{n+1}, s^{n+1}) + 2\tau\|\omega^{n+\frac{1}{2}}\|_1^2 + \mathcal{A}_{\beta h}(s^{n+1}, s^{n+1}) \\
&\le (\omega^n, \omega^n) + \mathcal{B}_{\delta h}(s^n, s^n) + \mathcal{A}_{\beta h}(s^n, s^n) + 2\tau\|T_1^n\|\|\omega^{n+\frac{1}{2}}\| + 2\tau\|T_2^n\|\|\omega^{n+\frac{1}{2}}\| \\
&\quad +2\tau\|T_2^n\|_1\|\omega^{n+\frac{1}{2}}\|_1.
\end{aligned}$$

Finally, applying the Young's inequality $ab \le \kappa a^2 + \frac{1}{\kappa}b^2$ for $a, b > 0$ and choosing $\kappa > 0$ appropriately, above relation leads us to

$$\begin{aligned}
&(\omega^{n+1}, \omega^{n+1}) + \mathcal{B}_{\delta h}(s^{n+1}, s^{n+1}) + \mathcal{A}_{\beta h}(s^{n+1}, s^{n+1}) \\
&\le (\omega^n, \omega^n) + \mathcal{B}_{\delta h}(s^n, s^n) + \mathcal{A}_{\beta h}(s^n, s^n) \\
&\quad +2\tau\Big(\|T_1^n\|^2 + \|T_2^n\|^2 + \|T_2^n\|_1^2\Big). \qquad (5.2.8)
\end{aligned}$$

TH-2392_146123010

Summing (5.2.8) from $n = 1$ to $n = l - 1$ with $2 \le l \le N$, we obtain

$$\max_{2\le n\le N} \|\omega^n\|^2 \le \|\omega^1\|^2 + \|s^1\|_1^2 + 2\tau \sum_{n=0}^{l-1} \big(\|T_1^n\|^2 + \|T_2^n\|_1^2\big). \tag{5.2.9}$$

For estimation of the terms ω^1 and s^1, we note that

$$s^1 = \tau\omega^{\frac{1}{2}} = \frac{\tau}{2}\omega^1 \ \ \& \ \ q^{\frac{1}{2}} = \frac{q^1}{2} = \frac{\omega^1}{\tau} - \alpha^0.$$

Now, putting $n = 0$ in the error equation (5.2.2) and using the above identities, we have

$$\begin{aligned} &\frac{2}{\tau^2}(\omega^1,\psi) + \frac{1}{\tau}\mathcal{B}_{\sigma h}(\omega^1,\psi) + \frac{1}{2}\mathcal{B}_{\delta h}(\omega^1,\psi) + \frac{1}{\tau}\mathcal{A}_{\epsilon h}(\omega^1,\psi) + \frac{1}{\tau}\mathcal{A}_{\beta h}(s^1,\psi) \\ &= (\rho^0,\psi) + \frac{2}{\tau}(\alpha^0,\psi) + \mathcal{B}_{\sigma h}(\alpha^0,\psi) + \mathcal{A}_{\epsilon h}(\alpha^0,\psi) \ \ \forall\psi \in V_h. \end{aligned} \tag{5.2.10}$$

Substituting $\psi = \omega^1 = \frac{2}{\tau}$ in (5.2.10) and using coercivity of the operators $\mathcal{B}$ and $\mathcal{A}$, we obtain

$$\|\omega^1\|^2 + \|s^1\|_1^2 \le \frac{\tau^2}{2}(\rho^0,\omega^1) + \tau(\alpha^0,\omega^1) + \frac{\tau^2}{2}\mathcal{B}_{\sigma h}(\alpha^0,\omega^1) + \tau\mathcal{A}_{\epsilon h}(\alpha^0,s^1).$$

Next, use Cauchy-Schwartz and Young's inequality to have

$$\begin{aligned} \|\omega^1\|^2 + \|s^1\|_1^2 \ &\le \ \frac{\tau^4}{4}\|\rho^0\|^2 + \kappa_1\|\omega^1\|^2 + \Big(\tau^2 + \frac{\tau^4}{4}\Big)\|\alpha^0\|^2 \\ &\quad + \kappa_2\|\omega^1\|^2 + \tau^2\|\alpha^0\|_1^2 + \kappa_3\|s^1\|_1^2. \end{aligned}$$

Finally, choosing $\kappa_i > 0$ appropriately leads us to

$$\|\omega^1\|^2 + \|s^1\|_1^2 \le C\Big(\tau^4\|\rho^0\|^2 + \tau^2\|\alpha^0\|_1^2\Big). \tag{5.2.11}$$

Combining (5.2.9) and (5.2.11), we have

$$\max_{1\le n\le N} \|\omega^n\|^2 \le C\Big(\tau^4\|\rho^0\|^2 + \tau^2\|\alpha^0\|_1^2 + 2\tau \sum_{n=0}^{l-1} \big(\|T_1^n\|^2 + \|T_2^n\|_1^2\big)\Big). \tag{5.2.12}$$

Now, we shall estimate both terms T_1^n and T_2^n. For the estimation of T_1^n, use triangle inequality and Cauchy-Schwartz inequality to have

$$\begin{aligned} \|T_1^n\|^2 \ &\le \ \frac{\tau^2}{4}\|\rho^n\|^2 + \tau^2\|\sum_{k=0}^{n-1}\rho^k\|^2 + \|\alpha^n\|^2 \\ &\le \ \frac{\tau^2}{4}\|\rho^n\|^2 + \tau^2 N\sum_{k=0}^{n-1}\|\rho^k\|^2 + \|\alpha^n\|^2 \\ &\le \ C\Big(\frac{\tau^2}{4}\|\rho^n\|^2 + \tau\sum_{k=0}^{n-1}\|\rho^k\|^2 + \|\alpha^n\|^2\Big). \end{aligned}$$

TH-2392_146123010

Then, using Lemma 5.1.2, we obtain

$$\|T_1^n\|^2 \leq C\left(\tau^5 \int_{t_n}^{t_{n+1}} \|u_{htttt}\|^2 dt + \tau^4 \int_0^T \|u_{htttt}\|^2 dt + \tau^3 \int_{t_n}^{t_{n+1}} \|u_{htt}\|^2 dt\right). \tag{5.2.13}$$

The following estimate for T_2^n is achieved using the same technique as used for deriving T_1^n

$$\|T_2^n\|_1^2 \leq C\left(\tau^5 \int_{t_n}^{t_{n+1}} \|u_{htt}\|_1^2 dt + \tau^4 \int_0^T \|u_{htt}\|_1^2 dt\right). \tag{5.2.14}$$

Finally, using (5.2.13)-(5.2.14) in (5.2.12), we obtain

$$\max_{1\leq n\leq N} \|\omega^n\|^2 \leq C\tau^4\left(\int_0^T \|u_{htttt}\|^2 dt + \int_0^T \|u_{htt}\|_1^2 dt\right). \quad \square$$

Now, we are in a position to state the main result of this section.

Theorem 5.2.1. *Let u and U^n be the solutions of the interface problem (5.1.1)-(5.1.3) and the finite element approximation (5.1.5)-(5.1.6), respectively. Assume that $u_0 \in H^6(\Omega) \cap H_0^1(\Omega)$, $v_0 \in H^6(\Omega) \cap H_0^1(\Omega)$ and $f \in H^3(J; H^2(\Omega))$, then we have*

$$\max_{0\leq n\leq N} \|u^n - U^n\| \leq C(u)\left(\left(h + \sqrt{\lambda} + \frac{\lambda}{h}\right)^2 + \tau^2\right),$$

where $C(u) = C\left\{\|u_0\|^2_{H^6(\Omega)} + \|v_0\|^2_{H^6(\Omega)} + \|u\|^2_{H^2(\mathcal{Y})}\right\}^{\frac{1}{2}}$.

Proof. Applying the triangle inequality to

$$u^n - U^n = u^n - u_h^n + u_h^n - U^n,$$

followed by estimates (4.4.16)-(4.4.17), Theorem 4.4.2 and Lemma 5.2.1 leads to desire result. $\square$

Remark 5.2.1. (a) *The proposed fully discrete finite element scheme can be easily extended for the numerical approximation of the solutions to the IBVP (5.1.1)-(5.1.2) coupled with the jump conditions*

$$[u] = 0, \quad \left[\epsilon(x)\frac{\partial u'}{\partial \mathbf{n}} + \beta(x)\frac{\partial u}{\partial \mathbf{n}}\right] = g \quad \text{along } \Gamma \times [0, T]. \tag{5.2.15}$$

TH-2392_146123010

For numerical validation, we refer to numerical Examples 5.3.1-5.3.2.
(b) *In developing numerical methods for interface problems, higher order of convergence is always one of the major research goals, because high order methods are more accurate and cost-efficient. Present analysis provides a scope for the generalization of these works to higher order finite element methods by combining the theory in this work with the analysis in [85]. A higher order finite element approximation and its convergence is illustrated in Example 5.3.3.*

5.3 Numerical Results

In this section, we present some numerical experiments to validate the theoretical findings presented in the previous section. To illustrate the flexibility of the method, different forms of interfaces along with a large scale of variation in the physical coefficients are considered. For our numerical experiment, globally continuous piecewise linear finite elements ($\mathbb{P}_1$) based on fitted triangulations of Ω_i, $i = 1, 2$ are used. The nodes of the triangulations of Ω_1 and Ω_2 coincide on the interface Γ. A higher order fitted finite element approximation has been carried out in Example 5.3.3. All the numerical computations are done in the time interval $J = (0, 1]$.

Table 5.1: Parameters used in computation (see, Xu *et al.* [138])

	Parameters	Domain Ω_1	Domain Ω_2
$k(W/mK)$	Thermal conductivity	0.235	0.445
$\rho(kg/m^3)$	Skin density	1500	1116
$c(J/kgK)$	Specific heat	3600	3300
$w_b(kg/m^3s)$	Blood perfusion rate	0.5	0.5
$c_b(J/kgK)$	Specific heat of blood	3770	43770
$\rho_b(kg/m^3)$	Density of blood	1060	1060

Example 5.3.1. *For our first numerical experiment, we consider a square domain* $\Omega = (-1, 1) \times (-1, 1)$, *where interface* Γ *is a circle centered at* $(0, 0)$ *with radius* $r_0 = 0.5$. *We select the data in (5.1.1)-(5.1.2) and (5.2.15) such that the exact solution* u *is given by*

$$u(x, y, t) = \begin{cases} (r_0^2 - r^2)t^2 & \text{if } r \le r_0, \\ (r_0^2 - r^2)t \sin(\pi x) \sin(\pi y) & \text{if } r > r_0, \text{ where } r^2 = x^2 + y^2. \end{cases}$$

TH-2392_146123010

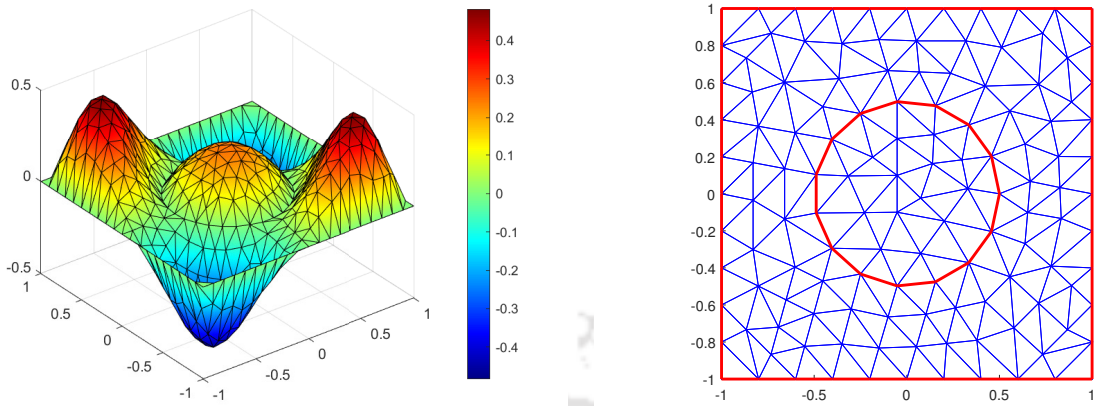

Figure 5.1: Exact solution (left) and triangulation(right) of Ω with $h = 0.305091$ (Test Example 5.3.1).

In Figure 5.1 we show the exact solution and triangulation of the domain Ω with mesh size $h = 0.305091$. In our numerical convergence test, we choose two different sets of physical coefficients borrowed from Xu *et al.* [138] that corresponds to two different forms of bio heat transfer model. Following [138], physical parameters employed in the computation are as in Table 5.1. Dual-phase-lag (DPL) bio heat transfer is characterized by thermal relaxation time τ_q and phase lag for temperature gradient τ_T. Vedavarz *et al.* [133] found that τ_q for some biological tissues lies in the range of $1s - 100s$ at room temperature. Following the paper by Mitra *et al.* [100], we take the thermal lag time (τ_q) and phase lag time (τ_T) as 16 seconds and 0.043 seconds, respectively. Then using Table 5.1, we have the first set of physical coefficients for the DPL bio heat model:

$$(\sigma, \delta, \epsilon, \beta) = \Big(\frac{\tau_q w_b \rho_b c_b + \rho c}{\tau_q \rho c}, \frac{w_b \rho_b c_b}{\tau_q \rho c}, \frac{\tau_T \kappa}{\tau_q \rho c}, \frac{\kappa}{\tau_q \rho c}\Big)$$

$$= \begin{cases} \big(0.4325, 0.0231, 1.1696 \times 10^{-10}, 2.7199 \times 10^{-9}\big) & \text{if } r \le r_0, \\ \big(0.6050, 0.0339, 1.2083 \times 10^{-7}, 7.5520 \times 10^{-9}\big) & \text{if } r > r_0. \end{cases}$$

In the absence of phase lag time (τ_T), equation (5.1.1) reduces to the thermal wave model of bio heat transfer [69, 70]. The second set of physical coefficients that corresponds to the thermal wave model of bio heat transfer is given by

$$(\sigma, \delta, \epsilon, \beta) = \begin{cases} \big(0.4325, 0.0231, 0, 2.7199 \times 10^{-9}\big) & \text{if } r \le r_0, \\ \big(0.6050, 0.0339, 0, 7.5520 \times 10^{-9}\big) & \text{if } r > r_0. \end{cases}$$

TH-2392_146123010

Table 5.2: Example 5.3.1. EOC for $\tau_T \neq 0$ at $t = 1$ and $\tau = 10^{-3}$

h	$\|u - u_h\|_{L^2(\Omega)}$	EOC	$\|u - u_h\|_{H^1(\Omega)}$	EOC
0.3050910	5.03668e-002	-	9.99850e-001	-
0.1673780	1.11142e-002	2.2414	4.64219e-001	1.1025
0.0828717	2.77700e-003	2.1093	2.30304e-001	0.9971
0.0420952	7.65119e-004	2.0718	1.20741e-001	1.0877

Table 5.3: Example 5.3.1. EOC for $\tau_T = 0$ at $t = 1$ and $\tau = 10^{-3}$

h	$\|u - u_h\|_{L^2(\Omega)}$	EOC	$\|u - u_h\|_{H^1(\Omega)}$	EOC
0.3050910	1.17510e-002	-	7.11408e-001	-
0.1673780	3.24310e-003	2.1444	3.54219e-001	1.1615
0.0828717	7.31190e-004	2.1191	1.70304e-001	1.0418
0.0420952	1.85119e-004	2.0280	8.47410e-002	1.0305

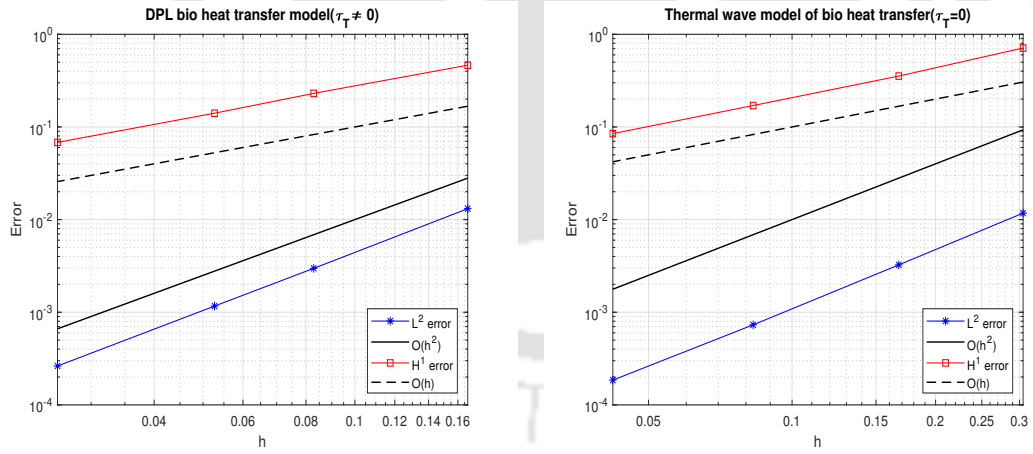

Figure 5.2: Log-log plot of the L^2 norm and H^1 norm versus the mesh size at time $t = 1$ in Example 5.3.1.

Tables 5.2-5.3 represent the numerical solution errors and convergence rates in both L^2 and H^1 norms for $\tau_T \neq 0$ (DPL bio heat transfer) and $\tau_T = 0$ (thermal wave bio heat transfer), respectively. In both cases, we choose the uniform time step size $\tau = 10^{-3}$. The errors at time $t = 1$ are listed in the Tables 5.2-5.3. Figure 5.2 clearly demonstrates

TH-2392_146123010

the second order of convergence in L^2 norm and first order of convergence in H^1 norm. Note that the second set of physical coefficients are chosen to emphasize the fact that our numerical scheme is consistent for the thermal wave model of bio heat transfer and is clearly depicted in Table 5.3.

Example 5.3.2. *For our second numerical example, we consider the interface to be a curve given by* $y = x^2$ *in the computational domain* $\Omega = (-1, 1) \times (-1, 1)$. *We select the data appearing in (5.1.1)-(5.1.2) and (5.2.15) by setting the exact solution as*

$$u(x, y, t) = \begin{cases} 0.25 \exp(t)(y - x^2) \sin(\pi x) \sin(\pi y) & \text{if } y \leq x^2, \\ -5t^2(y - x^2)(y - 1) & \text{if } y > x^2. \end{cases}$$

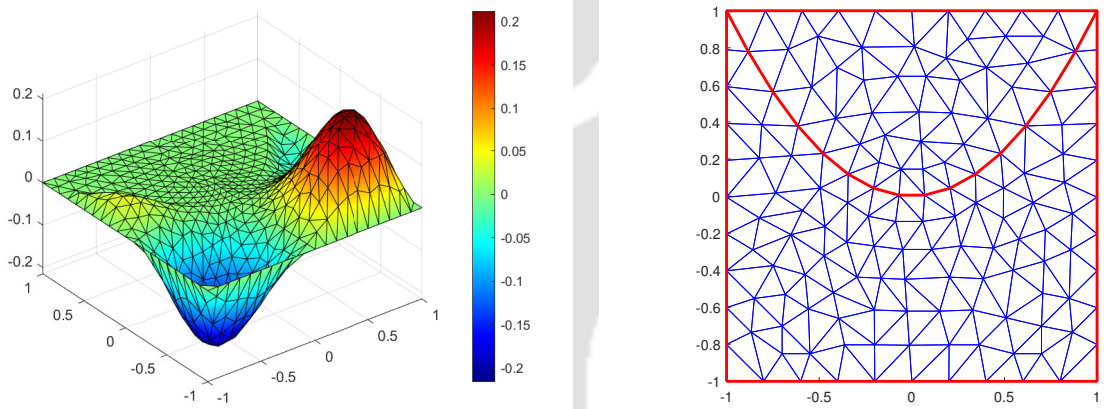

Figure 5.3: Exact solution (left) and triangulation(right) of Ω with $h = 0.2861720$ (Test Example 5.3.2).

With the development of high-power short impulse lasers, use of dual-phase-lag (DPL) model has become common in the study of heat transport in metallic films during ultrafast laser heating [112, 128]. The phase-lag time varies for different materials and it may take values in the range of $10^{-3}s - 10^{3}s$ for heterogeneous materials (*cf.* [96]). To mark the significance of our model problem, we choose the physical coefficients from the paper by Tzou *et al.* [129]

$$(\sigma, \delta, \epsilon, \beta) = \left(\frac{C_E^2}{\alpha_E}, 0, \alpha_e, C_E^2\right)$$
$$= \begin{cases} \left(1.2 \times 10^{12}, 0, 1.2 \times 10^{-4}, 1.44 \times 10^{8}\right) & \text{if } y \leq x^2, \\ \left(1.2 \times 10^{12}, 0, 1.6 \times 10^{-4}, 1.96 \times 10^{8}\right) & \text{if } y > x^2. \end{cases}$$

TH-2392_146123010

Table 5.4: Example 5.3.2. *EOC* at $t = 10^{-12}$ and $\tau = 10^{-14}$

h	$\|u - u_h\|_{L^2(\Omega)}$	*EOC*	$\|u - u_h\|_{H^1(\Omega)}$	*EOC*
0.2861720	1.14180e-002	-	2.16910e-001	-
0.1656240	3.05842e-003	2.4088	1.09996e-001	1.2417
0.0888431	7.67597e-004	2.2195	5.48601e-002	1.1169
0.0478408	1.946711e-004	2.2164	2.74689e-002	1.1175

Here C_E represents the equivalent thermal wave speed, α_E denotes the equivalent thermal diffusivity and α_e is the electron thermal diffusivity of the material. In Figure 5.3, we show the exact solution and the triangulation of the domain Ω with mesh size $h = 0.2861720$. The numerical solution errors and convergence rates in both L^2 and H^1 norms at final time $t = 10^{-12}$ are listed in Table 5.4. The final time step is taken in pico-second (ps) as the thermal lagging model describes the pico-second (ps) heat transport in metal films (*cf.* [128, 129]). It is clear from Figure 5.4 that we have achieved optimal order of convergence in both L^2 and H^1 norms, which confirm the theoretical prediction as proved in Theorem 5.2.1.

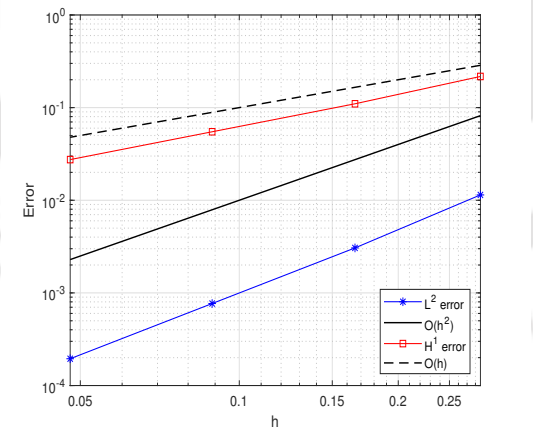

Figure 5.4: Log-log plot of the L^2 norm and H^1 norm versus the mesh size at time $t = 10^{-12}$ in Example 5.3.2.

Example 5.3.3. *For our final numerical example, the computational domain* $\Omega = (-1, 1) \times (-1, 1)$ *is divided into four subdomains* Ω_i, $i = 1, 2, 3, 4$ *using the interface* $\Gamma := \{(x, y) \in \Omega : xy = 0\}$. *We select the data appearing in (5.1.1)-(5.1.2) and (5.2.15)*

TH-2392_146123010

by setting the exact solution as

$$u(x,y,t) = \begin{cases} -0.5x^2\sin(\pi x)\sin(\pi y^2) & \text{if } (x,y) \in \Omega_1, \\ 0.5ty^2\sin(\pi x^2)\sin(\pi y) & \text{if } (x,y) \in \Omega_2, \\ 0.5\sin(t)x^2\sin(\pi x)\sin(\pi y^2) & \text{if } (x,y) \in \Omega_3, \\ -0.5y^2\sin(\pi x^2)\sin(\pi y) & \text{if } (x,y) \in \Omega_2. \end{cases}$$

Table 5.5: Parameters used in computation for Example 5.3.3 (*cf.* [13, 107])

Parameters	Domain Ω_1	Domain Ω_2	Domain Ω_3	Domain Ω_4
σ	5	4	4	7
δ	0	0	0	0
ϵ	6×10^{-9}	4×10^{-9}	4×10^{-2}	4×10^{-9}
β	1500^2	1000^2	1000^2	3000^2

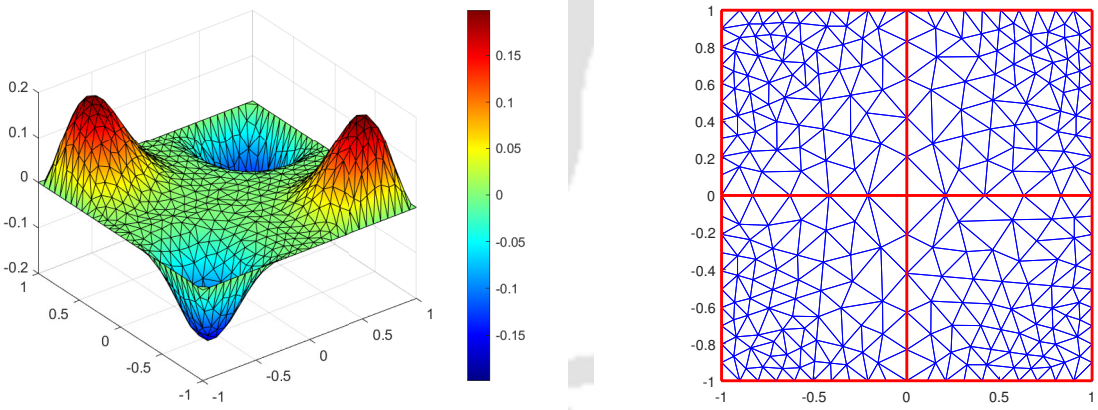

Figure 5.5: Exact solution (left) and triangulation(right) of Ω with $h = 0.2969850$ (Test Example 5.3.3).

In Figure 5.5, we show the exact solution and triangulation of the domain Ω with mesh size $h = 0.2969850$. Equation (5.1.1) also represents the linearized Westervelt's equation for classical model for nonlinear ultrasound propagation through thermoviscous fluids [107]. Following [13, 107], in each subdomain we use different material parameters for the physical coefficients, given in Table 5.5.

TH-2392_146123010

Table 5.6: Example 5.3.3. *EOC* at $t = 1$ and $\tau = 10^{-2}$ for $\mathbb{P}_1$ elements

h	$\|u - u_h\|_{L^2(\Omega)}$	*EOC*	$\|u - u_h\|_{H^1(\Omega)}$	*EOC*
0.2969850	9.90197e-003	-	2.39631e-002	-
0.1542410	2.70301e-003	1.9817	1.20437e-002	1.0501
0.0765776	6.69095e-004	1.9940	6.01226e-003	0.9922
0.0410173	1.80135e-004	2.1019	2.92771e-003	1.1526

Table 5.7: Example 5.3.3. *EOC* at $t = 1$ and $\tau = 10^{-2}$ for $\mathbb{P}_2$ elements

h	$\|u - u_h\|_{L^2(\Omega)}$	*EOC*	$\|u - u_h\|_{H^1(\Omega)}$	*EOC*
0.2969850	4.75802e-004	-	2.77468e-002	-
0.1542410	6.63167e-005	3.0077	7.11948e-003	2.0762
0.0781625	8.56805e-006	3.0106	1.82065e-003	2.0062
0.0435878	1.47599e-006	3.0114	5.47462e-004	2.0576

Table 5.8: Example 5.3.3. *EOC* at $t = 1$ and $\tau = 10^{-2}$ for $\mathbb{P}_3$ elements

h	$\|u - u_h\|_{L^2(\Omega)}$	*EOC*	$\|u - u_h\|_{H^1(\Omega)}$	*EOC*
0.2969850	4.32487e-005	-	1.9120e-003	-
0.1542410	3.02790e-006	4.0587	2.60082e-004	3.0449
0.0781625	1.94952e-007	4.0353	2.97168e-005	3.1914
0.0435878	1.85633e-008	4.0266	4.63975e-006	3.1798

Tables 5.6-5.8 represent the numerical solution errors and convergence rates in both L^2 and H^1 norms for $\mathbb{P}_1$, $\mathbb{P}_2$ and $\mathbb{P}_3$ finite elements, respectively. In all cases, we choose the uniform time step size $\tau = 10^{-2}$. The errors at time $t = 1$ are listed in the Tables 5.6-5.8. Note that the finite element spaces $\mathbb{P}_2$ and $\mathbb{P}_3$ are chosen to emphasize the fact that our numerical scheme is consistent for the higher order finite element spaces under the assumption that $\lambda = \mathrm{O}(h^3)$ and $\lambda = \mathrm{O}(h^4)$, respectively. It is clear from Figure 5.6 that we have achieved optimal order of convergence in both L^2 and H^1 norms which consolidates our theoretical findings.

TH-2392_146123010

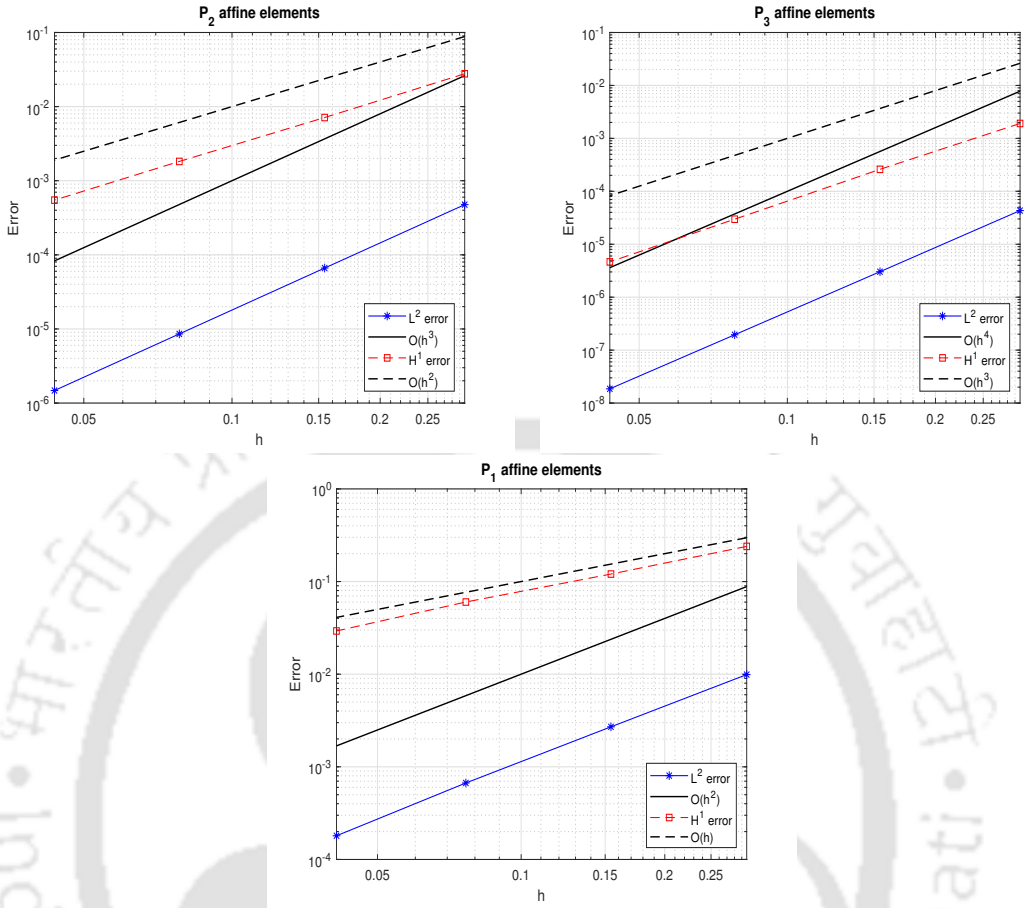

Figure 5.6: Log-log plot of the L^2 norm and H^1 norm versus the mesh size at time $t = 1$ in Example 5.3.3.

TH-2392_146123010

TH-2392_146123010

6

Conclusions and Extensions

In this chapter, we highlight the significance of current thesis work and the corresponding results and techniques to derive them. We also provide information for the scope of possible extensions and future investigations.

6.1 Critical Review of the Results

In this thesis, an interface fitted finite element method is proposed to study *a priori* analysis of finite element approximations for some interface problems arising in biological media as described in Chapter 1-5. The interface are assumed to be of arbitrary shape but are smooth for our purpose. The performance of interface-fitted FEMs depends on the quality of underlying finite element partition and how well the interface is resolved by the finite element mesh. For that, a new λ-strip argument has been introduced for quantifying the relation of error near the interface in terms of the mismatch parameter λ. The critical review of the results of each chapter is presented below.

In Chapter 2, we have studied *a priori* error analysis for the finite element approximations to the electric interface problem (1.1.1)-(1.1.3) in a bounded convex polygonal domain in $\mathbb{R}^d$ $(d = 2, 3)$. Optimal order of convergence in $L^\infty(L^2)$, $H^1(L^2)$ and $L^\infty(H^1)$ norms are established for the semidiscrete solution. For the $L^\infty(H^1)$ norm error estimate for the semidiscrete solution, the splitting technique have been used, where the Ritz projection operator $\mathcal{Q}_h$ (*cf.* Lemma 2.2.1) is used to split the error into two parts. Optimal order of convergence in $L^\infty(H^1)$ norm has been established when the global regularity of the solution is low on the entire domain (see Theorem 2.3.1). $L^\infty(L^2)$ norm error analysis is based on the newly established optimal error estimates in $H^1(L^2)$ norm (see Theorem 2.3.2) for the semidiscrete solution. We have also proved stability of the semidiscrete solution and derive some estimates which are very crucial to prove the optimal convergence rate of the fully discrete solution. A discrete in time scheme based

TH-2392_146123010

on Crank-Nicolson scheme is considered and analyzed for the fully discrete approximation. For the error analysis we split the total error into two parts using semidiscrete solution as an intermediate operator. Optimal order of convergence for $L^\infty(L^2)$ and $L^\infty(H^1)$ norms are established when the global regularity of the solution is low on the entire domain (*cf.* Theorem 2.4.1). Finally, we give numerical examples to validate our theoretical findings.

Chapter 3 deals with the *a priori* analysis for the finite element approximations to the hyperbolic heat conduction model problem (1.1.4)-(1.1.6). Existence, uniqueness and regularity of the weak solution are discussed. We recall some basic approximation properties associated with the finite element spaces and derive some new error estimates involving λ-strip (see Lemma 3.3.1), which are crucial for the argument of convergence. Next, we have derived *a priori* error bound for the elliptic/Ritz projection operator $\mathcal{Q}_h$ involving λ-strip when the exact solution u is having a lower regularity, i.e., $u \in \mathcal{X}$. Optimal order of convergence in both $L^\infty(L^2)$ and $L^\infty(H^1)$ norms are obtained for the semidiscrete solution (see Theorem 3.4.1). Stability for the semidiscrete solution (*cf.* Lemma 3.4.1 and Lemma 3.4.2) are also derived. The fully discrete scheme can be reinterpreted as the Crank-Nicolson discretization of the reformulation of the governing equation in the first-order system, as in Baker [15]. In fact time discretization method is the well-known Newmark method for wave equation when we adopt the particular choice for the parameters in the Newmark scheme (*cf.* [51, 104]). Optimal order of convergence in $L^\infty(L^2)$-norm is established (*cf.* Theorem 3.5.1). Finally, we have presented numerical examples to consolidate our theoretical results. To illustrate the flexibility of the method, different form of interfaces along with a large scale of variations in physical coefficients are considered.

In Chapter 4, we have studied *a priori* error analysis for the spatially semidiscrete scheme for the Dual-phase-lag(DPL) bio heat model problem (1.1.7)-(1.1.9) . Existence, uniqueness and regularity of its solution are discussed. Apart from standard elliptic/Ritz projection operator $\mathcal{Q}_h$, a new non-standard elliptic type projection operator ξ_u has been introduced and *a priori* error bound for the projection operator has been discussed (see Lemma 4.3.1). The derivation of the error bound for the semidiscrete solution heavily depends on this new non-standard elliptic type projection operator ξ_u. We have also recalled some basic approximation properties along with some new analytical tools and techniques, including a λ-strip argument for quantifying the relation of error near the interface in terms of the mismatch parameter λ. Optimal order of convergence for $L^\infty(L^2)$ and $L^\infty(H^1)$ norms are established (see Theorem 4.4.2). Stability of the semidiscrete solution are derived which are very crucial to prove the optimal convergence

TH-2392_146123010

rate of the fully discrete solution.

In Chapter 5, we have extended the spatially discrete *a priori* error analysis to the fully discrete approximation for the Dual-phase-lag(DPL) bio heat model problem (1.1.7)-(1.1.9). The fully discrete scheme is the well-known Newmark method for wave equation when we adopt the particular choice for the parameters in the Newmark scheme (*cf.* [51, 104]). Optimal order of convergence in $L^\infty(L^2)$-norm is derived (*cf.* Theorem 5.2.1). Finally, numerical results for two dimensional test problems are presented in support of our theoretical findings. In each of these numerical experiments we have used different form of interfaces along with a large scale of variations in the physical coefficients indicating the flexibility of the method.

6.2 Extensions and Remarks

***A priori* error analysis of Immersed FEMs:** In this thesis, we have considered fitted finite element methods where the discretization is done in such a way that the grid points lie on the interface. In unfitted finite element method, the discretization of domain is independent of the interface. Unfitted FEMs are helpful in a number of contexts including multi-phase and multi-physics applications with moving interfaces (*e.g.*, fracture mechanics, fluid-structure interaction or free surface flows) or in situations in which one wants to avoid the generation of body-fitted meshes to reduce as much as possible the computational costs. The immersed finite element method (IFEM) is a class of unfitted mesh methods for interface problems. The main idea of IFEM is to locally adjust the approximation function instead of solution mesh to resolve the solution around the interface. Local basis functions are constructed according to the interface jump conditions, hence, structured Cartesian meshes can be used to solve interface problems with non-trivial interfaces. As a future extension, one can consider the *a priori* analysis of the present work to Immersed finite element methods.

A *priori* error analysis of Local Discontinuous Galerkin methods(LDG): A major disadvantage of interface-fitted conforming Galerkin FEMs is that performance of such methods depends not only on the quality of underlying finite element partition but also on the variational formulation of the problem. While the flux discontinuity of the solution can be captured in variational formulation, the discontinuity of the solutions neither fit in the variational formulation nor satisfied in classical FEM solution spaces. More recently, local discontinuous Galerkin (LDG) method has been proposed to solve not only the homogeneous but also nonhomogeneous parabolic interface problems in [10] based on fitted mesh. Using the LDG method for space discretization, authors have derived the approximations for the potential and the flux at the same time. Moreover,

TH-2392_146123010

unlike the conforming Galerkin methods which need special treatment for the discontinuity across an interface, the LDG method provides a natural framework to enforce the discontinuities in both the potential and the flux weakly in the discrete formulation. Theoretical convergence analysis of the LDG method for parabolic interface problems is still open. A future extension of the present work could be *a priori* error analysis of Local Discontinuous Galerkin methods.

***A priori* error analysis of Interface Problems on Polygonal Meshes:** Despite of numerous advancements in the numerical solution of interface problems, there are still a few remaining challenges in the field. One of these challenges concerns the issue of interface problems arises from nonsmooth interfaces or interfaces with Lipschitz continuity. Nonsmooth interfaces are also referred to as geometric singularities, such as sharp edges, cusps and tips, which commonly occur in real-world applications. It is a challenge to design high order interface schemes for geometric singularities both numerically and analytically. Recently, finite element methods using polygonal elements are gaining popularity because of their applicability in handling complex geometries usually appeared in real life problem. Two of the major methods on this regard are the Weak Galerkin FEMs and Virtual element Methods. The numerical solution of elliptic interface problems by means of Weak Galerkin FEMs and Virtual element Methods are investigated in [101] and [30] respectively. Very recently, Deka *et al.* has studied the prabolic interface problem on polygonal meshes using Weak Galerkin FEMs in [43]. Convergence analysis for other time dependent Interface problems on polygonal meshes are still open. A further extension could be *a priori* analysis of time dependent interface problems on polygonal meshes.

Nonlinear second order Hyperbolic Interface Problem: Consider the nonlinear damped wave equation of the form

$$c^{-2}u_{tt} - \nabla \cdot \left(\nabla u + \beta \nabla u'\right) = \gamma(u^2)_{tt} \text{ in } (0,T] \times \Omega. \tag{6.2.1}$$

The equation (6.2.1) is known as Westervelt equation which is widely used to simulate high-intensity focused ultrasound fields generated by medical ultrasound transducers. High intensity focused ultrasound has numerous applications starting from treatment of kidney and bladder stones via thermotherapy, ultrasound cleaning, and welding to sonochemistry. Westervelt equation (6.2.1) with interfaces are motivated by lithotripsy where a silicone acoustic lens focuses the ultrasound traveling through a nonlinearly acoustic fluid to a kidney stone. In [106], the authors have investigated interface coupling problems involving Westervelt equation for different types of boundary conditions. Well-posedness of such model interface problems and the regularity of its solutions are

TH-2392_146123010

established. It will be interesting and challenging to extend the present the analysis discuss in this thesis to the interface problems discussed in [106].

TH-2392_146123010

TH-2392_146123010

Bibliography

[1] R. Adams and J. Fournier, *Sobolev Spaces, sec. ed*, Academic Press, Amsterdam, 2003.

[2] S. Adjerid, N. Chaabane, and T. Lin, *An immersed discontinuous finite element method for stokes interface problems*, Comput.Methods Appl. Mech. Engrg., 293 (2015), pp. 170–190.

[3] S. Adjerid, N. Chaabane, T. Lin, and P. Yue, *An immersed discontinuous finite element method for the stokes problem with a moving interface*, J. Comput. Appl. Math., 362 (2019), pp. 540–559.

[4] S. Adjerid, R. Guo, and T. Lin, *High degree immersed finite element spaces by a least squares method*, Int. J. Numer. Anal. Model, 14 (2017), pp. 604–626.

[5] S. Adjerid and T. Lin, *A p-th degree immersed finite element for boundary value problems with discontinuous coefficients*, Appl. Numer. Math., 59 (2009), pp. 1303–1321.

[6] S. Adjerid and K. Moon, *A higher order immersed discontinuous galerkin finite element method for the acoustic interface problem*, Adv. Appl. Math., (2014), pp. 57–69.

[7] S. Adjerid and K. Moon, *An immersed discontinuous galerkin method for acoustic wave propagation in inhomogeneous media*, SIAM J. Sci. Comput., 41 (2019), pp. A139–A162.

[8] H. Ammari, D. Chen, and J. Zou, *Well-posedness of an electric interface model and its finite element approximation*, Math. Models Methods Appl. Sci., 26 (2016), pp. 601–625.

TH-2392_146123010

[9] H. Ammari, J. Garnier, L. Giovangigli, W. Jing, and J.-K. Seo, *Spectroscopic imaging of a dilute cell suspension*, J. Math. Pures Appl. (9), 105 (2016), pp. 603–661.

[10] N. An, X. Yu, and C. Huang, *Local discontinuous galerkin methods for parabolic interface problems with homogeneous and non-homogeneous jump conditions*, Comput. Math. Appl., 74 (2017), pp. 2572–2598.

[11] F. Andre and L. Mir, *DNA electrotransfer: its principles and an updated review of its therapeutic applications*, Gene Ther., 11 (2004), pp. S33–S42.

[12] A. Angersbach, V. Heinz, and D. Knorr, *Effects of pulsed electric fields on cell membranes in real food systems*, Innov. Food Sci. Emerg. Technol., 1 (2000), pp. 135–149.

[13] P. Antonietti, I. Mazzieri, M. Muhr, V. Nikolić, and B. Wohlmuth, *A high-order discontinuous galerkin method for nonlinear sound waves*, J. Comput. Phys., 415 (2020), p. 109484.

[14] I. Babuška, *The finite element method for elliptic equations with discontinuous coefficients*, Computing, 5 (1970), pp. 207–213.

[15] G. A. Baker, *Error estimates for finite element methods for second order hyperbolic equations*, SIAM J. Numer. Anal., 13 (1976), pp. 564–576.

[16] A. Bamberger, R. Glowinski, and Q. H. Tran, *A domain decomposition method for the acoustic wave equation with discontinuous coefficients and grid change*, SIAM J. Numer. Anal., 34 (1997), pp. 603–639.

[17] J. W. Barrett and C. M. Elliott, *Fitted and unfitted finite-element methods for elliptic equations with smooth interfaces*, IMA J. Numer. Anal., 7 (1987), pp. 283–300.

[18] M. Basson, B. Stapelberg, and N. F. J. van Rensburg, *Error estimates for semi-discrete and fully discrete Galerkin finite element approximations of the general linear second-order hyperbolic equation*, Numer. Funct. Anal. Optim., 38 (2017), pp. 466–485.

[19] P. Bastian and C. Engwer, *An unfitted finite element method using discontinuous galerkin*, Int. J. Numer. Methods Engrg., 79 (2009), pp. 1557–1576.

[20] D. Boffi, L. Gastaldi, and M. Ruggeri, *Mixed formulation for interface problems with distributed lagrange multiplier*, Comput. Math. Appl., 68 (2014), pp. 2151–2166.

TH-2392_146123010

[21] J. H. Bramble and J. T. King, *A finite element method for interface problems in domains with smooth boundaries and interfaces*, Adv. Comput. Math., 6 (1996), pp. 109–138.

[22] F. Brezzi and M. Fortin, *Mixed and hybrid finite element methods*, vol. 15, Springer Science & Business Media, 2012.

[23] E. Burman and A. Ern, *An unfitted hybrid high-order method for elliptic interface problems*, SIAM J. Numer. Anal., 56 (2018), pp. 1525–1546.

[24] E. Burman and P. Hansbo, *Interior-penalty-stabilized lagrange multiplier methods for the finite-element solution of elliptic interface problems*, IMA J. Numer. Anal., 30 (2010), pp. 870–885.

[25] C. R. Butson and C. C. McIntyre, *Tissue and electrode capacitance reduce neural activation volumes during deep brain stimulation*, Clin Neurophysiol., 116 (2005), pp. 2490–2500.

[26] Z. Cai, X. Ye, and S. Zhang, *Discontinuous galerkin finite element methods for interface problems: a priori and a posteriori error estimations*, SIAM J. Numer. Anal., 49 (2011), pp. 1761–1787.

[27] Z. Cai and S. Zhang, *Recovery-based error estimators for interface problems: mixed and nonconforming finite elements*, SIAM J. Numer. Anal., 48 (2010), pp. 30–52.

[28] W. Cao, X. Zhang, and Z. Zhang, *Superconvergence of immersed finite element methods for interface problems*, Adv. Comput. Math., 43 (2017), pp. 795–821.

[29] Y. Cao, Y. Chu, X. He, and T. Lin, *An iterative immersed finite element method for an electric potential interface problem based on given surface electric quantity*, J. Comput. Phys., 281 (2015), pp. 82–95.

[30] L. Chen, H. Wei, and M. Wen, *An interface-fitted mesh generator and virtual element methods for elliptic interface problems*, J. Comput. Phys., 334 (2017), pp. 327–348.

[31] Z. Chen and J. Zou, *Finite element methods and their convergence for elliptic and parabolic interface problems*, Numer. Math., 79 (1998), pp. 175–202.

[32] S.-H. Chou, D. Y. Kwak, and K. T. Wee, *Optimal convergence analysis of an immersed interface finite element method*, Adv. Comput. Math., 33 (2010), pp. 149–168.

TH-2392_146123010

[33] W. Dai, H. Wang, P. M. Jordan, R. E. Mickens, and A. Bejan, *A mathematical model for skin burn injury induced by radiation heating*, Int. J. Heat Mass Transf., 51 (2008), pp. 5497–5510.

[34] R. Dautray and J.-L. Lions, *Mathematical Analysis and Numerical Methods for Science and Technology: I*, vol. 5, Springer-Verlag, Berlin, 1992.

[35] B. Deka, *Finite element methods with numerical quadrature for elliptic problems with smooth interfaces*, J. Comput. Appl. Math., 234 (2010), pp. 605–612.

[36] ——, *A priori $L^\infty(L^2)$ error estimates for finite element approximations to the wave equation with interface*, Appl. Numer. Math., 115 (2017), pp. 142–159.

[37] ——, *A weak galerkin finite element method for elliptic interface problems with polynomial reduction.*, Numer. Math. Theory Methods Appl., 11 (2018).

[38] ——, *A posteriori error estimates for finite element approximations to the wave equation with discontinuous coefficients*, Numer. Methods Partial Differential Equations, 35 (2019), pp. 1630–1653.

[39] B. Deka and T. Ahmed, *Convergence of finite element method for linear second-order wave equations with discontinuous coefficients*, Numer. Methods Partial Differential Equations, 29 (2013), pp. 1522–1542.

[40] B. Deka and J. Dutta, *$L^\infty(L^2)$ and $L^\infty(H^1)$ norms error estimates in finite element methods for electric interface model*, Appl. Anal. DOI: 10.1080/00036811.2019.1643010., (2019).

[41] ——, *Convergence of finite element methods for hyperbolic heat conduction model with an interface*, Comput. Math. Appl., 79 (2020), pp. 3139–3159.

[42] ——, *Finite element methods for non-fourier thermal wave model of bio heat transfer with an interface*, J. Appl. Math. Comput., 62 (2020), pp. 701–724.

[43] B. Deka and P. Roy, *Weak galerkin finite element methods for parabolic interface problems with nonhomogeneous jump conditions*, Numer. Funct. Anal. Optim., 40 (2019), pp. 259–279.

[44] ——, *Weak galerkin finite element methods for electric interface model with nonhomogeneous jump conditions*, Numer. Methods Partial Differential Equations, 36 (2020), pp. 734–755.

[45] B. Deka and R. K. Sinha, *$L^\infty(L^2)$ and $L^\infty(H^1)$ norms error estimates in finite element method for linear parabolic interface problems*, Numer. Funct. Anal. Optim., 32 (2011), pp. 267–285.

TH-2392_146123010

[46] H. Dong, B. Wang, Z. Xie, and L.-L. Wang, *An unfitted hybridizable discontinuous galerkin method for the poisson interface problem and its error analysis*, IMA J. Numer. Anal., 37 (2017), pp. 444–476.

[47] J. Dutta and B. Deka, *Optimal a priori error estimates for the finite element approximation of dual-phase-lag bio heat model in heterogeneous medium*, Revised version Submitted.

[48] J. Dutta, B. Deka, and N. Kumar, *Finite element methods for the electric interface model: Convergence analysis*, Math. Methods Appl. Sci., 43 (2020), pp. 4598–4613.

[49] L. C. Evans, *Partial Differential Equations*, vol. 19, American Mathematical Soc., 2010.

[50] Y. Gong, B. Li, and Z. Li, *Immersed-interface finite-element methods for elliptic interface problems with nonhomogeneous jump conditions*, SIAM J. Numer. Anal., 46 (2007/08), pp. 472–495.

[51] O. Gorynina, A. Lozinski, and M. Picasso, *Time and space adaptivity of the wave equation discretized in time by a second-order scheme*, IMA J. Numer. Anal., 39 (2018), pp. 1672–1705.

[52] W. M. Grill, *Modeling the effects of electric fields on nerve fibers: influence of tissue electrical properties*, IEEE Trans. Biomed. Engrg., 46 (1999), pp. 918–928.

[53] R. Guo and T. Lin, *A group of immersed finite-element spaces for elliptic interface problems*, IMA J. Numer. Anal., 39 (2019), pp. 482–511.

[54] J. S. Gupta, *A Posteriori error Analysis of Finite Element Method for Parabolic Interface Problems*, PhD thesis, 2015.

[55] G. Guyomarc'h, C.-O. Lee, and K. Jeon, *A discontinuous galerkin method for elliptic interface problems with application to electroporation*, Comms. Numer. Methods Engrg., 25 (2009), pp. 991–1008.

[56] D. Han, P. Wang, X. He, T. Lin, and J. Wang, *A 3d immersed finite element method with non-homogeneous interface flux jump for applications in particle-in-cell simulations of plasma–lunar surface interactions*, J. Comput. Phys., 321 (2016), pp. 965–980.

[57] A. Hansbo and P. Hansbo, *An unfitted finite element method, based on nitsches method, for elliptic interface problems*, Comput. Methods Appl. Mech. Engrg., 191 (2002), pp. 5537–5552.

TH-2392_146123010

[58] G. H. Hardy, J. E. Littlewood, and G. Pólya, *Inequalities*, Cambridge Univ. Press, London, 1964.

[59] X. He, T. Lin, and Y. Lin, *A selective immersed discontinuous galerkin method for elliptic interface problems*, Math. Methods Appl. Sci., 37 (2014), pp. 983–1002.

[60] X. He, T. Lin, Y. Lin, and X. Zhang, *Immersed finite element methods for parabolic equations with moving interface*, Numer. Methods Partial Differential Equations, 29 (2013), pp. 619–646.

[61] S. Hou, P. Song, L. Wang, and H. Zhao, *A weak formulation for solving elliptic interface problems without body fitted grid*, J. Comput. Phys., 249 (2013), pp. 80–95.

[62] Q. Hu and R. Joshi, *Transmembrane voltage analyses in spheroidal cells in response to an intense ultrashort electrical pulse*, Phys. Rev. E, 79 (2009), p. 011901.

[63] J. Huang and J. Zou, *Some new a priori estimates for second-order elliptic and parabolic interface problems*, J. Differ. Equ., 184 (2002), pp. 570–586.

[64] L. Huynh, N. Nguyen, J. Peraire, and B. Khoo, *A high-order hybridizable discontinuous galerkin method for elliptic interface problems*, Int. J. Numer. Methods Engrg., 93 (2013), pp. 183–200.

[65] H. Ji, J. Chen, and Z. Li, *A symmetric and consistent immersed finite element method for interface problems*, J. Sci. Comput., 61 (2014), pp. 533–557.

[66] ——, *A new augmented immersed finite element method without using SVD interpolations*, Numer. Algorithms, 71 (2016), pp. 395–416.

[67] ——, *A high-order source removal finite element method for a class of elliptic interface problems*, Appl. Numer. Math., 130 (2018), pp. 112–130.

[68] H. Ji, Q. Zhang, and B. Zhang, *Inf-sup stability of petrov-galerkin immersed finite element methods for one-dimensional elliptic interface problems*, Numer. Methods Partial Differential Equations, 34 (2018), pp. 1917–1932.

[69] D. D. Joseph and L. Preziosi, *Heat waves*, Rev. Mod. Phys., 61 (1989), p. 41.

[70] A. Joshi and A. Majumdar, *Transient ballistic and diffusive phonon heat transport in thin films*, J. Appl.Phys., 74 (1993), pp. 31–39.

[71] B. Kaltenbacher and I. Lasiecka, *Global existence and exponential decay rates for the westervelt equation*, Discrete Contin. Dyn. Syst. Ser. S, 2 (2009), p. 503.

[72] W. Kaminski, *Hyperbolic heat conduction equation for materials with a nonhomogeneous inner structure*, J. Heat Transfer., 112 (1990), pp. 555–560.

TH-2392_146123010

[73] J. D. Kandilarov and L. G. Vulkov, *The immersed interface method for two-dimensional heat-diffusion equations with singular own sources*, Appl. Numer. Math., 57 (2007), pp. 486–497.

[74] S. Karaa, *Error estimates for finite element approximations of a viscous wave equation*, Numer. Funct. Anal. Optim., 32 (2011), pp. 750–767.

[75] K. Kelly, R. Ward, S. Treitel, and R. Alford, *Synthetic seismograms: A finite-difference approach*, Geophysics, 41 (1976), pp. 2–27.

[76] K. Kim and Z. Guo, *Multi-time-scale heat transfer modeling of turbid tissues exposed to short-pulsed irradiations*, Comput. Methods Programs Biomed., 86 (2007), pp. 112–123.

[77] T. Kotnik, D. Miklavčič, and T. Slivnik, *Time course of transmembrane voltage induced by time-varying electric fields a method for theoretical analysis and its application*, Bioelectrochem. Bioenerg, 45 (1998), pp. 3–16.

[78] H.-O. Kreiss and N. A. Petersson, *An embedded boundary method for the wave equation with discontinuous coefficients*, SIAM J. Sci. Comput., 28 (2006), pp. 2054–2074.

[79] O. A. Ladyzhenskaya, V. Y. Rivkind, and N. N. Ural'tseva, *The classical solvability of diffraction problems*, Tr. Mat. Inst. Steklova, 92 (1966), pp. 116–146.

[80] J. E. Lagnese, G. Leugering, and E. G. Schmidt, *Modeling, analysis and control of dynamic elastic multi-link structures*, Springer Science & Business Media, 2012.

[81] S. Larsson, V. Thomée, and L. B. Wahlbin, *Finite-element methods for a strongly damped wave equation*, IMA J. Numer. Anal., 11 (1991), pp. 115–142.

[82] C. Lehrenfeld and A. Reusken, *Analysis of a high-order unfitted finite element method for elliptic interface problems*, IMA J. Numer. Anal., 38 (2018), pp. 1351–1387.

[83] ——, *L2-error analysis of an isoparametric unfitted finite element method for elliptic interface problems*, J. Numer. Math., 27 (2019), pp. 85–99.

[84] R. J. Leveque and Z. Li, *The immersed interface method for elliptic equations with discontinuous coefficients and singular sources*, SIAM J. Numer. Anal., 31 (1994), pp. 1019–1044.

[85] J. Li, J. M. Melenk, B. Wohlmuth, and J. Zou, *Optimal a priori estimates for higher order finite elements for elliptic interface problems*, Appl. Numer. Math., 60 (2010), pp. 19–37.

TH-2392_146123010

[86] Z. Li, *The immersed interface method using a finite element formulation*, Appl. Numer. Math., 27 (1998), pp. 253–267.

[87] Z. Li, T. Lin, Y. Lin, and R. C. Rogers, *An immersed finite element space and its approximation capability*, Numer. Methods Partial Differential Equations, 20 (2004), pp. 338–367.

[88] Z. Li, T. Lin, and X. Wu, *New cartesian grid methods for interface problems using the finite element formulation*, Numer. Math., 96 (2003), pp. 61–98.

[89] H. Lim, S. Kim, and J. Douglas Jr, *Numerical methods for viscous and nonviscous wave equations*, Appl. Numer. Math., 57 (2007), pp. 194–212.

[90] T. Lin, Y. Lin, and X. Zhang, *Partially penalized immersed finite element methods for elliptic interface problems*, SIAM J. Numer. Anal., 53 (2015), pp. 1121–1144.

[91] T. Lin, Q. Yang, and X. Zhang, *Partially penalized immersed finite element methods for parabolic interface problems*, Numer. Methods Partial Differential Equations, 31 (2015), pp. 1925–1947.

[92] ——, *A priori error estimates for some discontinuous galerkin immersed finite element methods*, J. Sci. Comput., 65 (2015), pp. 875–894.

[93] J. L. Lions and E. Magenes, *Non-homogeneous boundary value problems and applications*, vol. 2, Springer Science & Business Media, 1972.

[94] K.-C. Liu and H.-T. Chen, *Investigation for the dual phase lag behavior of bio-heat transfer*, Int. J. Therm. Sci., 49 (2010), pp. 1138–1146.

[95] K.-C. Liu, Y.-N. Wang, and Y.-S. Chen, *Investigation on the bio-heat transfer with the dual-phase-lag effect*, Int. J. Therm. Sci., 58 (2012), pp. 29–35.

[96] A. Luikov, *Application of irreversible thermodynamics methods to investigation of heat and mass transfer*, Int. J. Heat Mass Transf., 9 (1966), pp. 139–152.

[97] G. H. Markx and C. L. Davey, *The dielectric properties of biological cells at radiofrequencies: applications in biotechnology*, Enzyme Microb. Technol., 25 (1999), pp. 161–171.

[98] R. Massjung, *An unfitted discontinuous galerkin method applied to elliptic interface problems*, SIAM J. Numer. Anal., 50 (2012), pp. 3134–3162.

[99] D. Miklavčič, N. Pavšelj, and F. X. Hart, *Electric properties of tissues*, Wiley Encyclopedia Biomed. Engrg., (2006).

TH-2392_146123010

[100] K. Mitra, S. Kumar, A. Vedevarz, and M. Moallemi, *Experimental evidence of hyperbolic heat conduction in processed meat*, J. Heat Transfer., 117 (1995), pp. 568–573.

[101] L. Mu, J. Wang, G. Wei, X. Ye, and S. Zhao, *Weak galerkin methods for second order elliptic interface problems*, J. Comput. Phys., 250 (2013), pp. 106–125.

[102] L. Mu, J. Wang, X. Ye, and S. Zhao, *A new weak galerkin finite element method for elliptic interface problems*, J. Comput. Phys., 325 (2016), pp. 157–173.

[103] A. Narasimhan and S. Sadasivam, *Non-fourier bio heat transfer modelling of thermal damage during retinal laser irradiation*, Int. J. Heat Mass Transf., 60 (2013), pp. 591–597.

[104] N. M. Newmark, *A method of computation for structural dynamics*, American Society of Civil Engineers, 1959.

[105] B. F. Nielsen, *Finite element discretizations of elliptic problems in the presence of arbitrarily small ellipticity: An error analysis*, SIAM J. Numer. Anal., 36 (1999), pp. 368–392.

[106] V. Nikolić and B. Kaltenbacher, *On higher regularity for the westervelt equation with strong nonlinear damping*, Appl. Anal., 95 (2016), pp. 2824–2840.

[107] V. Nikolić and B. Wohlmuth, *A priori error estimates for the finite element approximation of Westervelt's quasi-linear acoustic wave equation*, SIAM J. Numer. Anal., 57 (2019), pp. 1897–1918.

[108] S. Ozen, S. Helhel, and O. Cerezci, *Heat analysis of biological tissue exposed to microwave by using thermal wave model of bio-heat transfer (twmbt).*, Burns, 34 (2008), pp. 45–49.

[109] A. K. Pani and J. Y. Yuan, *Mixed finite element method for a strongly damped wave equation*, Numer. Methods Partial Differential Equations, 17 (2001), pp. 105–119.

[110] H. H. Pennes, *Analysis of tissue and arterial temperature in the resting human forearm*, J. Appl. Physiol., 1 (1948), pp. 93–122.

[111] Y. Polevaya, I. Ermolina, M. Schlesinger, B.-Z. Ginzburg, and Y. Feldman, *Time domain dielectric spectroscopy study of human cells:II. normal and malignant white blood cells*, Biochim. Biophys. Acta, 1419 (1999), pp. 257–271.

TH-2392_146123010

[112] T. Qiu and C. Tien, *Short-pulse laser heating on metals*, Int. J. Heat Mass Transf., 35 (1992), pp. 719–726.

[113] M. Rama Mohan Rao, *Ordinary differential equations theory and aplications*, East-West Press Pvt. Ltd., 1980.

[114] L. Rems, M. Ušaj, M. Kandušer, M. Reberšek, D. Miklavčič, and G. Pucihar, *Cell electrofusion using nanosecond electric pulses*, Sci. Rep., 3 (2013), p. 3382.

[115] X. Ren and J. Wei, *On a two-dimensional elliptic problem with large exponent in nonlinearity*, Trans. Amer. Math. Soc., 343 (1994), pp. 749–763.

[116] J. C. Robinson, *Infinite-dimensional dynamical systems: an introduction to dissipative parabolic PDEs and the theory of global attractors*, vol. 28, Cambridge University Press, 2001.

[117] E. Salimi, *Nanosecond pulse electroporation of biological cells: The effect of membrane dielectric relaxation*, PhD thesis, 2011.

[118] K. H. Schoenbach, F. E. Peterkin, R. W. Alden, and S. J. Beebe, *The effect of pulsed electric fields on biological cells: Experiments and applications*, IEEE Trans. Plasma Sci., 25 (1997), pp. 284–292.

[119] H. Schwan, *Mechanisms responsible for electrical properties of tissues and cell suspensions.*, Med. Prog. Technol., 19 (1993), pp. 163–165.

[120] R. E. Showalter, *Hilbert space methods in partial differential equations*, Courier Corporation, 2010.

[121] S. Singh, S. Singh, and Z. Li, *A high order compact scheme for a thermal wave model of bio-heat transfer with an interface*, Numer. Math. Theory Methods Appl., 11 (2018), pp. 321–337.

[122] R. K. Sinha and B. Deka, *Optimal error estimates for linear parabolic problems with discontinuous coefficients*, SIAM J. Numer. Anal., 43 (2005), pp. 733–749.

[123] ——, *An unfitted finite-element method for elliptic and parabolic interface problems*, IMA J. Numer. Anal., 27 (2007), pp. 529–549.

[124] L. Song and S. Zhao, *Symmetric interior penalty galerkin approaches for two-dimensional parabolic interface problems with low regularity solutions*, J. Comput. Appl. Math., 330 (2018), pp. 356–379.

[125] E. M. Stein, *Singular integrals and differentiability properties of functions (PMS-30)*, vol. 30, Princeton university press, 2016.

TH-2392_146123010

[126] V. Thomée, *Galerkin finite element methods for parabolic problems*, vol. 1054, Springer, 1984.

[127] Q. H. Tran, L. Jannaud, and P. Adler, *Coda spectral power and apparent attenuation factor of acoustic waves in 3-d random media*, J. Acoust. Soc. Am., 94 (1993), pp. 2397–2407.

[128] D. Tzou and K. Chiu, *Temperature-dependent thermal lagging in ultrafast laser heating*, Int. J. Heat Mass Transf., 44 (2001), pp. 1725–1734.

[129] D. Y. Tzou, *A unified field approach for heat conduction from macro-to micro-scales*, J. Heat Transfer., 117 (1995), pp. 8–16.

[130] ——, *Macro-to microscale heat transfer: the lagging behavior*, John Wiley & Sons, 2014.

[131] N. van Rensburg and B. Stapelberg, *Existence and uniqueness of solutions of a general linear second-order hyperbolic problem*, IMA J. Appl. Math., 84 (2018), pp. 1–22.

[132] N. Van Rensburg and A. Van Der Merwe, *Analysis of the solvability of linear vibration models*, Appl. Anal., 81 (2002), pp. 1143–1159.

[133] A. Vedavarz, S. Kumar, and M. K. Moallemi, *Significance of non-fourier heat waves in conduction*, J. Heat Transfer., 116 (1994), pp. 221–226.

[134] K. Virta and K. Mattsson, *Acoustic wave propagation in complicated geometries and heterogeneous media*, J. Sci. Comput., 61 (2014), pp. 90–118.

[135] X. Wang and J. Zou, *Identification of conductivity and permittivity in a pulsed electric field model*, Appl. Anal., 95 (2016), pp. 2736–2749.

[136] J. C. Weaver and Y. A. Chizmadzhev, *Theory of electroporation: a review*, Bioelectrochem. Bioenerg, 41 (1996), pp. 135–160.

[137] F. Xu, T. Lu, K. Seffen, and E. Ng, *Mathematical modeling of skin bioheat transfer*, Appl. Mech. Rev., 62 (2009), p. 050801.

[138] F. Xu, K. Seffen, and T. Lu, *Non-fourier analysis of skin biothermomechanics*, Int. J. Heat Mass Transf., 51 (2008), pp. 2237–2259.

[139] L. Yang, *Electrical impedance spectroscopy for detection of bacterial cells in suspensions using interdigitated microelectrodes*, Talanta, 74 (2008), pp. 1621–1629.

[140] Q. Yang and X. Zhang, *Discontinuous galerkin immersed finite element methods for parabolic interface problems*, J. Comput. Appl. Math., 299 (2016), pp. 127–139.

TH-2392_146123010

[141] C. Zhang and R. J. LeVeque, *The immersed interface method for acoustic wave equations with discontinuous coefficients*, Wave Motion, 25 (1997), pp. 237–263.

[142] S. Zhang, *Robust and local optimal a priori error estimates for interface problems with low regularity: Mixed finite element approximations*, J. Sci. Comput., 84 (2020).

[143] X. Zhang, *Nonconforming immersed finite element methods for interface problems*, PhD thesis, Virginia Tech, 2013.

TH-2392_146123010